Hydrothermal Synthesis of Spinel Nanoparticles in the Al_2O_3-Ga_2O_3 and $ZnAl_2O_4$-$ZnGa_2O_4$ Systems

2017

Kazuki Sakoda

Aichi Institute of Technology

Contents

Chapter 1
Introduction

1-1 Spinel compounds

Spinel compounds are one of representative and useful materials in ceramics and minerals. Spinel is also a constituent that is located in the transition zone below the upper layer of the earth's mantle. Various spinel compounds that have a variety of characteristics are known. In the ideal structure of spinel oxide, oxygen atoms have a face centered cubic (fcc) and cubic closest packed arrangements in which cations occupy one-eighth of the tetragonal and one-half of the octahedral interstices. In the arrangement of atoms, perpendicular to each three-fold axis, layers are occupied only by cations in octahedral coordination alternate with others. In that structure, the tetrahedral and octahedral sites are included in the ratio two to one [1, 2] The unit cell of spinel oxide includes 32 oxygen anions, 16 octahedral cations, and 8 tetragonal cations for example. The formula of a binary spinel can be represented as AB_2X_4, in which X is an anion and A and B represent cations. Possible two types of extreme distribution of the cations among the available sites exist in the spinel structures. One is "normal" distribution $A[B]_2X_4$, and the other is "inverse" distribution $B[AB]X_4$, where the cations in octahedral coordination are indicated in a brackets "[ ]". In the case that the cation distribution becomes random over each type of site, eight formula units exist in the unit cell and its symmetry can be lowered by means of Jahn-Teller and other effects [3-5]. When the cations are distributed intermediately, it may be indicated as $A_{1-x}B_x[A_xB_{2-x}]X_4$, where x is what is called degree of inversion. The x which is equal to zero and unity corresponds to the normal and inverse arrangements, respectively [6]. On the other hand, many spinel compounds with cation vacancies are also known. γ-type Fe_2O_3 (maghemite), which is a representative example that contains high concentration of cation vacancies, is what is called a defective spinel. All the iron cations in γ-Fe_2O_3 are in trivalent state, and the charge neutrality of the cell is compensated by the presence of cation vacancies. These vacancies are known to be situated in the octahedral sites. This type of spinel is usually metastable and transforms into stable phase via high temperature heating.

Spinel compounds show interesting, unique, and a variety of properties which can be applied in a wide variety of industrial fields. Magnesium aluminate $MgAl_2O_4$, among all the spinels, is the most representative one and is an excellent refractory oxide as a structural ceramics because of high melting temperature (2135°C) and high resistance to attack by most of the acids and alkalis [7]. Other compounds, e.g., $ZnAl_2O_4$ (gahnite), $FeAl_2O_4$ (hercynite), and $MnAl_2O_4$ (galaxite) are known as aluminate spinel. Magnetite (Fe_3O_4) is also a famous mineral as a common magnetic iron oxide that crystallizes in the cubic inverse spinel structure having

ferrous and ferric ions on the octahedral sites of the spinel lattice [8-11]. Ferrimagnetic substances referred to as ferrites XFe_2O_4 (X signifies a divalent metal as Mg, Mn, Ni, Cu, Zn, etc.) that have extensive use as magnetic materials in electronic technology are also important members of spinel compounds. Manganese-zinc and nickel-zinc ferrites are most widely used as magnetically-soft ferrites. Among magnetically-hard ferrites the most widespread ones are barium and strontium ferrites. On the other hand, there are other complex oxides with spinel structure based on chromium oxide such as chromite ($FeCr_2O_4$), magnesiochromite ($MgCr_2O_4$), etc. Chromium spinel oxides AB_2O_4 (A=Hg, Cd, Mg, and Zn), in which magnetic chromium ions occupy the B site, forming a pylochlore lattice, show interesting magnetic properties of geometrical frustration in high magnetic fields due to that strong geometrical frustration and significant spin-lattice coupling inherent in the chromium spinel oxides result in unconventional magnetic phase transitions [12].

Spinel compounds with negative temperature coefficient (NTC) resistance, i.e., NTC thermistors that belong to semi-conducting ceramics are widely used in the areas on modern microelectronics, especially in temperature and heating sensors, integrated temperature-humidity sensors, fire detectors, power-sensing terminations, temperature-compensating attenuators, etc. [13-17]. Spinel compounds based on nickel manganite or mixed spinel-type manganites in the system $NiMn_2O_4$-$CuMn_2O_4$-$MnCo_2O_4$ show many essential advantages as a material for NTC thermistor [18,19]. Actually, nanostructured ceramics consisting of magnesium aluminate spinel and mixed transition metal manganite spinel are widely used for temperature and humidity measurement [13, 20, 21]. Spinel-type $LiMnO_4$ is one of candidate cathode materials for lithium ion rechargeable batteries which play an important part in an energy source with high energy and power density for small portable electronic devices such as cell phones, lab-top computers, portable power tools, and vehicle electrification [22-25]. Among many cathode materials, the most promising candidate for a large scale lithium ion batteries of electric vehicles has been considered to be the $LiMnO_4$ spinel because of its advantages of low cost, environmental friendliness, high abundance, and low safety hazard [26-28].

1-2 Materials based on gallium oxide and spinel-type gallate compounds

Gallium oxide (gallia, Ga_2O_3), which belongs to transparent wide-band gap oxide semiconductor, is one of important functional materials because it becomes a semiconductor above 800 °C though an insulator having a forbidden energy gap of 4.9 eV at room temperature [29,30]. Ga_2O_3 has been known to have five different polymorphs: α, β, γ, δ, and ε [31] similar to those of aluminum oxide (alumina, Al_2O_3). The γ-type Ga_2O_3 is metastable phase and has defective spinel structure. The monoclinic β-Ga_2O_3 is the most stable crystalline modification and its melting temperature is 1740 °C. The transformation of γ-Ga_2O_3 into stable β-Ga_2O_3

occurs above 873 K [32]. The materials based on Ga_2O_3 find application in catalysis [33-35], phosphors [33,36], gas sensors [37], and transparent conducting oxide [38]. Aluminum oxide (alumina, Al_2O_3) and gallium oxide (gallia, Ga_2O_3) have several similarities in structural and optical properties though alumina is a typical insulator. The structure of the γ-type Al_2O_3 is also defective-spinel-type. In the Al_2O_3-Ga_2O_3 system, the possibility that they can form defective-spinel-type $(Al,Ga)_2O_3$ solid solution is suggested.

On the other hand, zinc aluminate ($ZnAl_2O_4$) and zinc gallate ($ZnGa_2O_4$), both of which belong to transparent and wide-band-gap semiconductor materials, e.g. ZnO, In_2O_3, and SnO_2 [39], are known to have the same normal spinel structure with all the Zn^{2+} ions in tetrahedral sites and Ga^{3+} or Al^{3+} ions in octahedral sites [40]. Zinc gallate shows a blue emission without any dopant via a self-activation center of Ga-O groups under excitation by both UV light and low-voltage electrons [41,42]. This emission can be tunable from blue to green or up to red when it is activated with Mn^{2+}, Cr^{3+}, Eu^{3+}, and Tb^{3+} [43-45]. As excellent phosphor host materials, the zinc gallate has been applied to thin film electroluminescent devices (TFED), vacuum fluorescent displays (VFD), and field emission displays (FED) [41,46-49]. The zinc aluminate also possesses a wide range of applications as phosphor materials [50-52], reflective optical coatings [53], UV-transport electro conductive oxide [54], photocatalyst for the degradation of toluene [55], and catalysts for dehydration, hydrogenation, dehydrogenation, and synthesis of fine chemicals [56-59]. It is expected that the properties of $ZnGa_2O_4$ can be tuned by the formation of solid solutions, e.g., through the substitutional incorporation of aluminum ion into the spinel lattice in the $ZnAl_2O_4$-$ZnGa_2O_4$ system. A large number of methods for the preparation of those spinel materials mentioned above are known in literature, but there are few reports on the low-temperature (< 250°C) and direct formation of those nanocrystals with high crystallinity.

1-3 Purpose of the present study

In the preparation of crystalline inorganic (ceramic) materials, their synthesis routes and processing have great effects on their phases, microstructures, characteristics and performances. The aqueous solution routes for the preparation of refractory crystalline materials based on the reaction in the presence of liquid phase such as hydrothermal synthesis method, which fall into a category “building up process”, can attain the formation of more homogeneous nanocrystalline materials at lower temperatures than the cases of the solid-state reactions and break down processes. From a view point of green processing, the aqueous solution routes have advantages. The direct formation of nanocrystalline inorganic materials at low temperatures has been one of technological and scientific interests. Although the spinel materials based on gallium oxide have attractive properties described above, the studies and reports on the hydrothermal synthesis of nanoparticles such as γ-Ga_2O_3, γ-$(Al,Ga)_2O_3$, and $Zn(Al,Ga)_2O_4$ with

a single phase of spinel-type structure from aqueous precursor solutions using the starting materials of simple inorganic salts are few. In the spinel-structured γ-Ga_2O_3 and $ZnGa_2O_4$ nanocrystals, the details of the effect of the substitutional incorporation of aluminum into the spinel lattice on their hydrothermal formation, structures, and optical properties, e.g., optical band gap and luminescence have not been clarified.

The purposes of this study are to synthesis spinel-structured γ-Ga_2O_3, γ-$(Al,Ga)_2O_3$, and $Zn(Al,Ga)_2O_4$ nanoparticles from the aqueous precursor solutions under mild hydrothermal conditions and to investigate the effects of the composition, hydrothermal treatment condition, and heat treatment in air on their crystalline phases, structures, phase transformations, and luminescence properties.

1-4 Construction of the present study

The present thesis consists of 7 chapters.

Chapter 1 presents the background and fundamentals on spinel compounds and materials discussed in this study. The purpose and outline of the present study are also added.

Chapter 2 describes the results on the preparation of luminescent γ-Ga_2O_3 nanocrystals from the aqueous precursor solutions of inorganic gallium salts via hydrothermal route using citric acid. It also contains the results of an investigation on the effects of hydrothermal treatment temperature and post-heat treatment in air on the crystallinity, phase stability, and photoluminescence properties of spinel-type γ-Ga_2O_3 nanocrystals.

Chapter 3 deals with the spinel-type γ-Ga_2O_3-based nanoparticles doped with Al_2O_3 in the Al_2O_3-Ga_2O_3 system that were hydrothermally formed under weakly basic conditions in the presence of citric acid. This chapter also presents the results of an investigation on the effects of the composition, hydrothermal treatment condition, and heat treatment in air on their crystalline phases, structures, phase transformations, and luminescence properties.

Chapter 4 presents the results of the hydrothermal synthesis of nanometer-sized $ZnAlGaO_4$ spinel and its structure and properties, e.g., the cell size, optical band gap, and photoluminescence. A discussion on the structural change in the course of hydrothermal treatment and post-heating is also contained.

Chapter 5 describes the results of hydrothermal treatment at low temperature (180°C) in a short time that was carried out to form nanoparticles in the $ZnAl_2O_4$-$ZnGa_2O_4$ system. It also presents the results of an investigation on the change in structure and optical and luminescence properties of as-prepared nanoparticles by means of comparing those of heat-treated samples.

Chapter 6 presents the results of an investigation on the formation of nano-sized and spinel-structured complete solid solutions in the $ZnAl_2O_4$-$ZnGa_2O_4$ system from the aqueous precursor solutions of inorganic salts under mild hydrothermal conditions in the presence of tetramethylammonium hydroxide for a short period of time.

Chapter 7 summarizes the results obtained in the present study.

References

1. W. H. Bragg, *Philos. Mag*., **30**:305-315 (1915)
2. S. Nishikawa, *Proc. Math. Phys. Soc. Tokyo*, **8**:199-209 (1915)
3. J. B. Goodenough, L. a. Loeb, *Phys. Rev*., **98**:391-408 (1955)
4. J. D. Dunitz, E. L. Orgel, *J. Phys. Chem. Solids*, **3**:20-29 (1957)
5. N. W. Grimes, J. A. Collett, *Phys. Status Solidi (B)*, **43**:591-599 (1971)
6. H. J. Roderick, C. R. James, and G.V. Gibbs, *Phys. Chem. Minerals*, **4**, 317-339 (1979)
7. K.W. White and G.P. Kelkar, *J. Am. Ceram. Soc.*, **74**:1732 (1991)
8. R. M. Cornell, U. Schwertmann, *The Iron Oxides: Structure, Properties, Reactions, Occurrence and Uses*; VCH: New York, 28-29 (1996)
9. E. J. W. Verwey, *Nature* **144**:327-328 (1939)
10. J. M. D. Coey, A. E. Berkowitz, L. I. Balcells, F. F. Putris, F. T. Parker, *Appl. Phys. Lett*., **72**:734-736. (1998)
11. S. Soeya, J. Hayakawa, H. Takahashi, K. Ito, C. Yamamoto, A. Kida, H. Asano, M. Matsui, *Appl. Phys. Lett*., **80**:823-825 (2002)
12. S. Kimura, M. Hagiwara, K. Aoba, *In: Spinels: Occurences, Physical Properties and Applications*, Editors: Lucien Maigny and Mathis Dupont, 2013 Nova Science Publishers, Inc. 115-132 (2013)
13. J. Zhong, H.H. Bau, *Am. Ceram. Soc. Bull*., **80**:39-42 (2001).
14. A.H. Feingold, R.L. Wahlers, P. Amstutz, C. Huang, S.J. Stein, J. Mazzochette, *Microwave J*., **1**:90-98 (2000).
15. W. Qu, *Meas. Sci. Technol.*, **11**:1111-1118 (2000).
16. N.W. White, J.D. Turner, *Meas. Sci. Technol.*, **8**:1-4 (1997).
17. A. Dziedzic, *Meas. Sci. Technol.*, **8**:78-81 (1997).
18. I. Hadzaman, H. Klym, O. Shpotuyk, and M. Brunner, *Acta Physica Polonica A*, **117**:234-237 (2010)
19. R. Metz, *J. Mater. Sci*., **35**:4705-4711 (2000)
20. Feingold AH, Wahlers RL, Amstutz P, Huang C, Stein SJ, Mazzochette J. *Microw J*., **9**:90–98 (2000)
21. H. Klym, I. Hadzaman, O. Shpotyuk and M. Brunner, *Nanoscale Res Lett*., **9**:149-154 (2014)
22. B. Scrosati, *Nature*, **373**:557-558 (1995).
23. S.-Y. Chung, J.T. Bloking, Y.-M. Chiang, *Nat. Matter.*, **1**:123-128 (2002).
24. M.S. Whittingham, *Chem. Rev*., **104**:4271-4302 (2004).
25. K. Kang, Y.S. Meng, J. Berger, C.P. Grey, G. Ceder, *Science*, **311**:977-980 (2006).

26. N.-S. Choi, Z. Chen, S.A. Freunberger, X. Ji, Y.-K. Sun, K. Amine, G.Yushin, L.F. Nazar, J. Cho, P.G. Bruce, *Angew. Chem. Int. Ed*., **51**:9994-10024 (2012).
27. B. Dunn, H. Kamath, J.-M. Tarascon, *Science*, **334**:928-935 (2011).
28. H.-W. Lee, P. Muralidharan, R.Ruffo, C.M. Mari, Y. Cui, D.K.Kim, *Nano Lett*., **10**:3852-3856 (2010).
29. L. Binet, D. Gourier, C. Minot, *J. Solid State Chem*., **113**:420-433 (1994)
30. S. Sharma, M. K. Sunkara, *J. Am. Chem. Soc*., **124**:12288-12293 (2002)
31. R. Roy, V. G. Hill, E. F. Osborn, *J. Am. Chem. Soc*., **74**:719-722 (1952)
32. M. Zinkevicha, F. M. Moralesa, H. Nitschea, M. Ahrensb, M. Rühlea and F. Aldingera, *Zeitschrift für Metallkunde*, **95**:756-762 (2004)
33. A. C. Tas, P. J. Majewski, F. Aldinger, *J. Am. Ceram. Soc*., **85**:1421-1429 (2002)
34. K. Nakagawa, C. Kajita, K. Okumura, N. O. Ikenaga, M. Nishitani-Gamo, T. Ando, T. Kobayashi, T. Suzuki, *J. Catal*., **203**:87-93 (2001)
35. A. L. Peter, A. Auroux, P. Gelin, M. Caldarau, N. I. Ionescu. *Therm. Acta*., **379**:177-185 (2001)
36. T. Miyata, T. Nakatani, T. Minami, *Thin Solid Films*, **373**:145-149 (2000)
37. T. Weh, J. Frank, M. Fleischer, H. Meixner, *Sens. Actuators B*, **78**:202-207 (2001)
38. N. Ueda, H. Hosono, R. Waseda, H. Kawazoe, *Appl. Phys. Lett*., **70**:3561-3563 (1997)
39. T. Minami, *MRS Bull*., **25**:38-44 (2000)
40. A. F. Wells, *Structural Inorganic Chemistry*, Oxford University Press, London, 489 (1975)
41. L. E. Shea, R. K. Datta, J. J., Jr. Brown, *J. Electrochem. Soc*., **141**:1950-1954 (1994)
42. T. Omata, N. Ueda, K. Ueda, H. Kawazoe, *Appl. Phys. Lett*., **64**:1077-1078 (1994)
43. J. G. Kho, H. D. Park, D. P. Kim, *Bull, Korean. Chem. Soc*., **20**:1035-1039 (1999)
44. P. D. Rack, J. J. Peterson, M. D. Potter, W. Park, *J.Mater. Res*., **16**:1429-1433 (2001)
45. Z. Xu, Y. Li, Z. Liu, D. Wang, *J. Alloys Comp*., **391**:202-205 (2005)
46. T. Minami, Y. Kuroi, S. Takata, *J. Vac. Sci. Technol. A*, **14**:1736-1740 (1996)
47. S. Itoh, H. Toki, Y. Sato, K. Morimoto T. Kishino, *J. Electrochem. Soc*., **138**:1509-1512 (1991)
48. T. K. Tran, W. Park, J. W. Tomm, B. K. Wagner, S. M. Jacobsen, C. J. Summers, P. N. Yocom, S. K. McClelland, *J. Appl. Phys*., **78**:5691-5695 (1995)
49. J. S. Kim, S. G. Lee, H. L. Park, J. Y. Park, S. D. Han, *Mater. Lett*., **58**:1354-1357 (2004)
50. H. Matsui, C. N. Xu, H. Tateyama, *Appl. Phys. Let*t., **78**:1068-1070 (2001)
51. E. Martinez-Sanchez, M. Garcia-Hipolito, J. Guzman, F. Ramos-Brito, J. Santoyo Salazar, R. Martinez-Martinez, O. Alvarez-Fregoso, M. I. Ramos-Cortes, J. J. Mendez-Delgado, C. Falcony, *Phys. Status Solidi A*, **202**:102-107 (2005)
52. Z. Lou, J. Hao, *Appl. Phys. A: Mater. Sci. Process*., **80**:151-154 (2005)
53. A. R. Phani, M. Passacantando, S. Santucci, *Mater. Chem. Phys*., **68**:66-71 (2001)
54. S. K. Sampsth, J. F. Cordaro, *J. Am. Ceram. Soc*., **81**:649-654 (1998)

55. X. Li, Z. Zhu, Q. Zhao, L. Wang, *J. Hazardous Mater*., **186**:2089-2096 (2011)
56. T. K. Shioyama, *U. S. Patent*, 4,260,845 (1981).
57. G. Aquilar-Rios, M. Valenzuela, P. Salas, H. Armendariz, P. Bosch, G. Del Toro, R. Sila, V. Bertin, S. Castillo, A. I. Schifter, *Appl. Catal. A: General*, **127**:65-75 (1995)
58. T. El-Nabarany, A. A. Attia, M. N. Alayn, Matter. Lett., **24**:319-325 (1995)
59. R. Roesky, J. Weiguny, H. Bestgen, U. Dingerdissen, *Appl. Catal. A: General*, **176**:213-220 (1999)

Chapter 2

Hydrothermal synthesis of γ-Ga_2O_3 nanocrystals

2-1 Introduction

Over the past decade, synthesis of nanocrystalline inorganic materials has been of great interest and many new nanostructured materials have been developed [1-4]. In general, their synthesis techniques and procedures have many effects on their microstructure and performances. Recently, aqueous solution routes as one of building up processes of inorganic materials have received intensive attention from the environmental viewpoint [5-7]. Among them, the interest in hydrothermal synthesis techniques has increased in view of their advantage in direct formation of nanocrystalline inorganic materials because their crystal structure, phase homogeneity, composition, particle size, morphology, etc. can be well controlled and designed, and various kinds of nanocrystals have been hydrothermally synthesized [8].

Gallium oxide (gallia, Ga_2O_3) is well known as an important functional material such as wide-band gap oxide semiconductor. Normally, it is a semiconductor above 800 °C though an insulator at room temperature with a forbidden energy gap of 4.9 eV [9,10]. Similar to aluminum oxide (alumina, Al_2O_3), Ga_2O_3 shows five different polymorphs: α, β, γ, δ, and ε [11]. It has been investigated for use in catalysis [12-14], phosphors [12, 15], gas sensors [16], and transparent conducting oxide [17]. The most stable crystalline modification of gallia is monoclinic β-Ga_2O_3 having a melting point of 1740 °C, which exhibits blue luminescence [18] and has potential applications in optoelectronic devices and stable gas sensors [19,20]. The metastable γ-Ga_2O_3 has defective-spinel-type structure. The γ-Ga_2O_3 and/or its mixed oxide powders have been synthesized via pulsed-laser deposition technique [21], calcination of gels [22], solvolysis of $GaCl_3$ in N, N-dimethylformamide [23], solvothermal technique [24], hydrothermal method [25], and coprecipitation technique [26]. Recently, some studies have been reported on the formation of γ-Ga_2O_3 via epitaxial stabilization [27] and combustion synthesis using urea as fuel [28]. Colloidal γ-Ga_2O_3 particles were also formed through synthesis route from gallium acetylacetonate using oleylamine at 200-310 °C [29,30]. A few studies have been reported on the metastable γ-phase because of the difficulty in synthesis of single crystalline phase in stark contrast to the β-Ga_2O_3. However, the studies and reports on the hydrothermal synthesis of γ-Ga_2O_3 nanoparticles with a single phase of spinel-type structure from aqueous precursor solutions using the starting materials of simple inorganic gallium salts are especially very few. We have performed the investigations on the formation of nanocrystals

of a single phase of zinc gallate and its solid solutions [31,32] having spinel-type structure similar to γ-Ga_2O_3 via simple aqueous solution route at low temperatures below 90 °C [33,34] or hydrothermal routes [35,36].

The aim of this study is to prepare luminescent γ-Ga_2O_3 nanocrystals from the aqueous precursor solutions of inorganic gallium salts via hydrothermal route using citric acid. The effects of hydrothermal treatment temperature and post-heat treatment in air on the crystallinity, phase stability, and photoluminescence properties of spinel-type γ-Ga_2O_3 nanocrystals were investigated.

2-2 Experimental

2-2-1 Sample preparation

In a Teflon container, reagent-grade $Ga(NO_3)_3$ or $Ga_2(SO_4)_3$ and citric acid $C_3H_4(OH)(COOH)_3 \cdot H_2O$ as starting materials were dissolved in distilled water. The pH of the solution was controlled by the addition of aqueous ammonia to have a weakly basic condition in the end stage of hydrothermal treatment. This precursor solution mixture with 0.40 mol/dm^3 Ga^{3+} concentration in the Teflon container was then placed in a stainless-steel vessel. The vessel was tightly sealed, and it was heated at 180-240 °C for 5 h under rotation at 1.5 rpm. After hydrothermal treatment, the precipitates were washed with distilled water until the pH value of the rinsed water became 7.0, separated from the solution by centrifugation, and dried in an oven at 60 °C. The prepared powders were heated in an alumina crucible at a heating rate 200 °C/h, held at 600-1000 °C for 1 h in air, and then cooled to room temperature in a furnace.

2-2-2 Characterization

X-ray diffraction (XRD) patterns of the as-prepared and heat-treated powders were recorded on a diffractometer (XRD; model RINT-2000, Rigaku, Tokyo, Japan) using CuKα radiation. The microstructure and morphology of the as-prepared samples were observed using transmission electron microscopy (TEM) and selected area electron diffraction (SAED) (TEM; model JEM-2010, JEOL, Tokyo, Japan). The crystallite size of cubic phase was evaluated from the line broadening of 311 diffraction peak, according to the Scherrer equation, $D_{XRD} = K\lambda / \beta \cos\theta$, where θ is the Bragg angle of diffraction lines, K is a shape factor ($K = 0.9$ in this work), λ is the wavelength of incident X-rays, and β is the corrected half-width given by $\beta^2 = \beta_m^2 - \beta_s^2$, where β_m is the measured half-width and β_s is the half-width of a standard sample.

The measurements of UV-Vis absorption spectra for these prepared powders were taken using an ultraviolet-visible spectrophotometer with an integrating sphere attachment (V-560, Nihon Bunko, Tokyo, Japan). The photoluminescence (PL) emission spectra of samples were

measured using a spectrofluorometer (F-2700, Hitachi High-Tech, Tokyo, Japan) with Xe lamp. Powder samples were excited with a 325 nm radiation from a 150-W xenon lamp. The emission wavelength was scanned from 350 to 750 nm at a scanning rate of 60 nm/min.

2-3 Results and discussion

2-3-1 Synthesis of γ-gallium oxide nanocrystals

Hydrothermal treatment was carried out at 180 °C for 5h for the precursor solution mixtures of citric acid and $Ga(NO_3)_3$ or $Ga_2(SO_4)_3$ under weakly basic conditions in the presence of aqueous ammonia. The XRD patterns of precipitates hydrothermally treated at 180 °C and dried at 60 °C are shown in Fig. 1. Each of the precipitates was detected as a single phase of spinel-type γ-Ga_2O_3. The crystallinity of the spinel-type γ-Ga_2O_3 formed from the precursor solution of $Ga_2(SO_4)_3$ was slightly high because the XRD lines corresponding to the γ-Ga_2O_3 obtained from $Ga_2(SO_4)_3$ was sharper than those from $Ga(NO_3)_3$. It was found that the starting inorganic salt of gallium, i.e., anions of gallium salt had effect on the crystallinity of the spinel-type γ-Ga_2O_3.

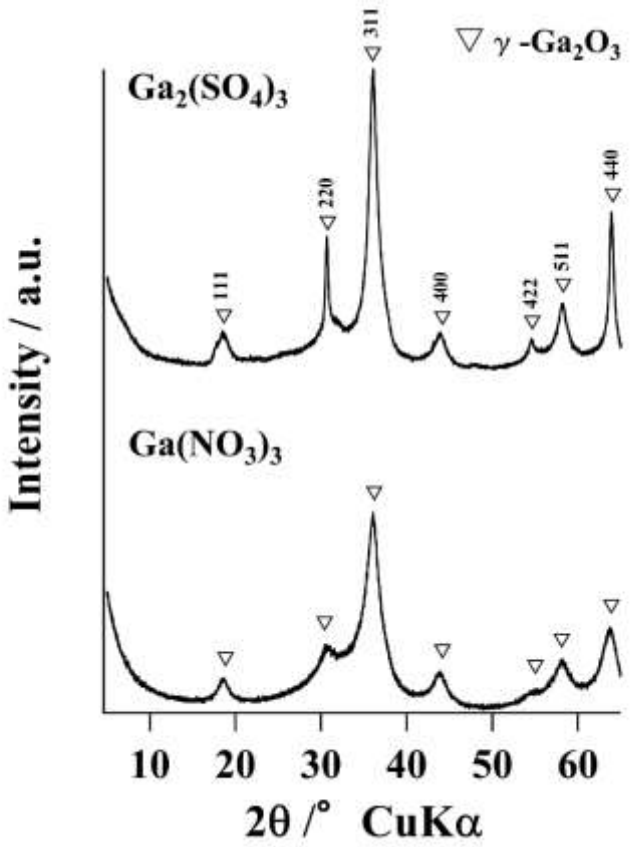

Fig.1 X-ray diffraction patterns of precipitates obtained from aqueous precursor solution of $Ga_2(SO_4)_3$ or $Ga(NO_3)_3$ using citric acid and aqueous ammonia under hydrothermal conditions at 180 °C for 5 h.

The effect of hydrothermal treatment temperature on the crystalline phase and crystallinity of solid products was investigated. The XRD patterns of precipitates that were obtained under weakly basic hydrothermal conditions at various temperatures and dried at 60 °C are shown in Fig. 2. All precipitates formed under these conditions were detected as a single-phase corresponding to spinel-type γ-Ga_2O_3. The XRD lines of the γ-Ga_2O_3 gradually became sharper as the hydrothermal treatment temperature rose. The crystallite size of the spinel-type γ-Ga_2O_3 is plotted against the hydrothermal treatment temperature in Fig. 3. The crystallite size of the γ-Ga_2O_3 spinel gradually grew from 5 to 9 nm when the hydrothermal treatment temperature rose from 180 to 240 °C. The crystallite size of the spinel in this study was in the dimension range as semiconductor quantum dots. Under these hydrothermal conditions, it was confirmed that a single-phase of spinel-type γ-Ga_2O_3 was formed as nanosized crystals.

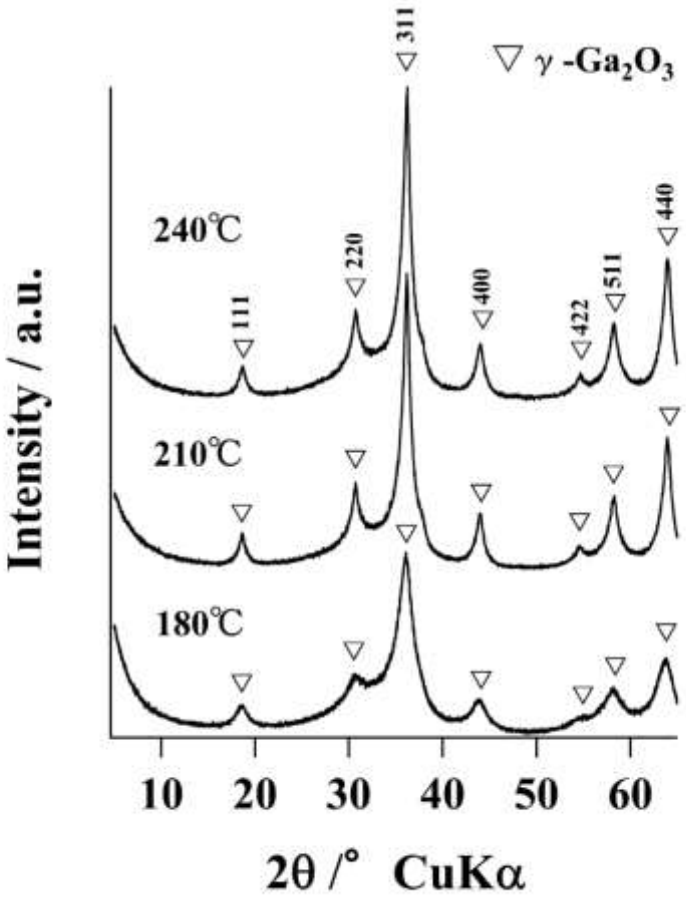

Fig.2 X-ray diffraction patterns of precipitates obtained from aqueous precursor solutions of $Ga(NO_3)_3$ using citric acid and aqueous ammonia under hydrothermal conditions at various temperatures for 5 h.

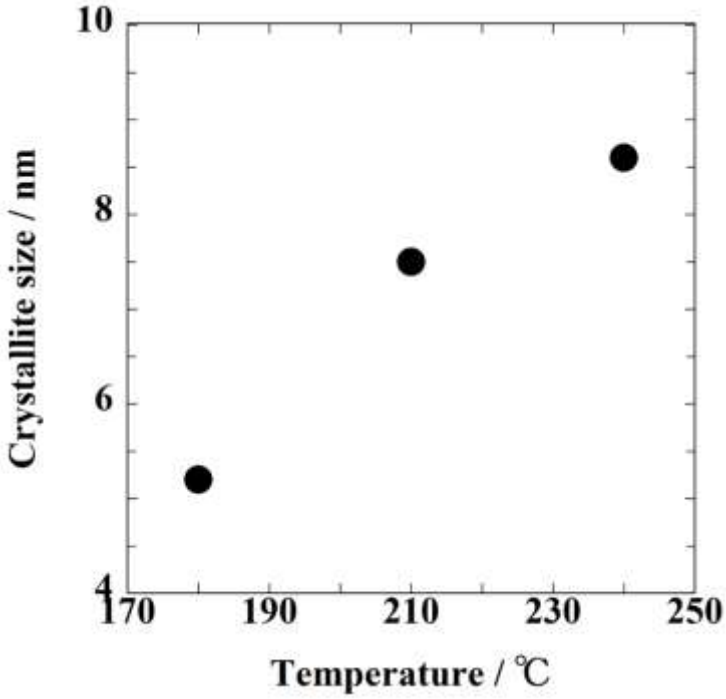

Fig.3 Crystallite size of as-prepared spinel-type γ-Ga_2O_3 precipitates against the hydrothermal treatment temperature.

When citric acid was not present in these weakly basic precursor solutions, a single phase of GaO(OH) was only formed after hydrothermal treatment. These results obtained in this study suggest that the presence of citric acid has a very important effect on the direct formation of a single phase of spinel-type γ-Ga_2O_3 nanocrystals as follows. In the weakly basic precursor solution in the presence of aqueous ammonia without citric acid, GaO(OH) phase with good crystallinity is apt to easily form at low temperatures such as room temperature. Once GaO(OH) crystals are formed in the precursor solution, the formation of the nuclei of spinel-type γ-Ga_2O_3 phase and their growth are considered not to be easy even though the solution is treated under hydrothermal conditions at elevated temperatures. From this reason, to inhibit the formation of GaO(OH) phase at low temperatures, citric acid was used and useful as chelating ligand. On the other hand, no precipitate was formed in the precursor solution containing citric acid as ligand after hydrothermal treatment at temperatures <120 °C. This fact shows that the gallium complex compound that is formed in the precursor solution using citric acid as chelating ligand is stably present under hydrothermal conditions <120 °C. It is supposed that the gallium complex compound will collapse under hydrothermal conditions at elevated temperatures higher than 120 °C. The formation of the nuclei of spinel-type γ-Ga_2O_3 and their growth are considered to be achieved via the collapse of the gallium complex compound at higher temperatures than 120 °C under weakly basic hydrothermal conditions.

The TEM image of dispersed γ-Ga_2O_3 precipitates and the TEM image with SAED pattern of aggregated γ-Ga_2O_3 precipitates, both of which were formed from the precursor solution of $Ga(NO_3)_3$ at 180 °C for 5 h, are shown in Fig. 4a, b, respectively. Both of the dispersed γ-Ga_2O_3 precipitates and aggregated γ-Ga_2O_3 precipitates were observed in the TEM images in the present study. In the TEM image of Fig. 4a, isolated nanosized particles in the range of 3~5 nm with roundish morphology exist. On the other hand, the aggregated precipitates consist of nanosized fine particles around 4~5 nm as shown in the TEM image in Fig. 4b. The SAED analysis suggests that the γ-Ga_2O_3 nanoparticles possess relatively good crystallinity and that the precipitates formed at 180 °C also contain amorphous-like phase with low crystallinity to a small degree. In the TEM image (b), fine particles seem to be piled up and gathered, but this aggregation may be considered to occur through the process of the preparation of the TEM sample due to the very fine size of particles and the presence of the amorphous-like phase with low crystallinity. As the particle size observed in the TEM images relatively well corresponded to the crystallite size evaluated from XRD line broadening, the observed γ-Ga_2O_3 fine particles are considered to be single crystals.

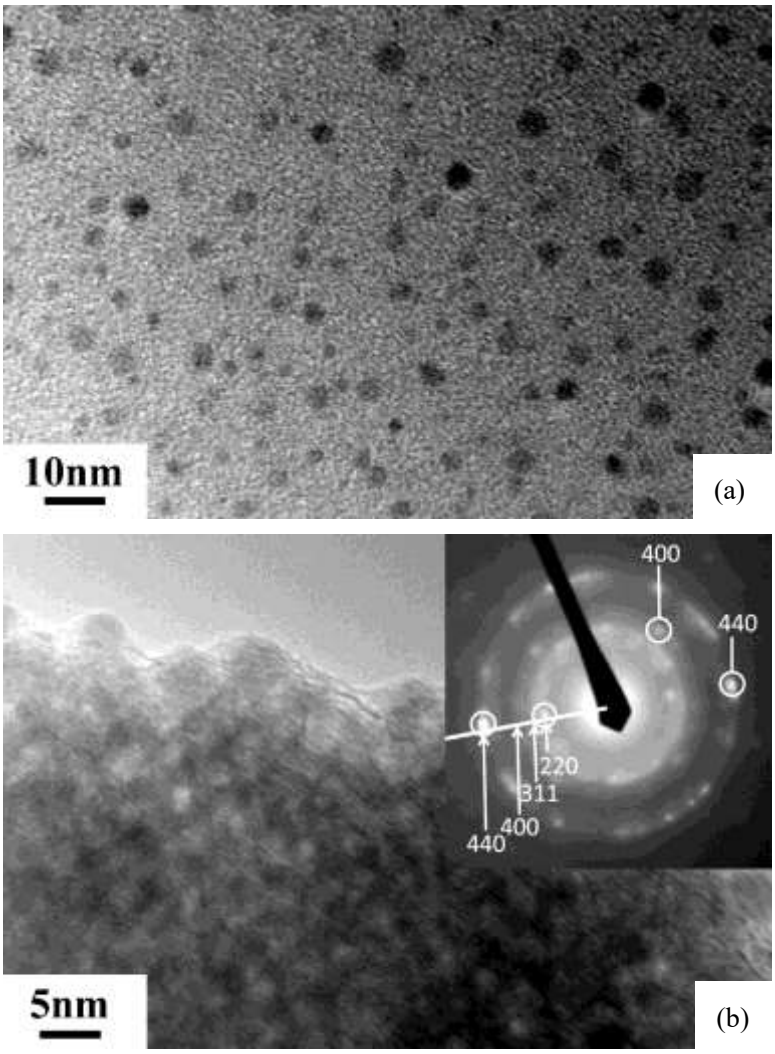

Fig.4 TEM image of (a) dispersed γ-Ga_2O_3 precipitates and (b) TEM image with SAED pattern of aggregated γ-Ga_2O_3 precipitates, both of which were obtained from aqueous precursor solutions of $Ga(NO_3)_3$ using citric acid under hydrothermal conditions at 180 °C for 5 h

2-3-2 Photoluminescence and phase transformation of γ-gallium oxide

The UV-Vis absorption spectra of the as-prepared γ-Ga_2O_3 spinel nanocrystals were measured. The plots of transformed Kubelka–Munk function versus the energy of light absorbed of the samples are shown in Fig. 5. The optical band gaps exhibited the tendency of dependence on the nanocrystal size, because the absorption edge in the spectra tended to slightly shift into shorter wavelengths as the hydrothermal treatment temperature fell, accordingly, the optical band gap of as-prepared γ-Ga_2O_3 spinel nanocrystals with smaller crystallite tended to

become slightly wider. The optical band gap value evaluated from the spectra measured for the γ-Ga_2O_3 spinel nanocrystals formed at 180 °C was 4.88 eV. But large absorptions in the visible region are observed in the as-prepared γ-Ga_2O_3 spinel nanocrystals formed at 210 and 240 °C, which is considered to be due to the residual impurities originating from the hydrothermal decomposition of citric acid in the starting materials.

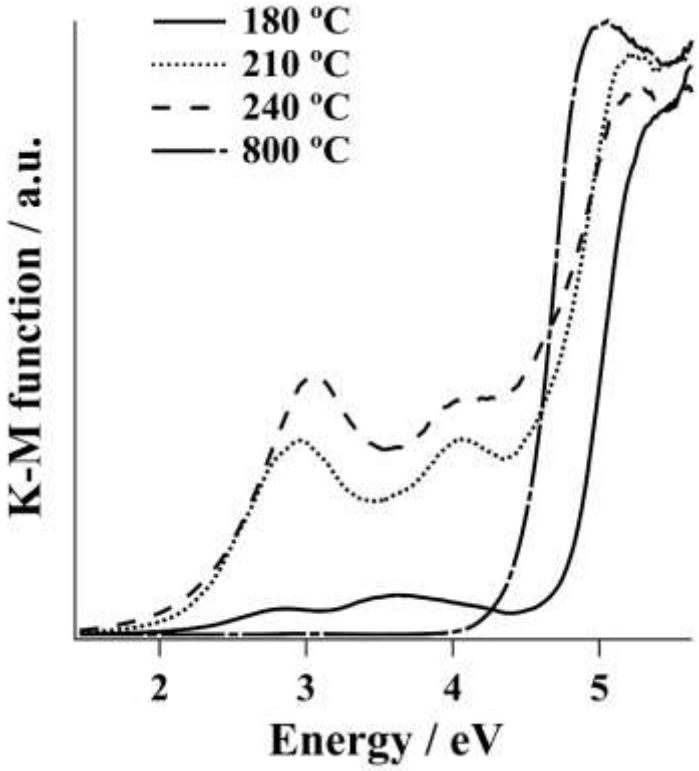

Fig.5 Plots of transformed Kubelka–Munk function versus the energy of light absorbed of γ-Ga_2O_3 formed at 180, 210, and 240 °C for 5 h and β-Ga_2O_3 formed after heating at 800 °C.

The photoluminescence spectra of the as-prepared γ-Ga_2O_3 spinel formed at various hydrothermal treatment temperatures that were measured under excitation at 325 nm at room temperature, are shown in Fig. 6. The γ-Ga_2O_3 spinel nanocrystals show a violet-blue, broad-band emission with a peak wavelength at 410 nm, centered at around 425 nm under excitation at 325 nm. The γ-Ga_2O_3 spinel nanocrystals formed at 180 °C presented the highest intensity of emission. The emission intensity decreased as hydrothermal treatment temperature rose, which is supposed to be due to the residual impurities that may act as luminescent quenchers included in the samples formed at 210 and 240 °C as observed in Fig. 5. It has been reported that the UV-blue emission of spinel oxide phosphors such as $ZnGa_2O_4$ and $ZnAl_2O_4$ similar to γ-Ga_2O_3 spinel originates from charge transfer between Ga^{3+} or Al^{3+} at octahedral sites and its

surrounding O^{2-} and it is due to inter-band gap defects, such as oxygen vacancies [37–39]. In general, the blue band emission around 430 nm from the self-activation center of Ga-O groups is observed in bulk $ZnGa_2O_4$ phosphors [39]. The observed luminescence spectrum centered at around 425 nm in these γ-Ga_2O_3 spinel nanocrystals is considered to be the characteristic vaiolet-blue band emission from the self-activation center of Ga-O groups.

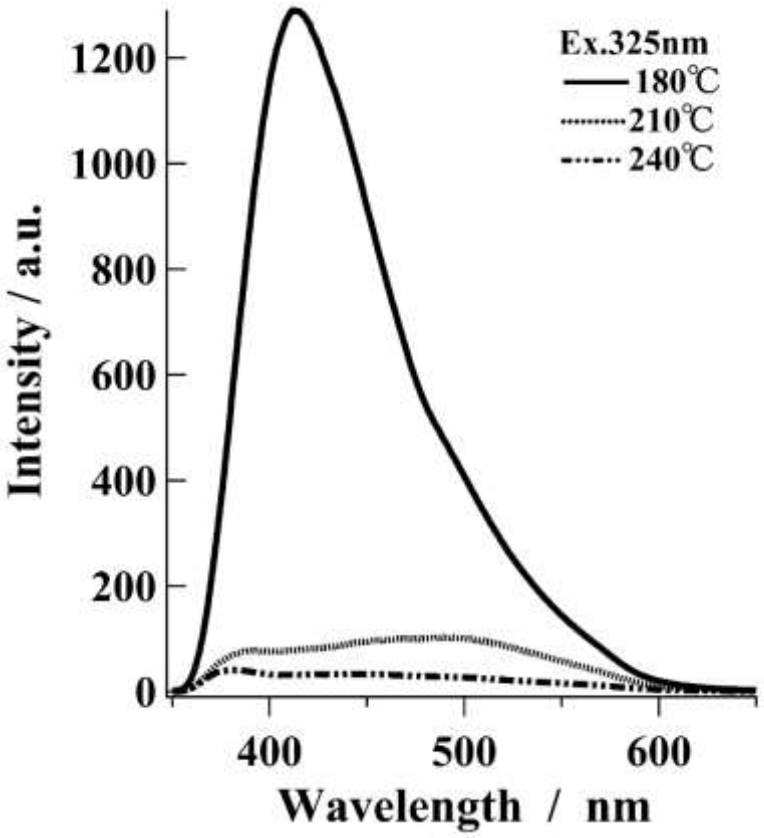

Fig.6 Emission spectra of γ-Ga_2O_3 precipitates obtained from aqueous precursor solutions of $Ga(NO_3)_3$ using citric acid under hydrothermal conditions at various temperatures for 5 h that were measured under excitation at 325 nm.

The effect of heat treatment temperature in air on the crystalline phase of γ-Ga_2O_3 spinel was investigated. Figure 7 shows XRD patterns before and after heating at 600, 800, and 1000 °C in air for the γ-Ga_2O_3 spinel sample formed under hydrothermal condition at 180 °C for 5 h. The crystalline phase detected in the as-prepared and heat treated samples at 600 °C was a single phase of γ-Ga_2O_3 spinel structure. The fact that the remarkable change in the crystallinity and the crystallite size of the spinel was not observed in the samples after heat treatment at temperatures lower than 600 °C 1 h shows that the formed γ-Ga_2O_3 spinel under hydrothermal

condition has relatively high thermal stability. However, the symptom of the appearance of β-Ga_2O_3 phase in the γ-Ga_2O_3 nanocrystals is slightly observed at the area of 2θ=30-40 ° marked with arrow in the XRD pattern of the sample heat-treated at 600 °C in Fig. 7. Since the XRD pattern of Ga_2O_3 after heat-treated at 800 °C shows a single phase of β-type structure, it is obvious that the γ-β phase transformation proceeded at the temperatures above 600 °C and concluded below 800 °C. The crystallite growth of β-Ga_2O_3 phase is observed in the sample heat-treated at 1000 °C.

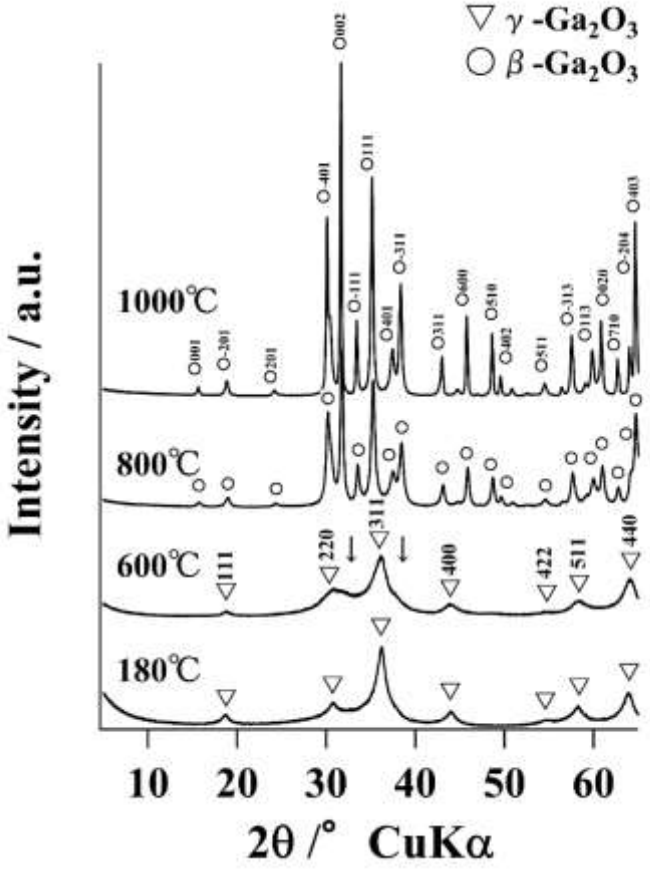

Fig.7 X-ray diffraction patterns of samples obtained from aqueous precursor solutions of $Ga(NO_3)_3$ using citric acid under hydrothermal conditions at 180 °C for 5 h before and after heating at 600~1000 °C for 1 h in air.

The plot of transformed Kubelka–Munk function versus the energy of light absorbed of β-Ga_2O_3 formed after heating at 800 °C is also shown in Fig. 5. The optical band gap value evaluated from the diffuse reflectance spectrum measured for the β-Ga_2O_3 was 4.51 eV. The change in the emission spectra of Ga_2O_3 is shown in Fig. 8. The luminescence intensity and the center wavelength of the emission are plotted against heat treatment temperature in Fig. 9a, b, respectively. The intensity of the emission decreases as the heat treatment temperature rises. The peak wavelength of the emission also shifts into lower wavelengths with an increase in heating temperature. In the present study, the as-prepared γ-Ga_2O_3 nanocrystals formed at 180 °C exhibited the emission with the highest intensity.

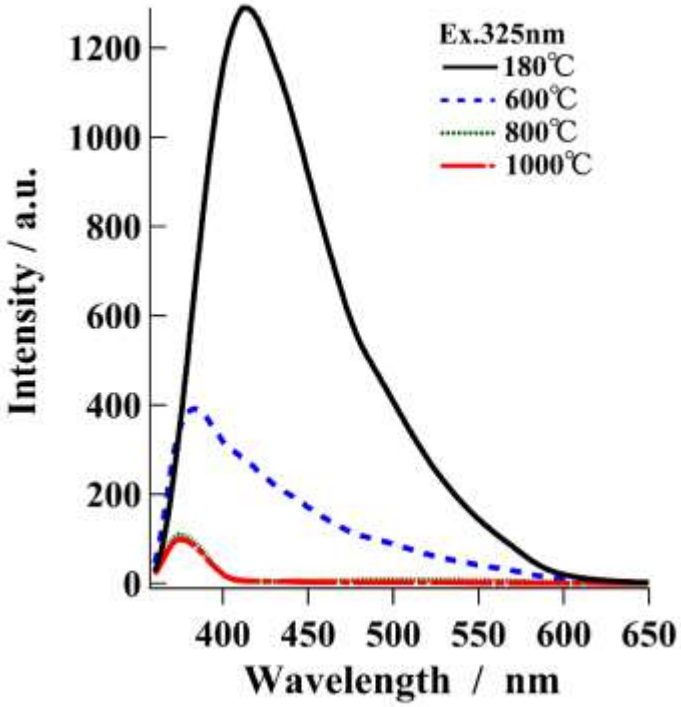

Fig.8 Emission spectra of Ga_2O_3 samples before and after heating at 600-1000 °C for 1 h in air that were measured under excitation at 325 nm.

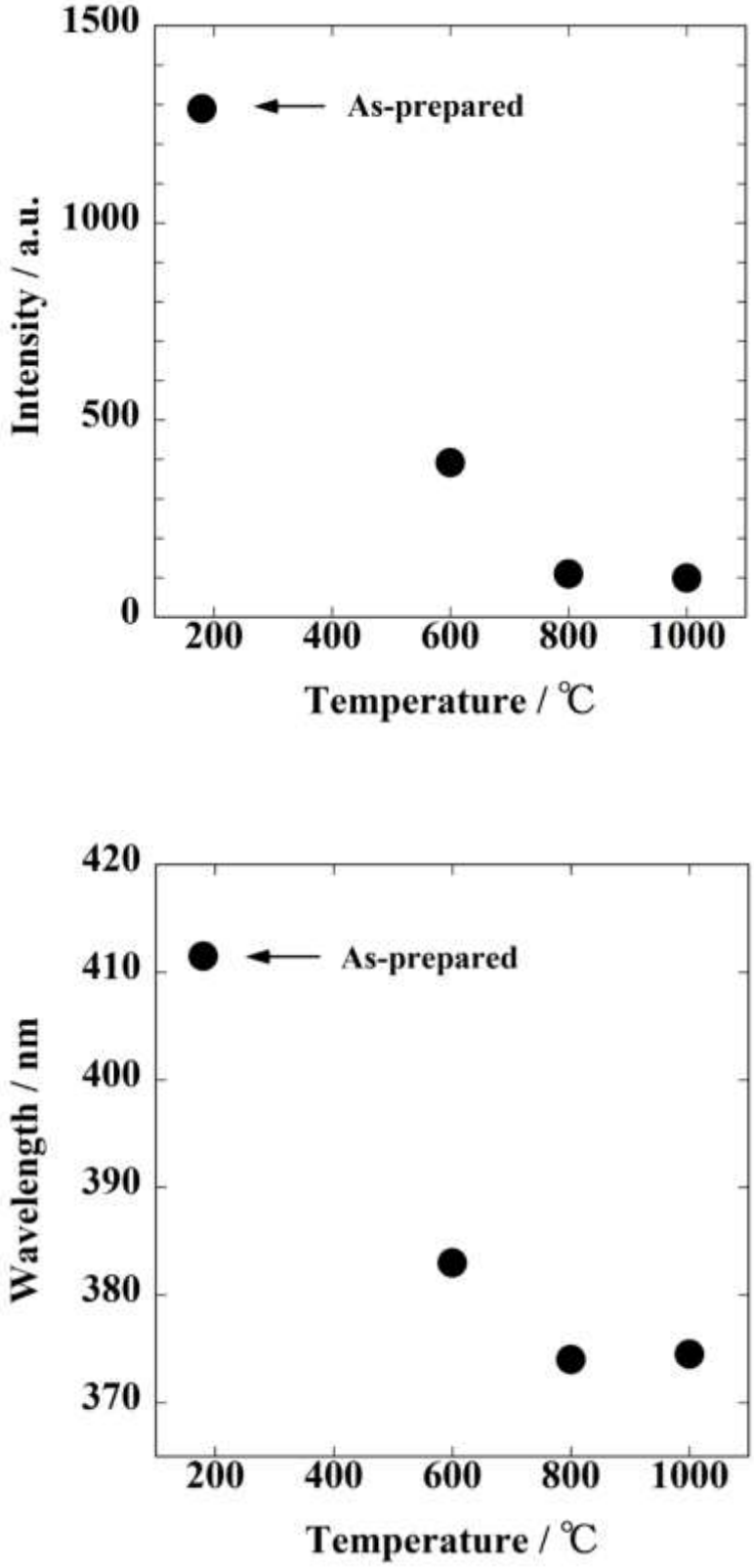

Fig.9 (a) intensity and (b) wavelength of the center of the broad band emission of Ga_2O_3 samples plotted against heat-treatment temperature.

2-4 Summary

A single-phase of spinel-type γ-Ga_2O_3 nanocrystals was directly synthesized from the aqueous precursor solution of $Ga(NO_3)_3$ or $Ga_2(SO_4)_3$ under weakly basic hydrothermal conditions at 180-240 °C in the presence of aqueous ammonia by inhibiting the formation of GaO(OH) phase using citric acid. The crystallite size of γ-Ga_2O_3 spinel was 5-9 nm. The γ-Ga_2O_3 spinel nanocrystals formed at 180 °C had the optical band gap of 4.88 eV and showed the highest intensity of broad-band visible violet-blue light emission centered at 425 nm under excitation at 325 nm. The phase transformation from γ-Ga_2O_3 to β-Ga_2O_3 was suggested to occur at elevated temperatures higher than 600 °C because the spinel phase was maintained after heating at 600 °C for 1 h. By the heat treatment in air, the emission intensity of Ga_2O_3 decreased and the center wavelength of the broad-band emission shifted into lower wavelengths.

References

1. P. Moriarty, *Rep Prog Phys,* **64**:297-381, (2001)
2. S. Mark Gudiksen, J. Lincoln Lauhon, Jlanfang Wang, C. David Smith, M. Charles Lieber, *Nature*, **415**:617-620, (2002)
3. H. A. Lu, L. E. Salabas, F. Schueth, *Angew Chem Int Ed*, **46**:1222-1244, (2007)
4. B. A. Djurisic, H. Y. Leung , *Small*, **2**:944-961, (2006)
5. V. D. Talapin, S. J. Lee, V. M. Kovalenko, V. E. Shevchenko, *Chem Rev*, **110**:389-45, (2010)
6. J. W. Dawson, *Am Ceram Soc Bull,* **67**:1673-1678, (1988)
7. M. Hirano, E. Kato, *J Ceram Soc Japan*, **104**:958-962, (1996)
8. M. Hirano, H. Morikawa, M. Inagaki, M. Toyoda, *J. Am Ceram Soc*, **85**:1915-1920, (2002)
9. L. Binet, D. Gourier, C. Minot, *J Solid State Chem*, **113**:420-433, (1994)
10. S. Sharma, K. M. Sunkara, *J Am Chem Soc*, **124**:12288-12293, (2002)
11. R. Roy, G. V. Hill, F. E. Osborn, *J Am Chem Soc*, **74**:719-722, (1952)
12. C. A. Tas, J. P. Majewski, F. Aldinger, *J Am Ceram Soc*, **85**:1421-1429, (2002)
13. K. Nakagawa, C. Kajita, K. Okumura, N. Ikenaga O. Nishitani, M. Gamo, T. Ando, T. Kobayashi, T. Suzuki, *J Catal*, **203**:87-93, (2001)
14. L. A. Peter, A. Auroux, P. Gelin, M. Caldarau, I. N. Ionescu, *Therm Acta*, **379**:177-185, (2001)
15. T. Miyata, T. Nakatani, T. Minami, *Thin Solid Films*, **373**:145-149, (2000)
16. T. Weh, J. Frank, M. Fleischer, H. Meixner, *Sens Actuators B*, **78**:202-207, (2001)
17. N. Ueda, H. Hosono, R. Waseda, H. Kawazoe, *Appl Phys Lett*, **70**:3561-3563, (1997)
18. L. Binet, D. Gourier, *J Phys Chem Solids*, **59**:1241-1249, (1998)
19. D. D. Edwards, O. T. Mason, F. Goutenoir, R. K. Poeppelmeier, *Appl Phys Lett*, **70**:1706-1708, (1997)

20. M. Ogita, K. Higo, Y. Nakanishi, Y. Hatanaka, *Appl Surf Sci*, **175-176**:721-725, (2001)
21. H. Hayashi, R. Huang, H. Ikeno, F. Oba, S. Yoshioka, I. Tanaka, S. Sonoda, *Appl Phys Lett*, **89**:181903/1-181903/3, (2006)
22. O. C. Arean, R. M. Delgado, V. Montouillout, D. Massiot, *Z Anorg Allg Chem*, **631**:2121-2126, (2005)
23. T. Chen, K. Tang, *Appl Phys Lett*, **90**:053104-1-053104-3, (2007)
24. M. Takahashi, T. Nakatani, S. Iwamoto, T. Watanabe, M. Inoue, *J Phys Cond Matter*, **18**:5745-5757, (2006)
25. K. Pohl, *Naturwissenschaften*, **55**:82-82, (1968)
26. M. Chen, J. Xu, Z. F. Su, M. Y. Liu, Y. Cao, Y. H. He, N. K. Fan, *J Catal*, **256**:293-300, (2008)
27. T. Oshima, T. Nakazono, A. Mukai, A. Ohtomo, *J Cryst Growth*, **359**:60-63, (2012)
28. V. Srihari, V. Sridharan, K. H. Sahu, G. Raghavan, S. V. Sastry, S. C. Sundar, *J Mater Sci*, **44**:671-675, (2009)
29. T. Wang, S. S. Farvid, A. Mutalifu, V. P. Radovanovic, *J Am Chem Soc*, **132**:9250-9250, (2010)
30. T. Wang, V. P. Radovanovic, *Chem Commun*, **47**:7161-7163, (2011)
31. K. Sakoda, M. Hirano, *Ceram Intl*, **40**:15841-15848, (2014)
32. K. Sakoda, M. Hirano, *J Nanosci Nanotechnol*, **15**: 6069-6077, (2015)
33. M. Hirano, S. Okumura, Y. Hasegawa, M. Inagaki, *Int J Inorg Mater*, **3**:797-801, (2001)
34. M. Hirano, S. Okumura, Y. Hasegawa, M. Inagaki, *J Solid State Chem*, **168**:5-10, (2002)
35. M. Hirano, M. Imai, M. Inagaki, *J Am Ceram Soc*, **83**:977-979, (2000)
36. M. Hirano, N. Sakaida, *J Am Ceram Soc*, **85**:1145-1150, (2002)
37. K. I. Jeong, L. H. Park, *Mho S I*, **105**:179-183, (1998)
38. M. Cao, I. Djerdj, M. Antonietti, M. Niederberger, *Chem Mater*, **19**:5830-5832, (2007)
39. D. A. Silva, S. A. Goçalves, R. M. Davolos, *J Sol–Gel Sci Technol*, **49**:101-105, (2009)

Chapter 3

Direct formation of spinel-type γ-Ga_2O_3-Al_2O_3 nanoparticles

3-1 Introduction

Aluminum oxide (alumina, Al_2O_3) and gallium oxide (gallia, Ga_2O_3) have several similarities in structural and optical properties though alumina is a typical insulator. Similar to alumina, five distinctive polymorphs: α, β, γ, δ, and ε [1] exist in gallium oxide which is one of attractive transparent and wide band-gap semiconductor materials [2]. Above all, the β-type Ga_2O_3 which has monoclinic structure is most stable crystalline modification and has high melting temperature of 1740 °C. On the other hand, γ-type Ga_2O_3 with defective-spinel-type structure is one of metastable phases. In general, β-Ga_2O_3 is commonly formed and observed after firing at elevated temperatures. The α-Ga_2O_3 has corundum type similar to the representative crystal structure of alumina. Gallium oxide-based materials have attracted considerable attentions, and they have been applied for catalysts [3-6], gas sensors [7,8], phosphors [9], spintronics devices [10], and transparent electronic devices [11]. The studies on the formation and properties of gallium oxide-based materials have been conducted using various synthesis methods e.g., coprecipitation [12], solvolysis of $GaCl_3$ in N, N-dimethylformamide [13], pulsed-laser deposition technique [14], calcination of gels [15], hydrothermal method [16], solvothermal or glycothermal technique [17,18], and colloidal synthesis route [19,20]. The catalytic properties of copper-doped gallium oxide with spinel-type structure formed through microwave hydrothermal method have been reported, but its crystallinity was very low [21].

The hydrothermal synthesis, which falls into one of aqueous solution routes, is well known to be useful as low-temperature synthesis techniques of nanocrystalline inorganic materials, especially metal oxide-based materials since their crystalline phases, compositions, particle sizes, and morphologies can be well designed and controlled. The investigations on the formation and characteristics of nanocrystalline phases and solid solutions focused on the spinel-structured complex oxide similar to γ-Ga_2O_3 have been performed [22-25]. As one of oxide systems related to the spinel-type oxide solid solutions in the γ-Al_2O_3-γ-Ga_2O_3 system, similar spinel-structured solid solutions in the $ZnAl_2O_4$–$ZnGa_2O_4$ system have also been directly formed as nanocrystals via the mild hydrothermal method using tetramethylammonium hydroxide, and the compositional dependence of their structure and optical and luminescence properties has been investigated [26,27]

Compared with many literatures on the β-type Ga_2O_3, there are not so many reports relating

to the γ-type Ga_2O_3 due to the difficulty in synthesis of metastable γ-type crystalline phase at low temperatures. In addition, hydrothermal techniques have hardly been applied to the synthesis of γ-type spinel-structured nanocrystals in the Al_2O_3-Ga_2O_3 system. This study is probably the first approach to the direct formation of spinel-type γ-Ga_2O_3-based nanoparticles doped with Al_2O_3, $(Al_xGa_{1.00-x})_2O_3$ under mild hydrothermal conditions at around 180 °C in a short period of time. The purpose of the present study is to investigate and clarify the effect of the composition, hydrothermal treatment condition, and heat treatment in air on the crystalline phase, structure, phase transformation, and luminescence properties of the spinel-structured γ-Ga_2O_3-based nanoparticles doped with Al_2O_3 in the Al_2O_3-Ga_2O_3 system, which were directly formed from the aqueous precursor solutions of $Ga(NO_3)_3$ and $Al_2(SO_4)_3$ under weakly basic hydrothermal conditions using aqueous ammonia in the presence of citric acid.

3-2 Experimental

3-2-1 Preparation of samples

For the preparation of nanoparticles in the Al_2O_3-Ga_2O_3 system, reagent-grade $Ga(NO_3)_3$, $Al_2(SO_4)_3$, and citric acid: $C_3H_4(OH)(COOH)_3 \cdot H_2O$ were used as starting materials and dissolved into distilled water in a Teflon container. The composition of the precursor solutions was controlled to be $(Al_xGa_{1.00-x})_2O_3$, x=0-1.00. The pH of the solution was controlled by the addition of aqueous ammonia to have a weakly basic condition in the end stage of hydrothermal treatment. This precursor solution mixture with Ga^{3+}+Al^{3+} concentration of 0.40 mol/dm^3 in the Teflon container was then placed in a stainless-steel vessel. The vessel was tightly sealed and it was heated at 170-240 °C for 5 h under rotation at 1.5 rpm. After hydrothermal treatment, the precipitates were washed with distilled water until the pH value of the rinsed water became 7.0, separated from the solution by centrifugation, and dried in an oven at 60 °C. The prepared powders were heated in an alumina crucible at heating rate 200 °C/h, held at 600-1000 °C for 1 h in air, and then cooled to room temperature in a furnace.

3-2-2 Characterization of samples

The powder X-ray diffraction (XRD) measurements were performed at room temperature for the as-prepared and heat-treated powders using CuKα radiation (XRD; model RINT-2000, Rigaku, Tokyo, Japan). The morphology of the as-prepared samples was observed using transmission electron microscopy (TEM; model JEM-2010, JEOL, Tokyo, Japan). The crystallite size of the spinel phase was calculated from the line broadening of 311 diffraction peak, according to the Scherrer equation, $D_{XRD} = K\lambda / \beta\cos\theta$, where θ is the Bragg angle of diffraction lines; K is a shape factor (K = 0.9 in this work); λ is the wavelength of incident X-

rays, and β is the corrected half-width given by $\beta^2 = \beta_m^2 - \beta_s^2$, where β_m is the measured half-width and β_s is the half-width of a standard sample. The lattice parameter was measured using silicon as the internal standard. The specific surface area of the prepared samples was calculated from the adsorption isotherm of nitrogen at 77 K based on the Brunauer–Emmett–Teller method (BET, model; NOVA 1200, Yuasa Ionics, Osaka, Japan). The diffuse reflectance spectra measurements for powder samples have been made. The optical absorption of these prepared powders was measured using an ultraviolet-visible spectrophotometer (V-560, Nihon Bunko, Tokyo, Japan).

All luminescence measurements were performed at room temperature using a spectrofluorometer (F-2700, Hitachi High-Tech, Japan) with Xe lamp. Powder samples were excited with 325 nm radiation from a 150 W xenon lamp. The emission wavelength was scanned from 350 nm to 750 nm at a scanning rate of 60 nm/min.

3-3 Result and discussion

3-3-1 Synthesis of spinel type γ-Ga_2O_3-Al_2O_3 nanoparticles

To investigate the effect of the composition in the Al_2O_3-Ga_2O_3 system on the crystalline phase of precipitates, hydrothermal treatment at 180 °C for 5 h was conducted for the precursor solutions of $Ga(NO_3)_3$ and $Al_2(SO_4)_3$ with various compositions ($(Al_xGa_{1.00-x})_2O_3$, x=0-1.00) under weakly basic conditions using citric acid and aqueous ammonia. The XRD patterns of precipitates with various compositions after dried, which were obtained under hydrothermal conditions at 180 °C, are shown in Fig. 1. A single phase of boehmite, AlO(OH) was formed at the composition of pure Al_2O_3. Only a single phase corresponding to spinel-type cubic structure was detected in the precipitates with compositions except for x=Al=1.00, and no diffraction peaks due to another crystalline phase were detected. It is noted that a single phase of cubic spinel was appeared in the wide composition range ($(Al_xGa_{1.00-x})_2O_3$, x=0-0.85). In Fig.1, slight and gradual shifts of the XRD lines, e.g., shifts of the 440 diffraction line of the spinel phase are clearly observed with the change in the composition in the Al_2O_3-Ga_2O_3 system.

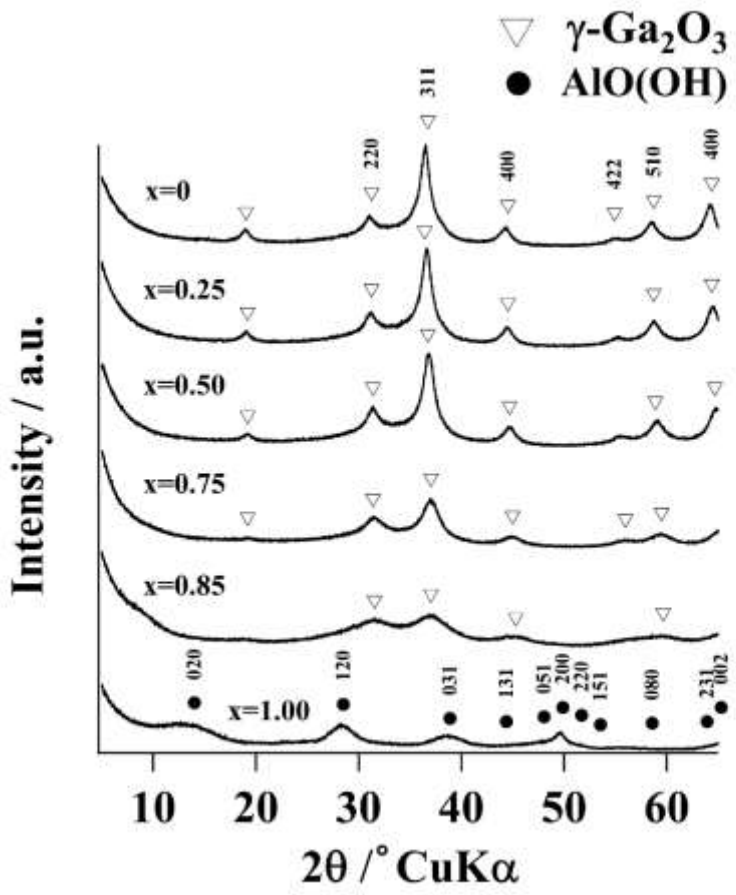

Fig.1 XRD patterns of precipitates obtained from aqueous precursor solutions with compositions of $(Al_xGa_{1.00-x})_2O_3$, x=0, 0.15, 0.25, 0.50, 0.75, and 1.00 under hydrothermal conditions at 180 °C for 5 h.

In Fig. 2, the change in the crystallite size of spinel phase, which is evaluated from the XRD line broadening, and the specific surface areas of as-prepared spinel-type precipitates in the Al_2O_3-Ga_2O_3 system are represented against the composition (Al/(Al+Ga) atomic ratio) of the samples. The crystallite size of the spinel phase of as-prepared samples was in the range of 4-5 nm, and it very slightly and gradually decreased with increased Al/(Al+Ga) atomic ratio. In contrast to the slight change in the crystallite size, the specific surface area of samples quite increased with increased Al/(Al+Ga) atomic ratio. This result implies that there is a possibility of the presence of substances with low crystallinity in the samples having the composition of high Al/(Al+Ga) atomic ratio.

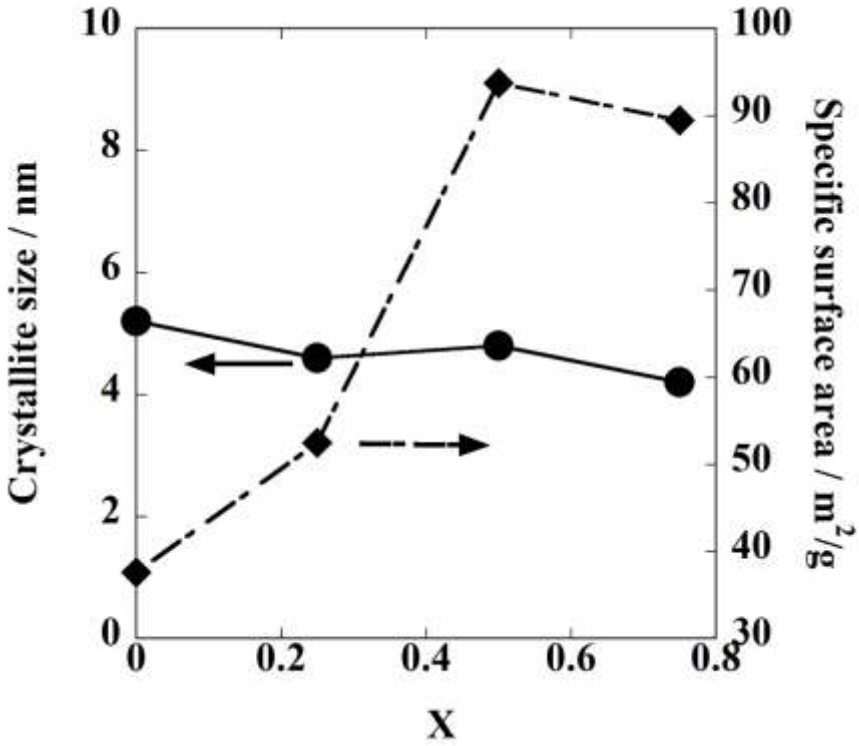

Fig.2 The crystallite size and BET specific surface area of precipitates obtained from aqueous precursor solutions with compositions of $(Al_xGa_{1.00-x})_2O_3$ under hydrothermal conditions at 180 °C for 5 h plotted against composition, Al atomic ratio.

The TEM images of precipitates formed from the solutions with compositions, x=Al=1.00, 0.75, and 0.50 at 180 °C are shown in Fig. 3. Although in the samples with compositions $(Al_{0.75}Ga_{0.25})_2O_3$ and $(Al_{0.50}Ga_{0.50})_2O_3$, the precipitates having cubic spinel phase are consisting of nano-sized very fine particles, the AlO(OH) precipitate formed from the precursor solution with a composition of pure Al_2O_3 has completely different morphology which is assembled nano-sized fibrous structure or sheet-like structure.

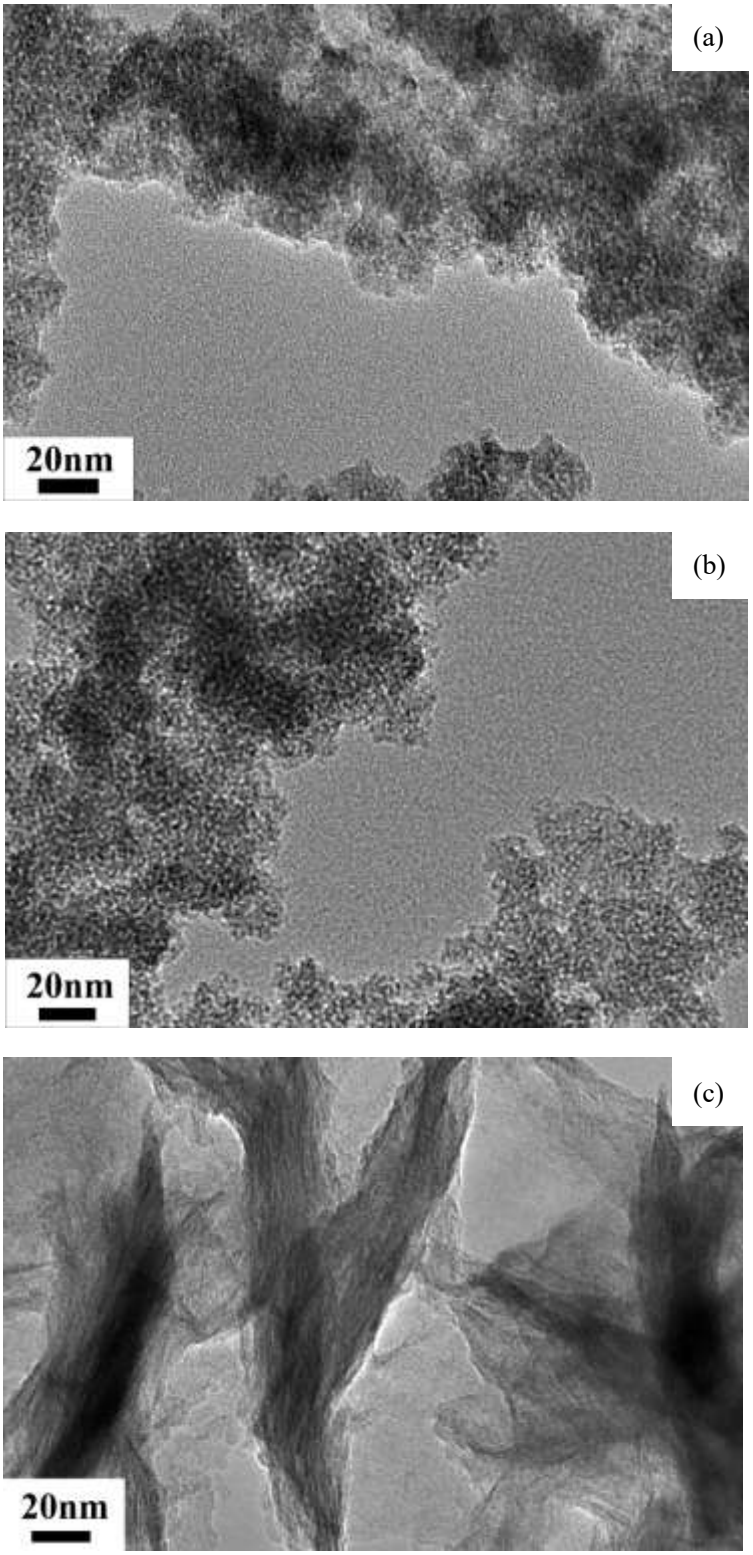

Fig.3 TEM images of precipitates obtained at various compositions of $(Al_xGa_{1.00-x})_2O_3$, x= (a) 0.50, (b) 0.75, and (c) 1.00 under hydrothermal conditions at 180 °C for 5 h

Fig. 4 shows the detail of region from 28 to 40 ° 2θ, i.e., shifts of the cubic 220 and 311 lines in the XRD patterns of the spinel-type nanoparticles that were directly formed from aqueous precursor solutions with various compositions via hydrothermal treatment at 180 °C, together with the XRD lines of the internal standard Si. It is observed that the cubic 220 and 311 lines slightly and gradually shift into higher angle as the value x: Al/(Al+Ga) atomic ratio increases. The lattice parameter of the as-prepared samples having cubic spinel structure is plotted against the value x, Al/(Al+Ga) atomic ratio in Fig. 5. The lattice parameter linearly decreased with increased aluminum concentration as suggested from the shift observed in the XRD lines (Figs. 1 and 4). But, as the concentration of aluminum increases, the lattice parameter values of as-prepared spinel nanoparticles exist considerably apart from the ideal linear relation, i.e., the line connecting with the lattice parameter of γ-Ga_2O_3 spinel and that of γ-Al_2O_3 spinel. This result implies that there is a possibility of the presence of substances with low crystallinity in the samples with compositions of high concentration of aluminum. But it is important to note that spinel-structured γ-Ga_2O_3-based nanoparticles doped with Al_2O_3, $(Al_xGa_{1.00-x})_2O_3$, x=0-0.85) were directly synthesized from the aqueous precursor solutions of $Ga(NO_3)_3$ and $Al_2(SO_4)_3$ under weakly basic conditions using aqueous ammonia in the presence of citric acid by the mild hydrothermal method at 180 °C for 5 h.

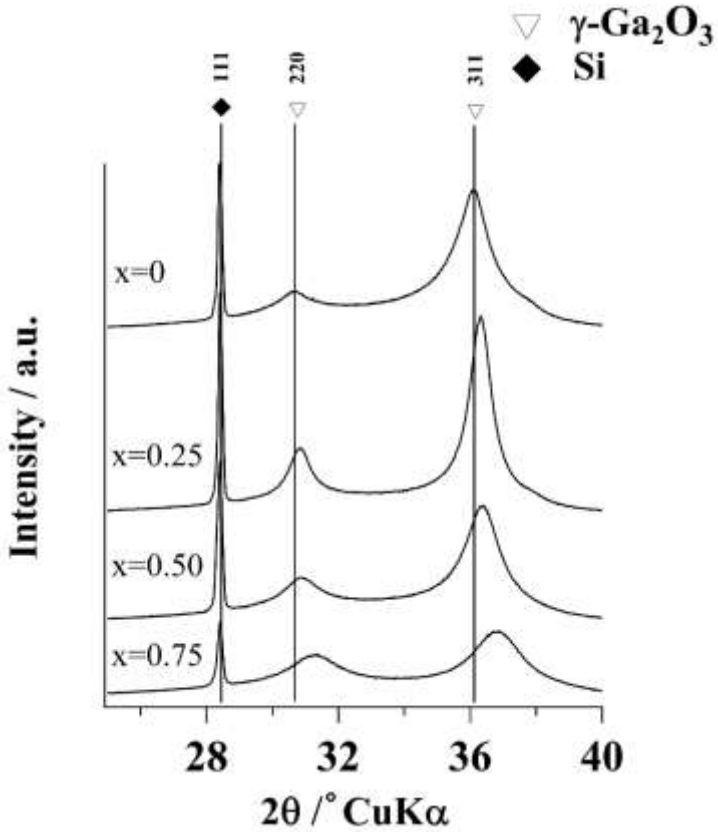

Fig.4 The close-up of the region around 36 ° 2θ of the X-ray diffraction patterns of precipitates obtained from aqueous precursor solutions with various compositions under hydrothermal conditions at 180 ºC for 5 h.

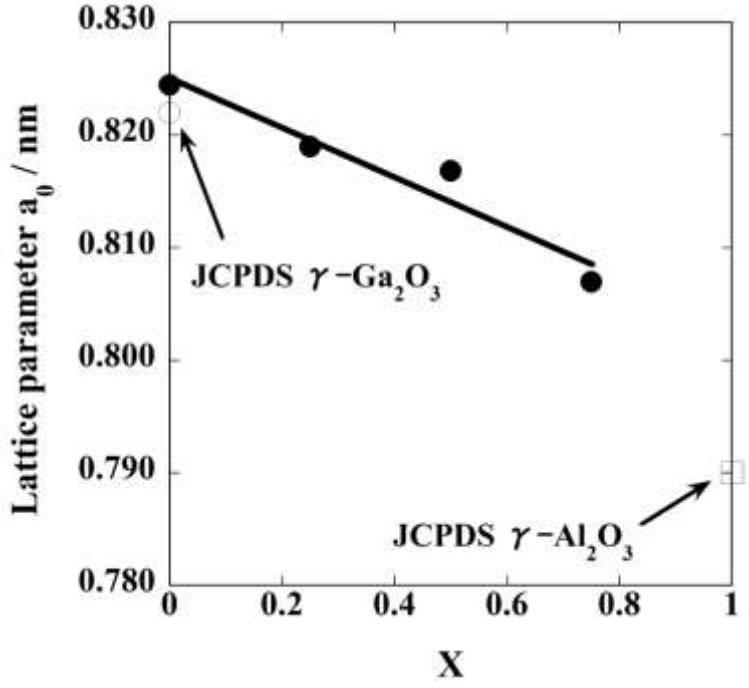

Fig.5 Lattice parameter of the cubic phase of as-prepared samples obtained from aqueous precursor solutions with compositions of $(Al_xGa_{1.00-x})_2O_3$ under hydrothermal conditions at 180 °C for 5 h plotted against composition, Al atomic ratio.

To examine the effect of the hydrothermal treatment temperature on the crystalline phase of precipitates in the Al_2O_3-Ga_2O_3 system, the hydrothermal treatment was carried out for the sample with a composition, $(Al_{0.25}Ga_{0.75})_2O_3$) at 170-240 °C for 5 h. The XRD patterns of the precipitates, $(Al_{0.25}Ga_{0.75})_2O_3$ that were hydrothermally formed at various temperatures are shown in Fig. 6. A single phase of spinel-type cubic structure was detected in all of the precipitates formed at all temperature ranges. The crystallite size of the spinel-type nanoparticles formed at 240 °C was rather smaller than that formed at 170 °C, and the crystallite size slightly and linearly decreased from 8 to 5 nm with increased heat treatment temperature. This strange and negative behavior implies that the spinel phase formed at lower temperature may have higher concentration of gallium than that formed at higher temperature, which is considered to be due to the insufficient crystallization of alumina component at low temperature under hydrothermal condition, because the treatment at higher temperature is necessary for the crystallization of aluminum oxide having higher refractoriness than the case of gallium oxide.

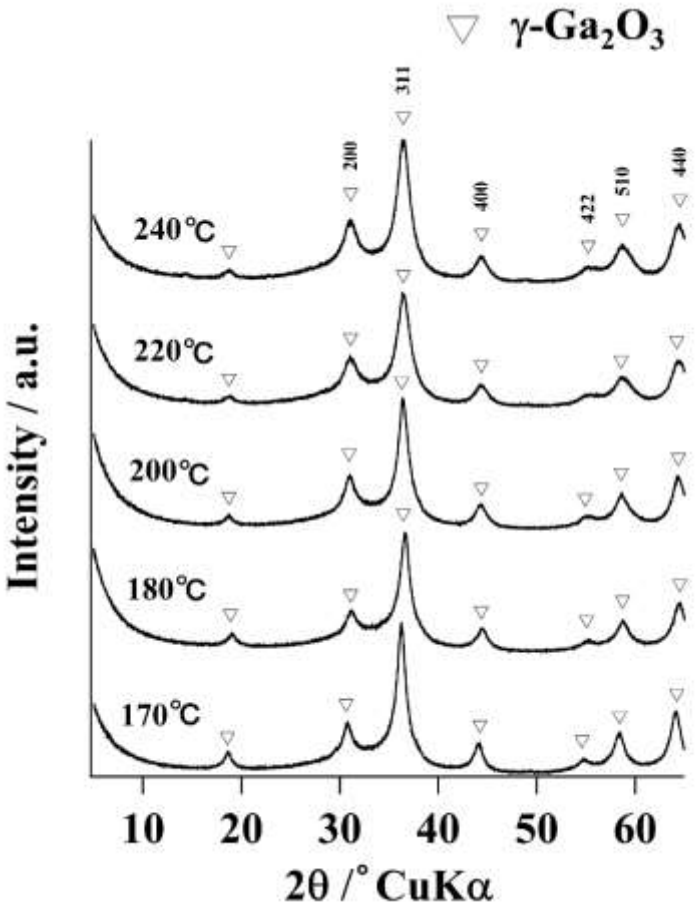

Fig.6 XRD patterns of precipitates obtained from aqueous precursor solutions with a composition of $(Al_{0.25}Ga_{0.75})_2O_3$ under hydrothermal conditions at 170-240 °C for 5 h.

The lattice parameter of the as-prepared spinel phase with a composition of $(Al_{0.25}Ga_{0.75})_2O_3$ evaluated as a cubic structure is represented against hydrothermal treatment temperature in Fig. 7. The lattice parameter of the cubic spinel phase of nanoparticles gradually and almost linearly decreased and approached the ideal lattice constant value corresponding to the $(Al_{0.25}Ga_{0.75})_2O_3$ composition as the hydrothermal treatment temperature rose. This result also implies that the precipitates formed at low temperatures may consist of the gallium-rich crystalline spinel phase and insufficient crystallization phase with low crystallinity, i.e., amorphous-like phase with high aluminum concentration. These results described above indicate that the present hydrothermal condition is insufficient for the crystallization of spinel phase with perfect crystallinity in the high alumina composition, that is, the hydrothermal treatment at elevated temperatures higher than 240 °C is necessary to obtain ideal solid solutions without containing

insufficiently crystallized alumina component in this system. However, the most important part of these results is that a single phase of cubic spinel was formed, the change in its lattice parameter was observed in the wide composition range ($(Al_xGa_{1.00-x})_2O_3$, x=0-0.85), and it was possible to prevent the AlO(OH) phase from crystallizing in the system by the presence of more than 15 mol% gallium component. Under the present hydrothermal conditions in the absence of citric acid, crystalline GaO(OH) and AlO(OH) phases were formed from the weakly basic precursor solutions in the system. It is considered that the direct formation of γ-Ga_2O_3-based spinel nanoparticles doped with alumina component was achieved because of the presence of citric acid as chelating ligand by prohibiting the aluminum and gallium hydroxide phases from crystallizing in the precursor solutions in the early stage of hydrothermal treatment at low temperature.

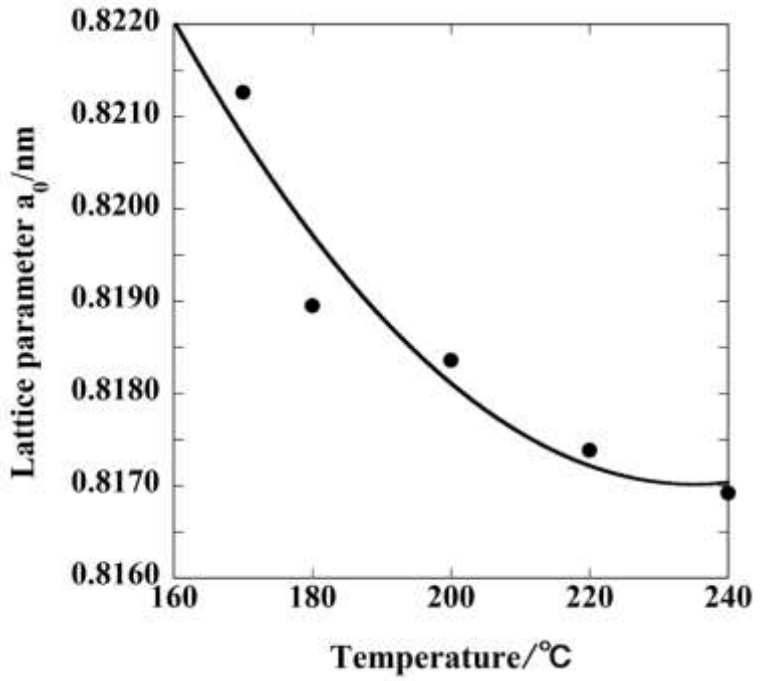

Fig.7 Lattice parameter of the cubic phase of as-prepared samples obtained from aqueous precursor solutions with a composition of $(Al_{0.25}Ga_{0.75})_2O_3$ under hydrothermal conditions at 170-240 °C for 5 h.

3-3-2 Effect of heat treatment on structure of γ-Ga_2O_3-Al_2O_3 nanoparticles

The effect of heat treatment on the crystalline phase, structure, crystallite growth, and phase transformation of γ-Ga_2O_3-Al_2O_3 nanoparticles was investigated. The XRD patterns of samples with various compositions in the Al_2O_3-Ga_2O_3 system before and after heating at 600, 800, and 1000 °C in air for 1 h are indicated in Fig. 8 (a)-(c), respectively. In the samples with composition range x=Al=0-0.75 after heating at 600 °C, although a slight increase in the crystallinity of their spinel phases is detected, the change in crystalline phase of the samples is hardly observed, and a single phase of spinel-type cubic phase was maintained. On the other hand, the AlO(OH) boehmite phase with a composition of Al=1.00 changed into a single phase of γ-Al_2O_3 via phase transition during heating at 600 °C. The spinel-type γ-Ga_2O_3 with pure Ga_2O_3 composition phase transformed into a single phase of β-Ga_2O_3 through heating at 800 °C. The crystalline phase of the samples with the compositions of x=Al=0.25 and 0.50 is composed of γ-Ga_2O_3 and β-Ga_2O_3 after heating at 800 °C. The sample with the composition of $(Al_{0.75}Ga_{0.25})_2O_3$ maintained a single phase of spinel structure corresponding to γ-Al_2O_3 (or γ-Ga_2O_3) even after heating at 800 °C. The sample Al=1.00 that was heat-treated at 800 °C also kept the spinel-type γ-Al_2O_3 phase formed via phase transition. Although almost a single phase of β-Ga_2O_3 structure was detected in the samples containing aluminum less than 50 mol%, $((Al_xGa_{1.00-x})_2O_3$, x=0~0.50), after heating at 1000 °C, the crystallinity of β-Ga_2O_3 phase was enhanced as the concentration of gallium in the sample increased. After the phase transformation from γ to β, β-Ga_2O_3-Al_2O_3 solid solutions having the structure similar to β-Ga_2O_3 were formed in the composition range, gallium=50-100 mol%, $((Al_xGa_{1.00-x})_2O_3$, x=0-0.50) since the shift of the XRD lines of β-Ga_2O_3 phase was clearly observed in the XRD patterns, e.g., 403 lines around 2θ=65 °. The phase transformation from γ-Ga_2O_3 phase to β-Ga_2O_3 structure doped with Al_2O_3 proceeded at lower temperature as the gallium concentration increased in the γ-Ga_2O_3-Al_2O_3 nanoparticles. Note that the spinel-type γ-Al_2O_3 (or γ-Ga_2O_3) phase was maintained in the samples containing 25 mol% gallium, $(Al_{0.75}Ga_{0.25})_2O_3$ even after heating at 1000 °C, though in the pure alumina composition, a single phase of θ-Al_2O_3 appeared via heating at 1000 °C. In this way, various changes in the crystalline phase of the Al_2O_3-Ga_2O_3 nanoparticles that were hydrothermally formed in the presence of citric acid and aqueous ammonia were observed depending on their composition and heat treatment condition.

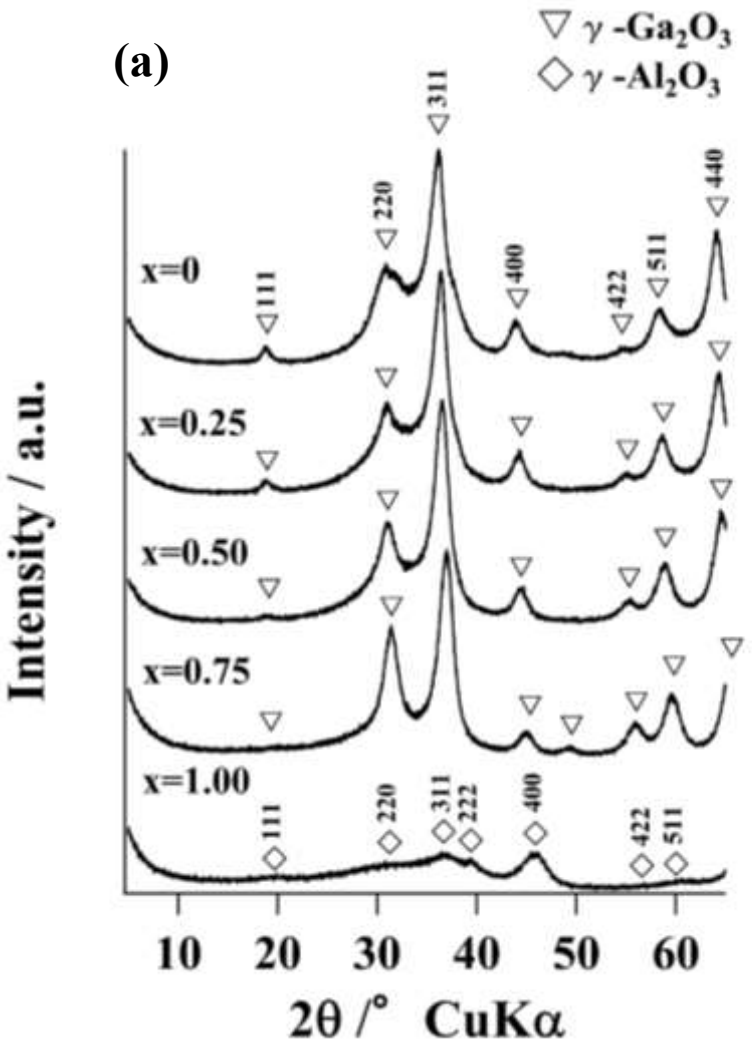

Fig.8 XRD patterns of samples after heating at (a) 600 °C for 1 h.

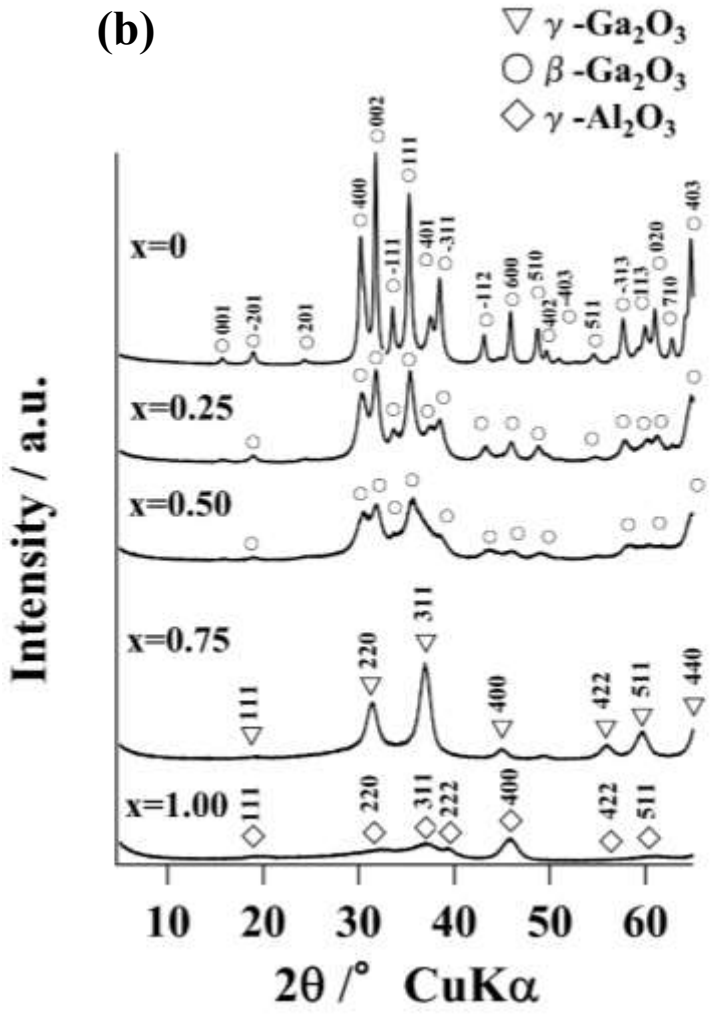

Fig.8 XRD patterns of samples after heating at (b) 800 °C for 1 h.

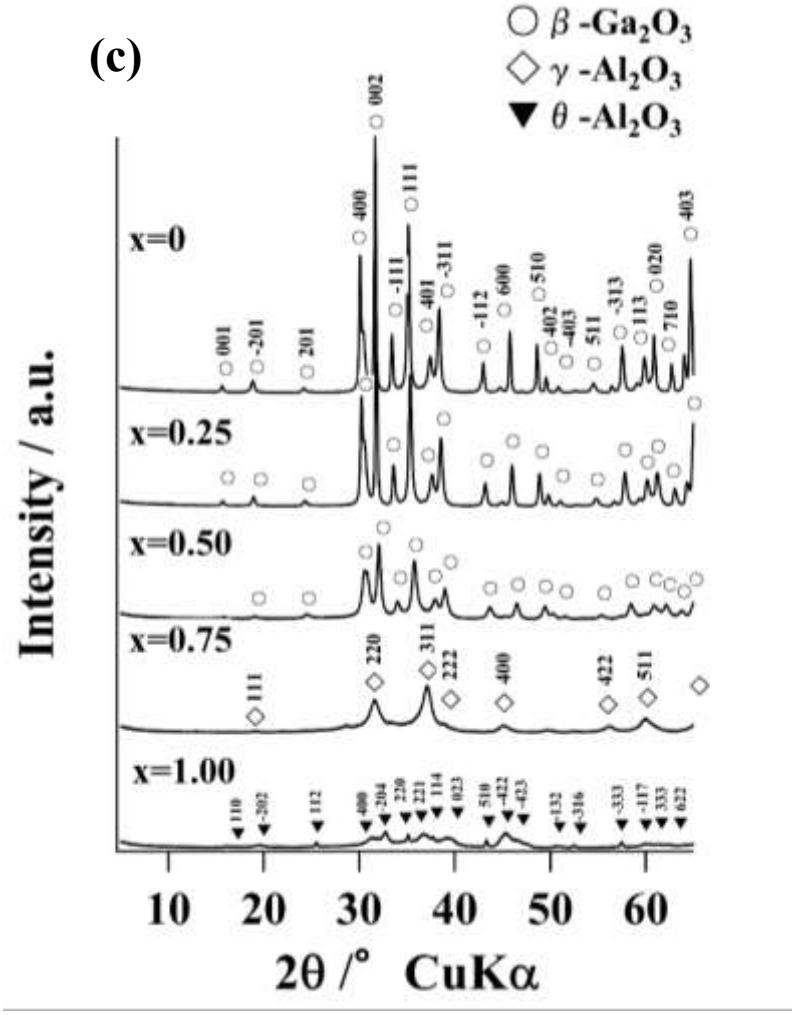

Fig.8 XRD patterns of samples after heating at (c) 1000 °C for 1 h.

3-3-3 Photoluminescence of γ-Ga_2O_3-Al_2O_3 nanoparticles

The effect of the composition and heat treatment on the photoluminescence properties of γ-Ga_2O_3-Al_2O_3 nanoparticles was investigated. The room temperature photoluminescence spectra of the samples with compositions $(Al_xGa_{1.00-x})_2O_3$, x=0.25, 0.50, and 0.75 measured under excitation at 325 nm are shown in Fig. 9(a)-(c), respectively. A violet-blue and broad band emission with a peak wavelength of 410-415 nm centered at around 440-450 nm under excitation at 325 nm was observed for each of the spinel-type nanoparticles with compositions of 25-75 mol% aluminum, ($(Al_xGa_{1.00-x})_2O_3$, x=0.25-0.75) formed at 180 °C. The three emission spectra of the nanoparticles with different compositions showed a great similarity. But the spinel-type nanoparticles with a composition of $AlGaO_3$, i.e., containing 50 mol% aluminum showed the highest luminescence intensity as shown in Fig. 9 (b). The luminescence intensities of the nanoparticles after heating at 600 °C became rather lower than those of the as-prepared samples, which corresponded to 1/2-1/6 of the emission intensities of as-prepared samples before heating. With increased heating temperature, the luminescence intensities of samples decreased, and the peak wavelength and the center wavelength of the broad band emission shifted into lower wavelength.

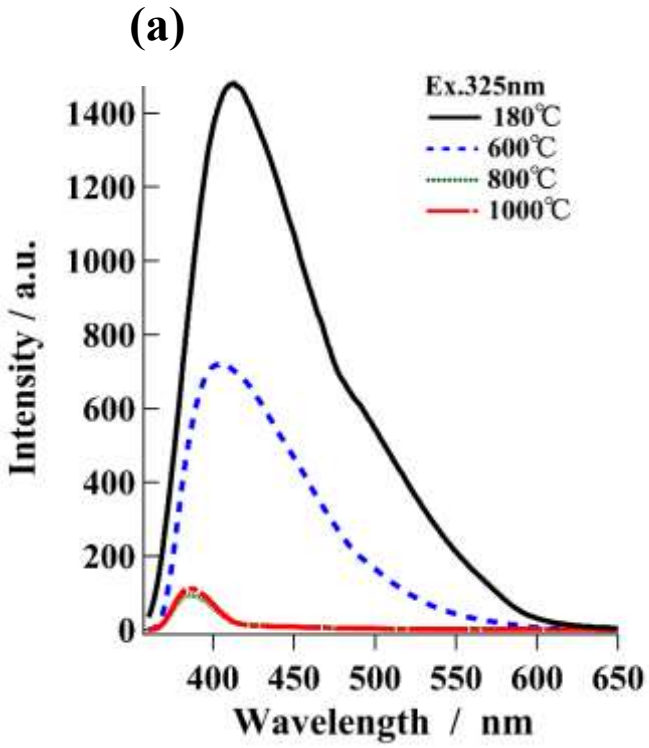

Fig.9 Emission spectra excited at 270 nm for the samples with composition of $(Al_xGa_{1.00-x})_2O_3$, x= (a) 0.25 before and after heat treatment in air.

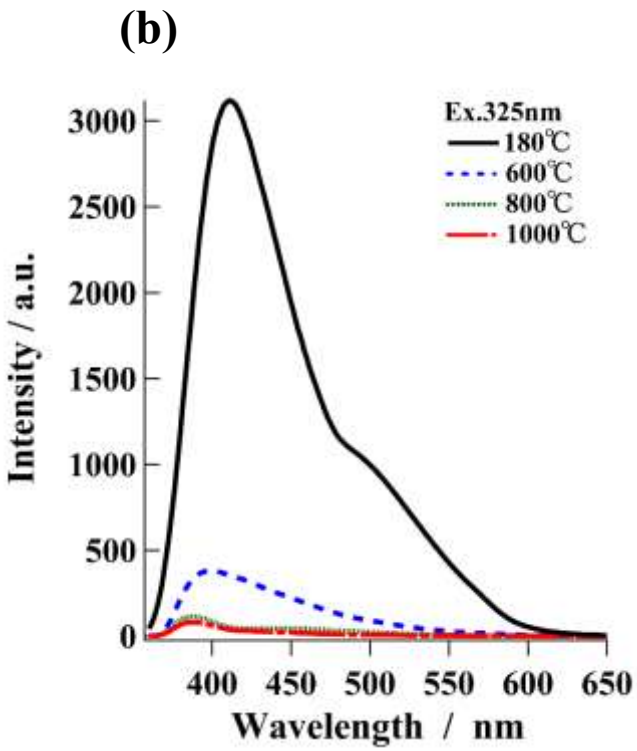

Fig.9 Emission spectra excited at 270 nm for the samples with composition of $(Al_xGa_{1.00-x})_2O_3$, (b) 0.50 before and after heat treatment in air.

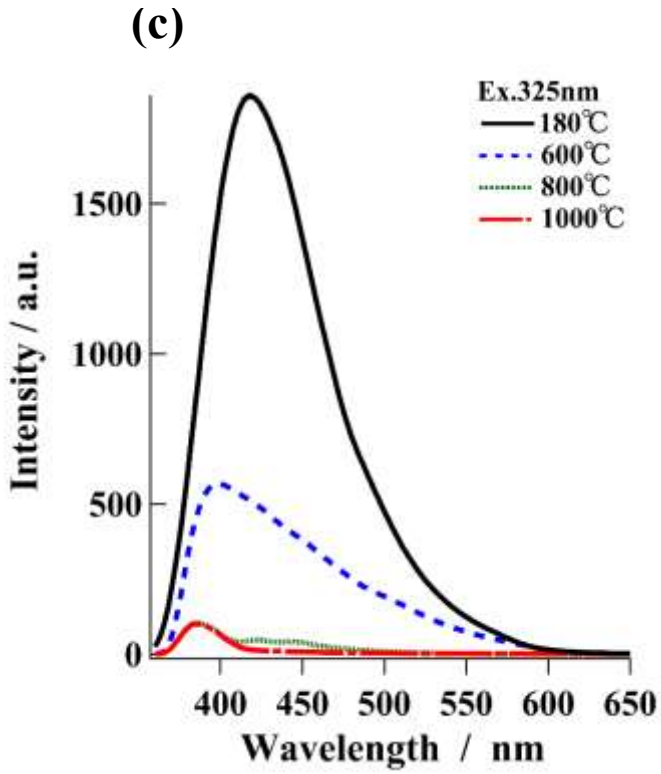

Fig.9 Emission spectra excited at 270 nm for the samples with composition of $(Al_xGa_{1.00-x})_2O_3$, x= (c) 0.75 before and after heat treatment in air.

3-4 Summary

The effect of the composition and heat treatment on the crystalline phase, structure, phase transformation, and luminescence properties was investigated for the spinel-structured γ-Ga_2O_3-based nanoparticles doped with Al_2O_3 component in the Al_2O_3-Ga_2O_3 system, which were hydrothermally formed from the aqueous precursor solutions of $Ga(NO_3)_3$ and $Al_2(SO_4)_3$ under weakly basic conditions using aqueous ammonia in the presence of citric acid. Under hydrothermal condition at 180 °C for 5 h, only a single phase corresponding to spinel-type cubic structure was formed as nanoparticles of 4-5 nm in the composition range of 0-85 mol% aluminum, $((Al_xGa_{1.00-x})_2O_3$, x=0-0.85) except for the pure alumina composition, which was due to the presence of citric acid as chelating ligand. After the phase transformation from γ to β, β-Ga_2O_3-Al_2O_3 solid solutions having the structure similar to β-Ga_2O_3 were formed in the composition range of aluminum=0-50 mol%, $((Al_xGa_{1.00-x})_2O_3$, x=0-0.50). As the gallium concentration increased in the γ-Ga_2O_3-Al_2O_3 nanoparticles, the phase transformation from γ-Ga_2O_3 phase to β-Ga_2O_3 structure proceeded at lower temperature The spinel-type γ-Al_2O_3 (or γ-Ga_2O_3) phase was maintained in the samples containing 75 mol% aluminum, $(Al_{0.75}Ga_{0.25})_2O_3$, even after heating at 1000 °C in contrast with a single phase of θ-Al_2O_3 in the case of pure alumina composition. A violet-blue and broad emission band with a peak wavelength of 410-415 nm centered at 440-450 nm under excitation at 325 nm was observed for each of the spinel-type γ-Ga_2O_3-based nanoparticles with compositions of $(Al_xGa_{1.00-x})_2O_3$, x=0.25, 0.50, and 0.75 formed at 180 °C.

References

1. R. Roy, V. G. Hill, E. F. Osborn, *J. Am. Chem. Soc.,* **74**:719-722 (1952)
2. A. J. Freeman, K. R. Poeppelmeier, T. O. Mason, R. P. H. Chang, T. J. Marks, *MRS Bull.,* **25**:45-51(2000).
3. A. C. Tas, P. J. Majewski, F. Aldinger, *J. Am. Ceram. Soc.,* **85**:1421-1429 (2002)
4. K. Nakagawa, C. Kajita, K. Okumura, N. O. Ikenaga, M. NishitaniGamo, T. Ando, T. Kobayashi, T. Suzuki, *J. Catal.,* **203**:87-93 (2001)
5. B. Xu, B. Zheng, W. Hua, Y. Yue, Z. Gao, *J. Catal.,* **239**:470-477 (2006)
6. A. L. Peter, A. Auroux, P. Gelin, M. Caldarau, N. I. Ionescu, *Thermochim. Acta.,* **379**:177-185 (2001)
7. T. Weh, J. Frank, M. Fleischer, H. Meixner, *Sens. Actuators B,* **78**:202-207 (2001)
8. M. Ogita, K. Higo, Y. Nakanishi, Y. Hatanaka, *Appl. Surf. Sci.*, **175-176**:721-725 (2001)
9. T. Miyata, T. Nakatani, T. Minami, *Thin Solid Films,* **373**:145-149 (2000)
10. H. Hayashi, R. Huang, H. Ikeno, F. Oba, S. Yoshioka, I. Tanaka, S. Sonoda, *Appl. Phys. Lett.*, **89**:181903/1-181903/3 (2006)

11. N. Ueda, H. Hosono, R. Waseda, H. Kawazoe, *Appl. Phys. Lett.,* **70**:3561-63 (1997)
12. M. Chen, J. Xu, F. Z. Su, Y. M. Liu, Y. Cao, H. Y. He, K. N. Fan, *J. Catal.,* **256**:293-300 (2008)
13. T. Chen, K. Tang, *Appl. Phys. Lett.,* **90**:053104-1-053104-3 (2007)
14. R. Huang, H. Hayashi, F. Oba, I. Tanaka, *J. Appl. Phys.,* **101**:063526-1-063526-6 (2007)
15. C. O. Arean, M. R. Delgado, V. Montouillout, D. Massiot, *Z. Anorg. Allg. Chem.,* **631**:2121-2126 (2005)
16. K. Pohl, *Naturwissenschaften,* **55**:82-82 (1968)
17. M. Takahashi, T. Nakatani, S. Iwamoto, T. Watanabe, M. Inoue, *J. Phys. Cond. Matter,* **18**:5745-5757 (2006)
18. M. Takahashi, N. Inoue, T. Takeguchi, M. Inoue, T. Watanabe, *J. Am. Ceram. Soc.*, **89**:2158-2166 (2006)
19. T. Wang, S. S. Farvid, A. Mutalifu, P. V. Radovanovic, *J. Am. Chem. Soc.,* **132**:9250-9250 (2010)
20. T. Wang, P. V. Radovanovic, *Chem. Commun.*, **47**:7161-7163 (2011)
21. F. Conrad, M. Bauer, S. Weyeneth, Y. Zhou, K. Hametner, D. Günther, G. R. Patzke, *Solis State Sci.,* **24**:125-132 (2013)
22. M. Hirano, S. Okumura, Y. Hasegawa, aM. Inagaki, *Int. J. Inorg. Mater.,* **3**:797-801 (2001)
23. M. Hirano, S. Okumura, Y. Hasegawa, M. Inagaki, *J. Solid State Chem.,* **168**:5-10 (2002)
24. M. Hirano, M. Imai, M. Inagaki, *J. Am. Ceram. Soc.,* **83**:977-79 (2000)
25. M. Hirano, N. Sakaida, *J. Am. Ceram. Soc.,* **85**:1145-1150 (2002)
26. K. Sakoda, M. Hirano, Formation of complete solid solutions, *Ceram. Intl.*, **40**:15841-15848 (2014)
27. K. Sakoda, M. Hirano, *J. Nanosci. Nanotechnol.,* **15**:6069-6077 (2015)

Chapter 4

Synthesis of $ZnAlGaO_4$ spinel through hydrothermal route

4-1 Introduction

In recent years, much attention has been devoted to wet chemical routes to synthesize nanometer-sized crystals of inorganic materials [1]. In order to improve the performance and properties of inorganic materials, investigating their synthesis routes is one approach in addition to designing the materials based on control of their microstructures and compositions. The mild hydrothermal synthesis technique, which is one of the wet chemical routes in the category of building-up processes, is well-known as being able to synthesize homogeneous nanocrystalline inorganic materials from aqueous precursor solutions at relatively low temperatures [2-5].

Zinc aluminum oxide (zinc aluminate, $ZnAl_2O_4$) and zinc gallium oxide (zinc gallate $ZnGa_2O_4$), which are representative materials of oxide spinel compounds, have attracted enormous attention as wide-band-gap semiconductors thanks to their interesting and superior properties [6]. The zinc gallate spinel possesses outstanding and excellent characteristics such as being potentially transparent and conductive in the near-UV region [7]. It shows a blue emission without any dopant via a self-activation center of Ga-O groups under excitation by both UV light and low-voltage electrons [8] and shows emissions from green to red when it is doped with Cr and Mn [9]. Zinc gallate has been applied in many uses, e.g., transparent electrodes, phosphors in vacuum florescent displays [8, 10], field emission displays [11], thin film electroluminescence displays [12], and photocatalysts for the decomposition of benzene [13]. As in the case of zinc aluminate spinel, it also exhibits excellent properties such as thermo-mechanical resistance, chemical stability, high thermal stability, and photoluminescence [14, 15]. Many applications of $ZnAl_2O_4$ as reflective optical coatings [16], UV-transport electro conductive oxide [17], and photocatalysts for the degradation of toluene [18] have been reported. The main applications of $ZnAl_2O_4$ are as catalysts for dehydration [19], hydrogenation [20], dehydrogenation [21], and synthesis of fine chemicals [22]. Although many studies on $ZnGa_2O_4$ and $ZnAl_2O_4$ spinel compounds have been reported, there are only few studies on $ZnAlGaO_4$ spinel with an intermediate composition in the $ZnGa_2O_4$ - $ZnAl_2O_4$ system.

Various synthetic approaches, for example, the solid-state reaction as the most common route [7, 11, 17], flux method using Li_3PO_4 at high temperature [10, 23, 24], sol-gel method [25], low-temperature direct synthesis [26, 27], co-precipitation [9, 28], homogeneous precipitation [29], hydrothermal method [30, 31], and combustion synthesis [32] have been employed for the

preparation of $ZnGa_2O_4$ spinel. On the other hand, there are many methods for the preparation of $ZnAl_2O_4$ spinel, e.g., solid-state reaction [33], co-precipitation [34], sol-gel [35, 36], and, template-assisted synthesis [37]. The glycothermal synthesis with post heating at 400°C and catalytic properties of $ZnAl_2O_4$ and $ZnGa_2O_4$ spinels have also been reported [38]. Some spinel-type $ZnAl_2O_4$ particles have been synthesized based on the hydrothermal synthesis routes [14, 15, 18, 39, 40]. Most of those hydrothermal $ZnAl_2O_4$ spinel have been prepared via the combination of post-heat treatment at 500-800 °C in air. There are few reports concerning the synthesis via the hydrothermal route and the properties of spinel-type $ZnAlGaO_4$ nanocrystals at the intermediate composition between $ZnGa_2O_4$ and $ZnAl_2O_4$. Moreover the details of the effect of heating on the structure and properties of the as-prepared spinel nanocrystals have not yet been determined sufficiently.

In the present study, nanometer-sized $ZnAlGaO_4$ spinel solid solution particles have been hydrothermally synthesized using tetramethylammonium hydroxide, and their structure and properties, e.g., the cell size, optical band gap, and photoluminescence have been investigated. In addition, a slight and gradual change in the cell size was observed in the as-prepared spinel nanoparticles during heating in air, the structural change of the $ZnAlGaO_4$ spinel in the course of hydrothermal treatment and post-heat treatment has been discussed.

4-2 Experimental

4-2-1 Sample preparation

The nanocrystalline $ZnAlGaO_4$ spinel particles were prepared with the hydrothermal method at 150-240 °C for 5 h using tetramethylammonium hydroxide ($N(CH_3)_4OH$, TMAH). An aqueous solution mixture of reagent-grade $ZnSO_4$, $Al(NO_3)_3$ and $Ga(NO_3)_3$ in the ratios of Zn:Al:Ga=1:1:1 was prepared in a Teflon container. Before hydrothermal treatment, $N(CH_3)_4OH$ solution was added into the solution mixture until the pH of the solution that was hydrothermally treated became weakly basic. This solution mixture with total cation concentrations (Zn + Al + Ga) of 0.20 mol/dm^3 in the Teflon container was then placed in a stainless steel vessel. The vessel was tightly sealed and it was heated at 150-240 °C for 5 h under rotation at 1.5 rpm. After hydrothermal treatment, the precipitates were washed with distilled water until the pH value of the rinsed water became 7.0, separated from the solution by means of centrifugation, and dried in an oven at 60 °C. The powders thus prepared under hydrothermal condition at 180 °C were heat treated in an alumina crucible at a heating rate of 200 °C/h, held at 400-1000 °C for 1 h in air, and then cooled to room temperature in a furnace.

4-2-2 Characterization

Phase identification of the as-prepared and heat-treated samples was conducted with an X-ray diffractometer (XRD, model: RINT-2000, Rigaku, Tokyo, Japan) using CuKα radiation. The morphology of the samples was observed using transmission electron microscopy (TEM, model: JEM-2010, JEOL, Tokyo, Japan). The crystallite size of the cubic spinel phase was evaluated from the line broadening of 311 diffraction peak, according to the Scherrer equation, $D_{XRD} = K\lambda / \beta\cos\theta$, where θ is the Bragg angle of diffraction lines; K is a shape factor ($K = 0.9$ in this work); λ is the wavelength of incident X-rays, and β is the corrected half-width given by $\beta^2 = \beta_m^2 - \beta_s^2$, where β_m is the measured half-width and β_s is the half-width of a standard sample. The peak-top positions of XRD patterns were measured using silicon as the internal standard. The specific surface area of the prepared samples was calculated from the adsorption isotherm of nitrogen at 77 K based on the Brunauer-Emmett-Teller method (BET, model: NOVA 1200, Yuasa Ionics, Osaka, Japan).

The UV-vis absorption (diffuse reflectance) spectra of the prepared powders were measured using an ultraviolet-visible spectrophotometer with an integrating sphere attachment (model: V-560, Nihon Bunko, Tokyo, Japan). The spectra were derived from the measured ones using the Kubelka-Munk equation [41]. The photoluminescence (PL) emission was measured using a fluorescence spectrophotometer (model: F-2700, Hitachi High-Tech, Japan) with a Xe lamp. Powder samples were excited with 270 nm radiation from a 150 W xenon lamp. The emission wavelength was scanned from 280 to 800 nm at a scanning rate of 60 nm/min.

4-3 Results and discussion

4-3-1 Synthesis of $ZnAlGaO_4$ spinel nanoparticles

The aqueous precursor solution (with composition: $ZnAlGaO_4$) was hydrothermally treated under weakly basic condition using TMAH. There was no presence of unreacted metal cations in the ultrafiltrated solution after hydrothermal treatment under weakly basic condition in all samples. The XRD patterns of as-prepared samples that were formed at 150~240 °C for 5 h are shown in Fig. 1. The precipitates formed at 150~240 °C were detected as a single phase corresponding to a spinel-type cubic structure, and no diffraction peaks due to another crystalline phase was detected. It was found that the crystalline products composed of a single phase of spinel-type cubic structure were obtained under hydrothermal conditions higher than 150 °C in the presence of TMAH.

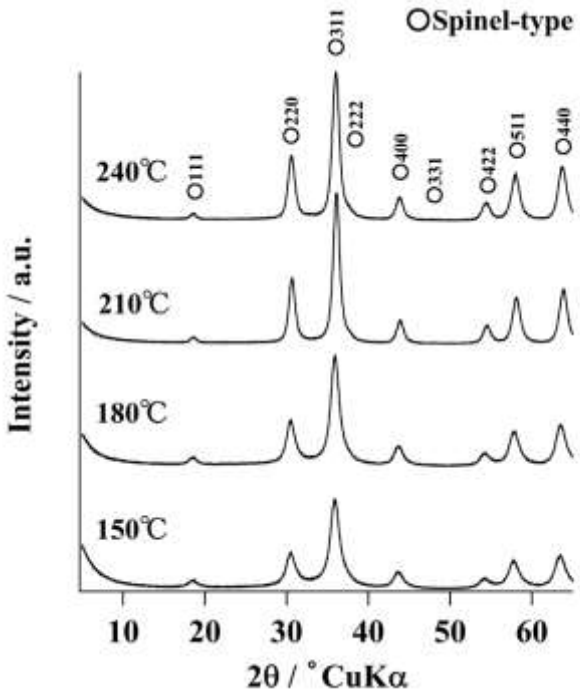

Fig.1 X-ray diffraction patterns of precipitates obtained under hydrothermal conditions at 150~240 ºC for 5 h.

The crystallite sizes of spinel-type cubic phase obtained after hydrothermal treatment at 150, 180, 210, and 240 °C, which were estimated from the line broadening of the 311 diffraction peak according to the Scherrer equation, were around 6, 8, 9, and 9 nm, respectively. The TEM images of precipitates formed at 150 and 210 °C are shown in Figs. 2(a) and (b), respectively. An increase in the particle size and crystallinity of spinel particles was seen as the treatment temperature rose. The particle sizes around 5-13 nm are observed for the precipitates obtained at 210 °C. As the crystallite size estimated from XRD line broadening corresponded relatively well to the particle size observed in TEM images, these particles are considered to be single crystals of spinel.

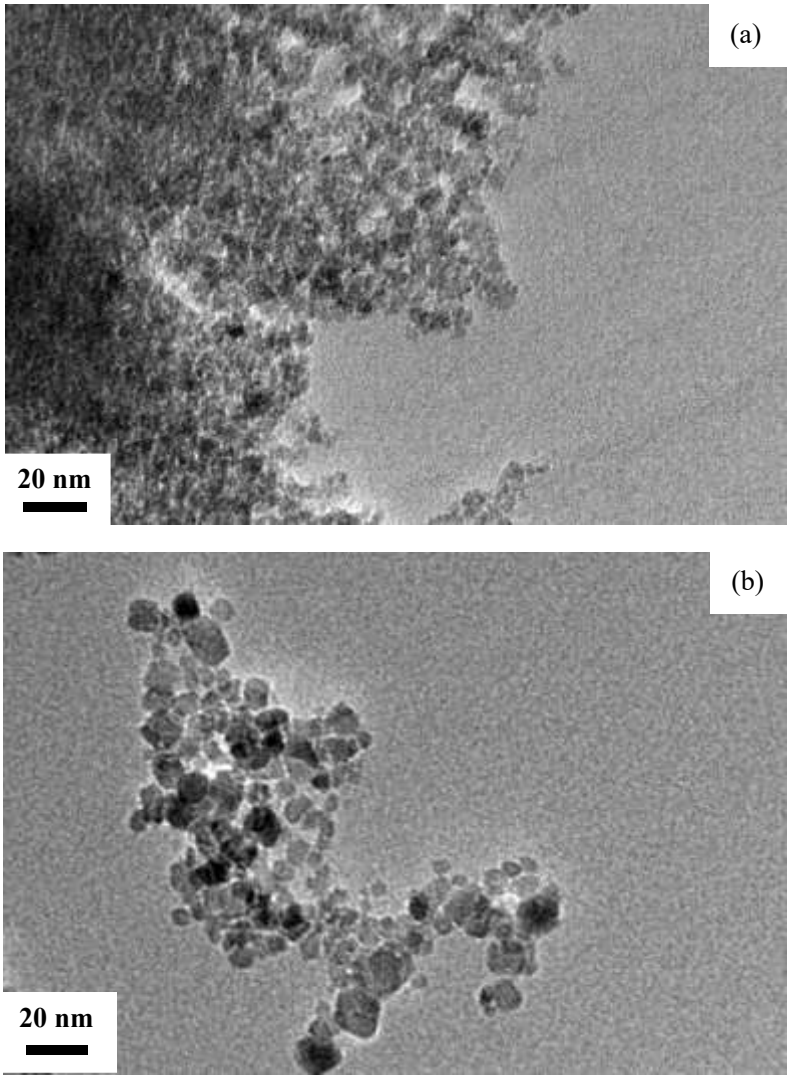

Fig.2 Transmission electron microscopy images of precipitates obtained under hydrothermal conditions at (a) 150 and (b) 210 °C for 5 h.

Fig. 3 shows the detail of region around 58 and 65° 2θ, i.e., a shift of the cubic 511 and 440 lines in the XRD patterns of the precipitates formed at 150-240 °C, together with the XRD lines of the internal standard Si. It is found that the XRD lines of the cubic 511 and 440 of the spinel phase shift very slightly to a higher degree of 2θ, as the hydrothermal treatment temperature rises from 150 to 240 °C. Fig. 4 presents the change in the peak-top position (d_{440}) of cubic spinel phase prepared at 150-240 °C for 5 h. The interplanar spacing, d_{440} evaluated from the peak-top position of samples decreased very slightly and gradually with increased hydrothermal treatment temperature. Since the interplanar spacing of $ZnGa_2O_4$ and $ZnAl_2O_4$ is d_{440}=0.1473 (JCPDS No. 38-1240) and d_{440}=0.1429 nm (JCPDS No. 05-0669), respectively, the peak-top position (d_{440}) of samples approached the intermediate value of $ZnGa_2O_4$ and $ZnAl_2O_4$, i.e., the

ideal value, little by little, as the hydrothermal treatment temperature rose from 150 to 240 °C. But the obtained values are larger than the ideal value. A gap exists between the peak-top position (d_{440}) of the as-prepared samples and ideal one. Then the as-prepared precipitates were heat treated in air and are discussed in the next section.

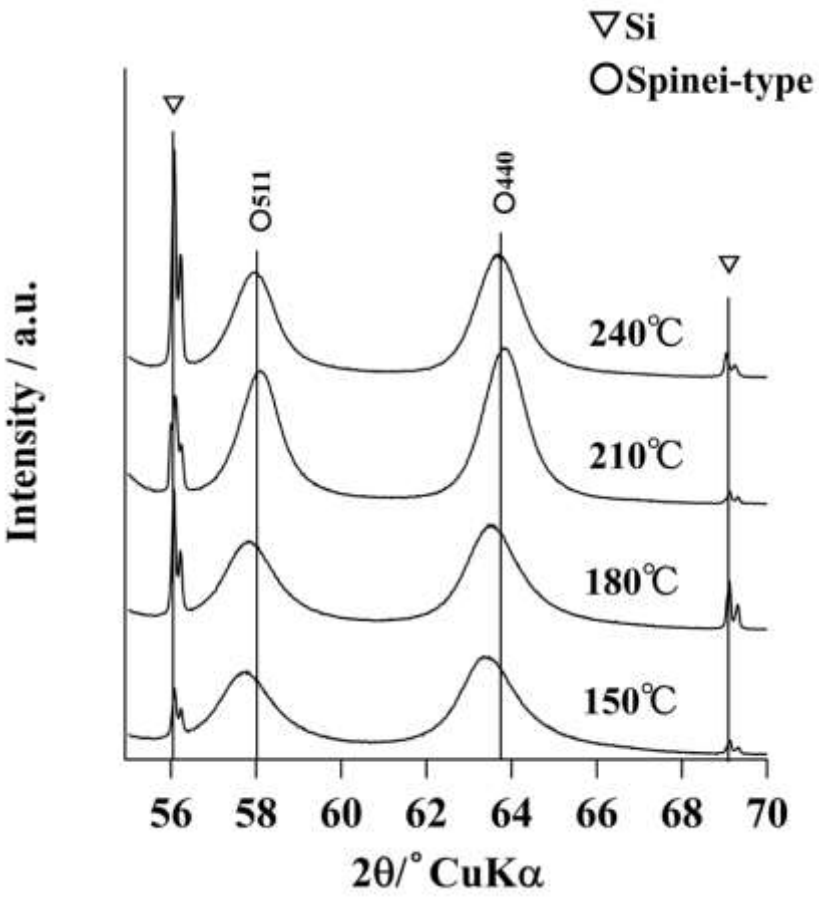

Fig.3 Close-up of the region around 58-64 ° 2θ of the X-ray diffraction patterns of samples obtained under hydrothermal conditions at 150-240 °C for 5 h.

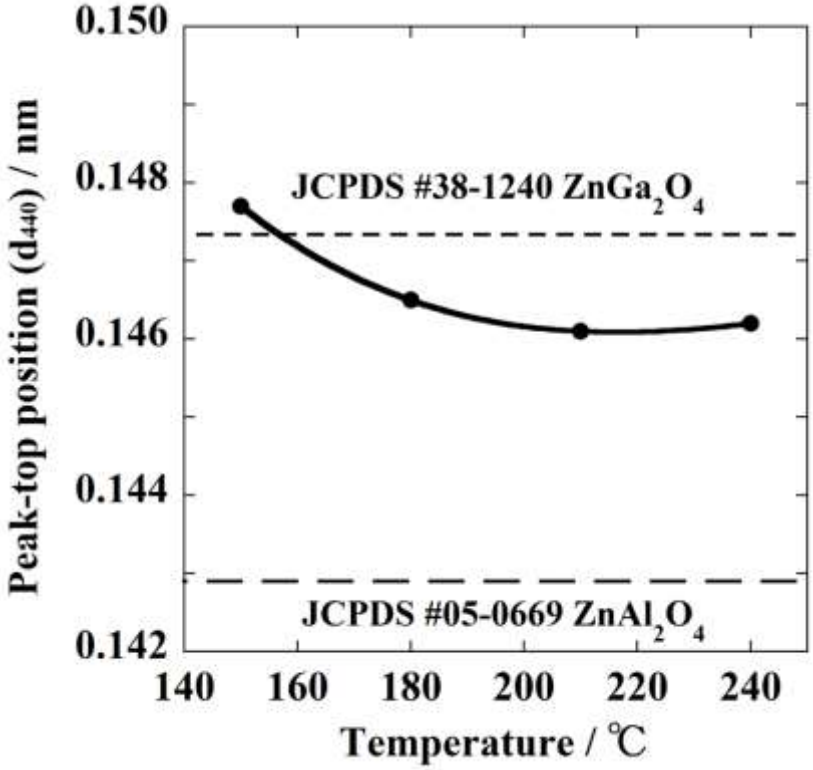

Fig.4 Peak-top position (d_{440}) of cubic spinel phase of samples obtained under hydrothermal conditions at 150-240 °C for 5 h.

4-3-2 Structural change through heat treatment

The effect of heat treatment in air on the crystallinity and structure of the as-prepared spinel nanoparticles was investigated. The precipitates with cubic spinel phase formed from the precursor solution with composition $ZnAlGaO_4$ under hydrothermal condition at 180 °C were heat-treated at 400°C-1000°C for 1 h in air. The XRD patterns of samples after heating in air at 400°C-1000°C are shown in Fig. 5. The crystalline phase of the samples after heating in air at temperatures of 400-1000 °C was a single phase of cubic spinel structure. The change in the sharpness of the XRD patterns is hardly observed between the as-prepared sample and samples heat treated at 400-600°C. The XRD lines corresponding to spinel phase gradually become sharp as the heating temperature rises from 700 to 1000 °C. This result suggests that the improvement in the crystallinity of the spinel phase occurs during heating at temperature higher than 700 °C.

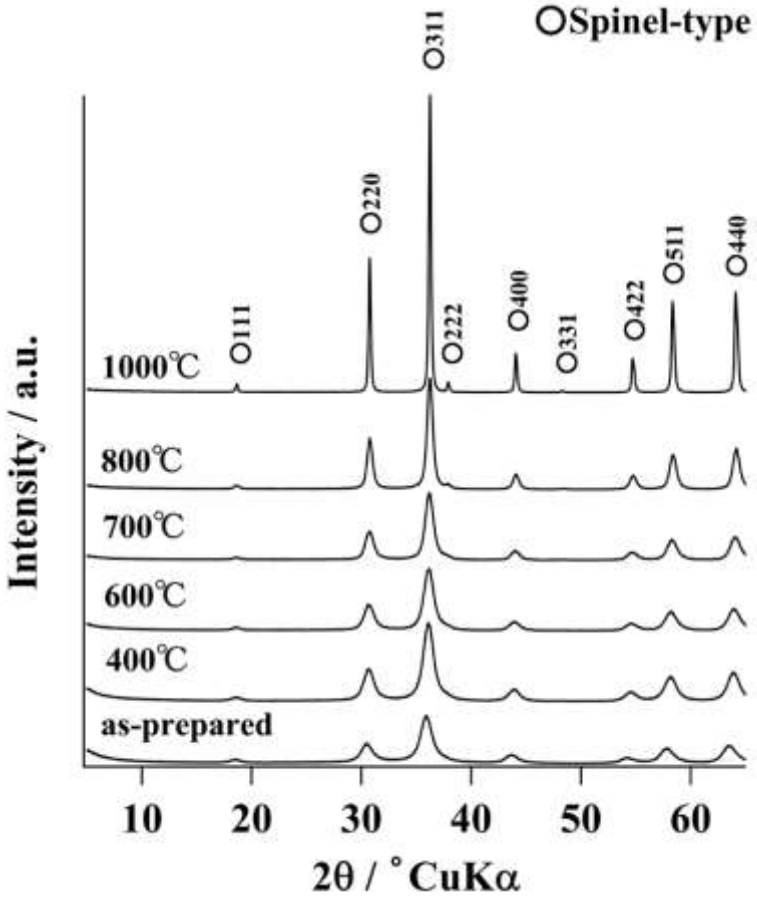

Fig.5 X-ray diffraction patterns of sample hydrothermally formed at 180 °C before and after heating at 400-1000 °C for 1 h.

The TEM images of the samples after heating at 600~1000 °C are shown in Figs. 6 (a)~(c), respectively. The as-prepared nanocrystals with cubic spinel phase gradually grew to become large crystals as the heating temperature rose from 600 to 800 °C. The spinel crystals around 20-70 nm with cubic morphology are observed in the sample after heating at 1000 °C. The crystallite growth of spinel in the samples as a function of heating temperature is presented in Fig. 7. The crystallite size of the spinel hardly changed in the samples before and after heat treatment up to 600°C for 1 h. The crystallite growth was accelerated by heating at temperatures higher than 800 °C. The resultant crystallite size of the spinel after heating at 1000 °C is around 45 nm, which corresponds relatively well to the average particle size estimated from the TEM observation in Fig. 6 (c). The BET surface areas of the spinel samples are plotted against the heating temperature in Fig. 8. The surface areas decreased almost linearly as the heating temperature rose.

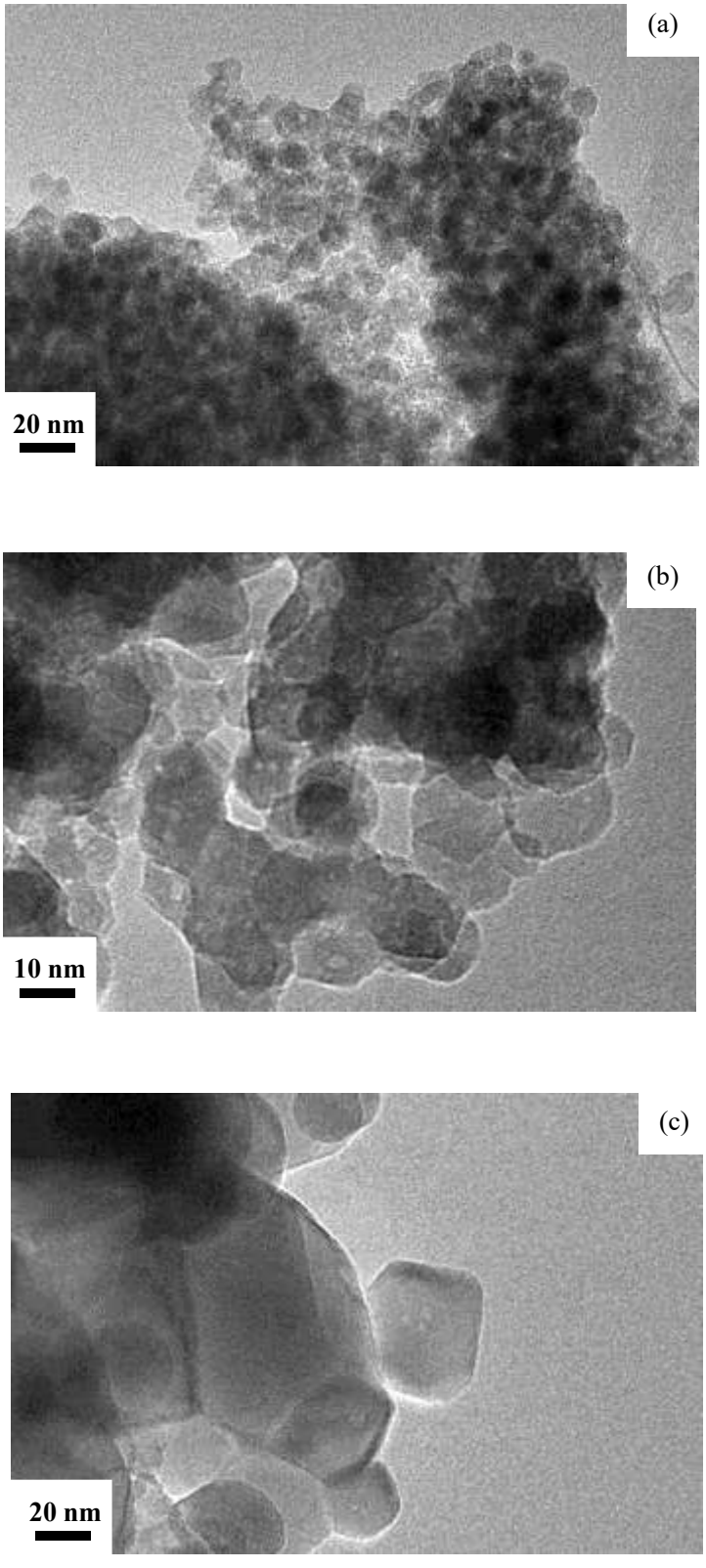

Fig.6 Transmission electron microscopy images of samples heated at (a) 600, (b) 800, and (c) 1000 °C for 1 h.

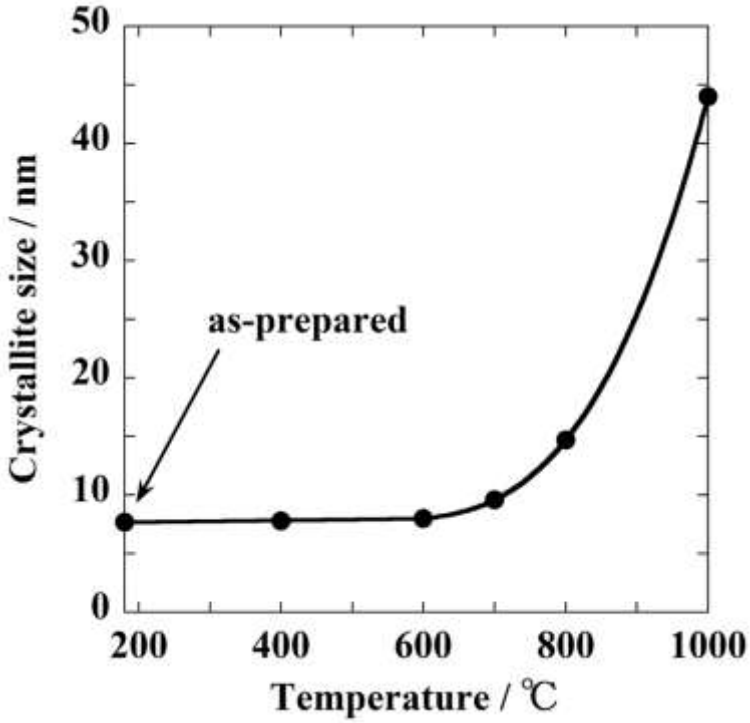

Fig.7 Crystallite size of samples with cubic phase hydrothermally formed at 180 °C before and after heating at 400-1000 °C for 1 h.

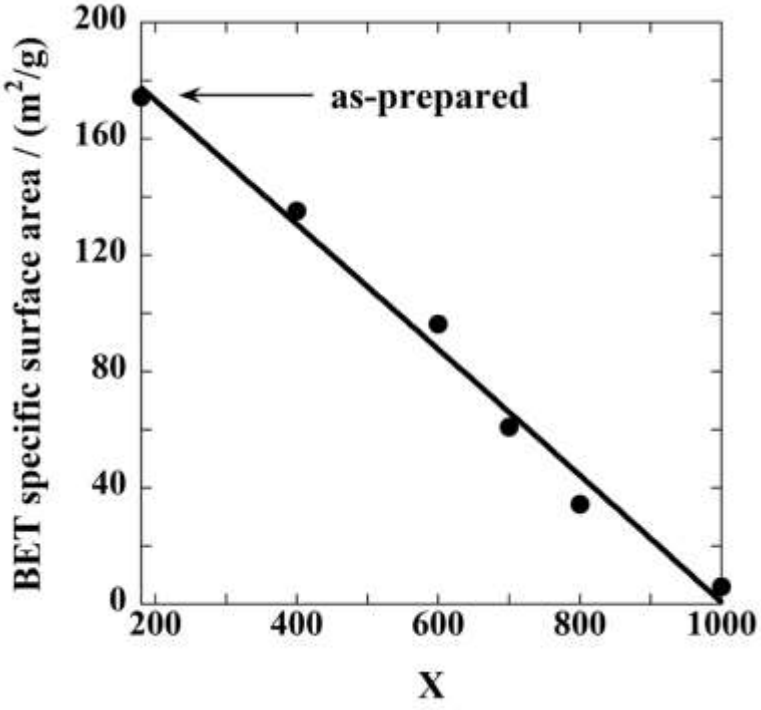

Fig.8 BET specific surface area of samples hydrothermally formed at 180 °C before and after heating at 400-1000 °C for 1 h.

Fig. 9 shows the detail of region around 58 and 65° 2θ, i.e., a shift of the cubic 511 and 440 lines in the XRD patterns of the samples as-prepared at 180 °C and heat treated at 400-1000°C, together with the XRD lines of the internal standard Si. It is observed that the XRD lines of the cubic 511 and 440 in the as-prepared spinel nanocrystals very slightly and gradually shift to higher degree of 2θ in accordance with heating at 400-800 °C. This phenomenon indicates that the as-prepared spinel nanocrystals undergo structural change as a result of the heat treatment.

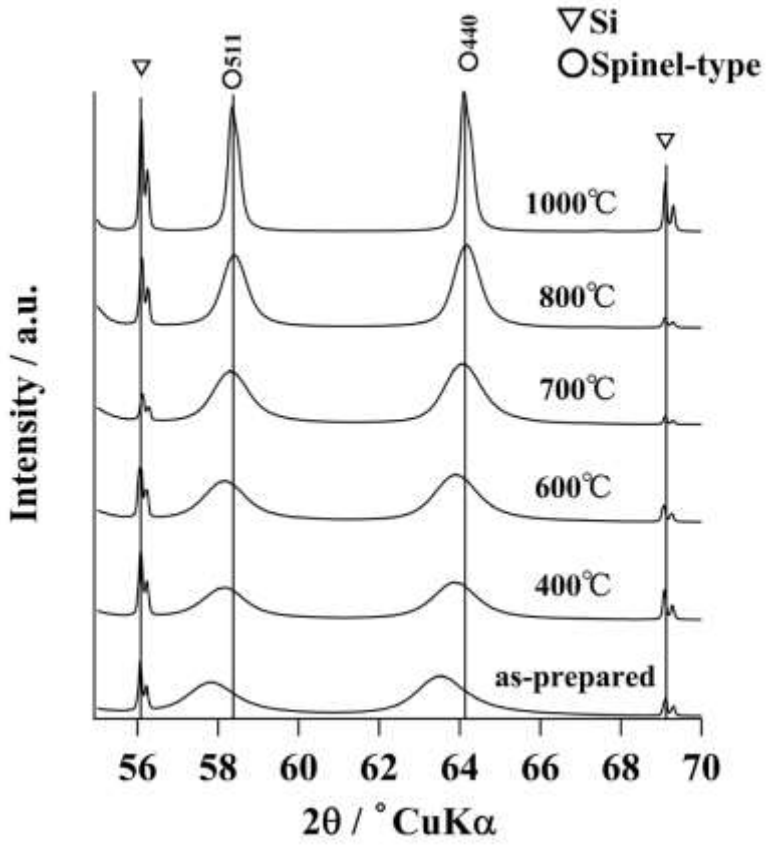

Fig.9 Close-up of the region around 58-64 ° 2θ of the X-ray diffraction patterns of samples hydrothermally formed at 180 °C before and after heating at 400-1000 °C for 1 h.

The peak-top position (d_{440}) of the as-prepared spinel phase formed under hydrothermal condition at 180 °C and that after heat-treatment at 400-1000 °C are shown as a function of heating temperature in Fig. 10. The interplanar spacing, d_{440} evaluated from the peak-top position of the as-prepared cubic spinel phase slightly and linearly decreased as the heating temperature rose from 400 to 800 °C. After heating at temperatures higher than 800 °C, the interplanar spacing, d_{440} reached almost the constant value: 0.1451 nm. The cause of this phenomenon is considered to be as follows. The ideal value of d_{440} for $ZnAlGaO_4$ spinel solid

solution estimated from the JCPDS data is around 0.1451 nm, which is an intermediate value between the d_{440} of $ZnAl_2O_4$ spinel: 0.1429 nm (JCPDS No. 05-669) and that of $ZnGa_2O_4$ spinel: 0.1473 nm (JCPDS No. 38-1240). Although it is not so easy to evaluate and discuss the cell size of the as-prepared spinel because the peaks are so broad, we have done this. The calculated value (d_{440}) for the as-prepared spinel formed under hydrothermal conditions at 180 °C from the precursor solution with composition $ZnAlGaO_4$ using XRD data is 0.1465 nm, which is slightly larger than that of the ideal value: 0.1451 nm. The peak-top position (d_{440}) of the as-prepared spinel which was located near that of $ZnGa_2O_4$ spinel: 0.1473 nm approached the intermediate ideal value of $ZnAlGaO_4$ spinel: 0.1451 nm with increased heating temperature. This result suggests that the possibility of the presences of spinel phase with low crystallinity or amorphous-like phase having a composition rich in Al in the as-prepared spinel nanocrystals in addition to the possibility of the presence of a small amount of OH^- species. The as-prepared state might be composed of Ga-rich $ZnAl_xGa_{1-x}O_4$ spinel phase and a small amount of Al-rich phase with low crystallinity or amorphous-like phase. As shown in Fig. 4, the cell size of the spinel phase gradually approached the ideal one of $ZnAlGaO_4$ as the hydrothermal treatment temperature rose.

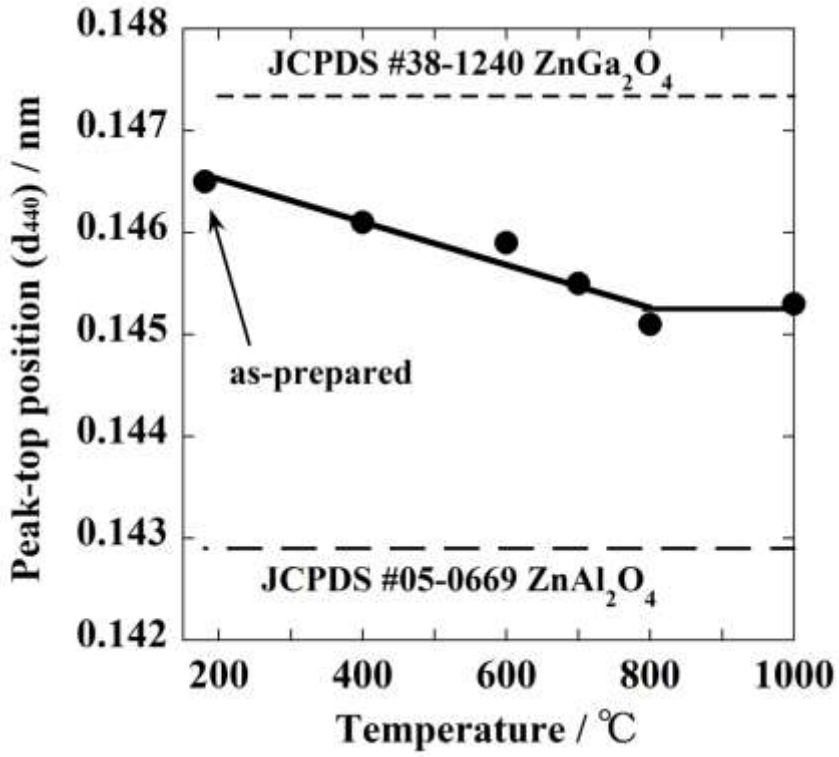

Fig.10 Peak-top position (d_{440}) of cubic spinel phase of samples hydrothermallty formed at 180 °C before and after heating at 400-1000 °C for 1 h.

In the course of heating up to 600 °C in air, a small amount of Al-rich phase with low crystallinity that is present in the as-prepared sample is considered to decrease as a result of the enhancement in crystallinity of spinel phase, which is the main reason why the surface area became smaller monotonically with the temperature (Fig. 8) although the crystallite sizes were almost constant up to 600 °C (Fig. 7). A substantial change in the cell size of the spinel phase after heating at temperatures higher than 800 °C could not be observed.

4-3-3 Optical and luminescence properties

In the present study, the diffuse reflectance spectra of powder samples were measured using an ultraviolet-visible spectrophotometer with an integrating sphere attachment. The diffuse reflectance spectra and plots of transformed Kubelka–Munk function vs. the energy of light absorbed of the as-prepared $ZnAlGaO_4$ spinel and the spinel after heating at 800 and 1000 °C are shown in Fig. 11(a) and (b), respectively. The absorption edge of the samples changed slightly depending on the heat treatment. The optical band gap data obtained for the $ZnAlGaO_4$ spinel as-prepared and after heating at 800 and 1000 °C, which were evaluated based on the plots of transformed Kubelka–Munk function vs. the energy of light absorbed of samples (Fig. 11 (b)), are listed in Table 1.

Table 1: Optical band gap of $ZnAlGaO_4$ spinel

Sample	Optical band gap (eV)
As-prepared	4.58
After heating at 800 °C	4.35
After heating at 1000 °C	4.53

There has been many investigations on the band gap of $ZnAl_2O_4$ and $ZnGa_2O_4$ spinel [42]. According to the results from the estimation on the band gap and structure, the $ZnAl_2O_4$ spinel possesses a larger band gap than $ZnGa_2O_4$ spinel. The band gap values of $ZnAl_2O_4$ spinel calculated using density functional theory (DFT) [43], the tight-binding muffin-tin orbital method (TB-LMTO) [44], GW approximation [43], and the modified Becke-Johnson potential (MBJ) [43] are 4.25, 4.11, 6.55, and 6.18 eV, respectively. On the other hand, the band gap values of $ZnGa_2O_4$ spinel estimated by means DFT, TB-LMTO, GW, and MBJ are 2.82 [43], 2.79 [44], 4.57 [43], and 4.71 eV [43], respectively. The obtained band gap values for $ZnAlGaO_4$ spinel in this study are around 4.5 eV, which may be fairly reasonable. This result is

supported by the report [45], in which the incorporation of aluminum ion into the $ZnGa_2O_4$ lattice results in the blue shifts of the absorption band of $ZnGa_2O_4$, bringing about the wider band gap. However, the band gap value of $ZnAlGaO_4$ spinel derived in this study are a little bit wider than those reported values based on the DFT and TB-LMTO method, on the one hand, and a little bit narrower than those based on the GW and MBJ method, on the other, according to the estimation as intermediate values between $ZnAl_2O_4$ and $ZnGa_2O_4$ spinel.

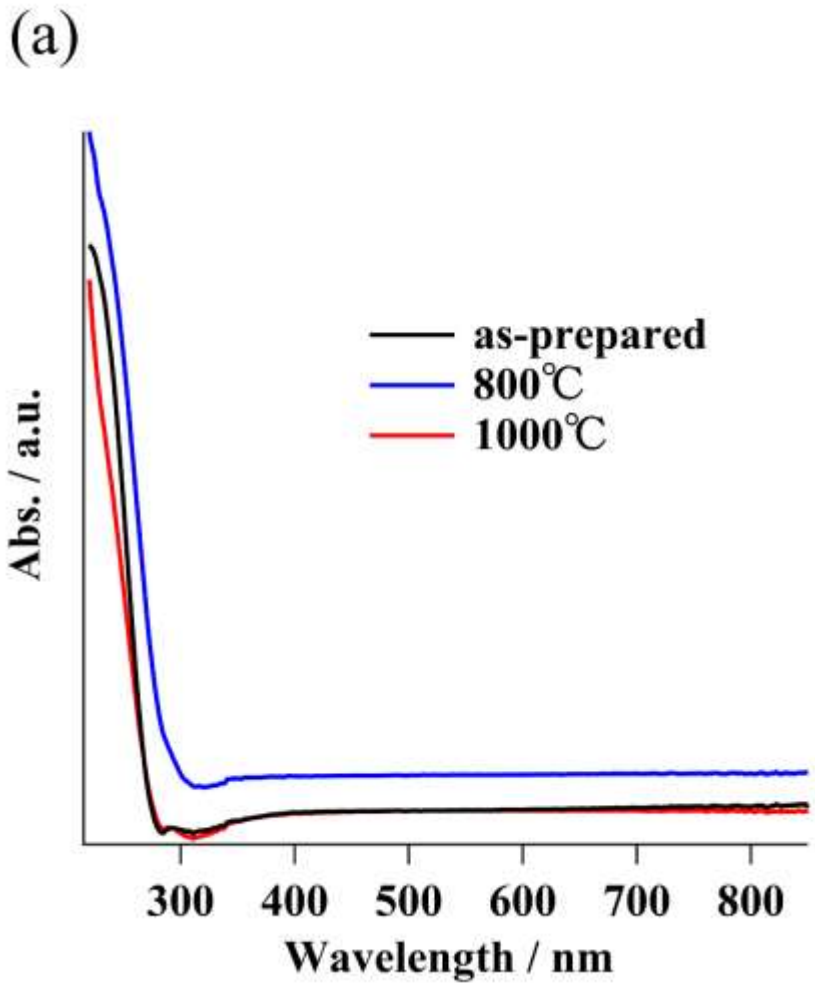

Fig.11(a) Diffuse reflectance spectra of samples hydrothermally formed at 180 °C before and after heating at 1000 °C for 1 h.

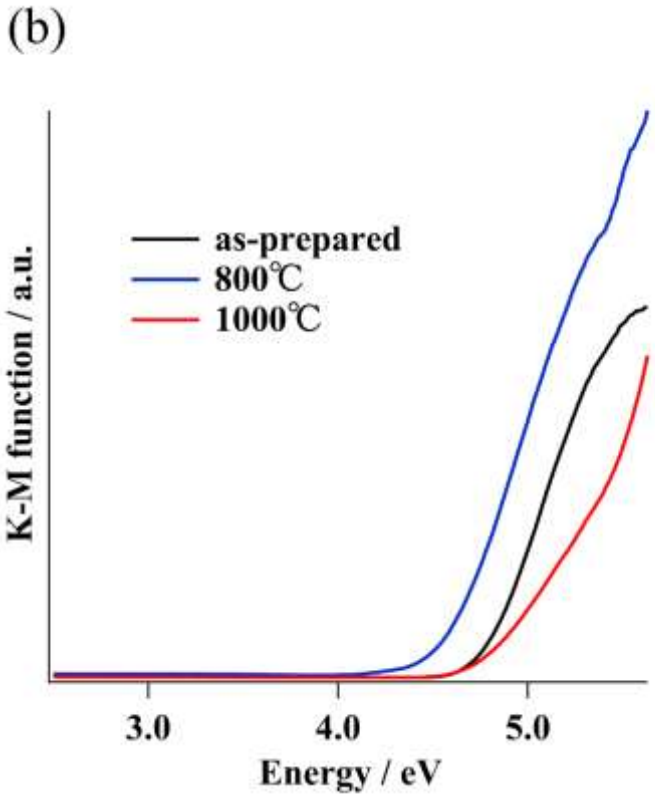

Fig.11(b) Plots of transformed Kubelka-Munk function vs. the energy of light absorbed of samples.

The room temperature photoluminescence spectra under excitation at 270nm for the $ZnAlGaO_4$ spinel as-prepared and after heating at 800 and 1000 °C are shown in Fig. 12. The spectrum of the as-prepared spinel contains a wide band emission in the UV-blue region. The photoluminescence spectrum of the as-prepared spinel changed depending on the heat treatment. The center wavelength of the broadband UV-blue emission for the as-prepared sample was around 360 nm. On the other hand, the center wavelength of the broad band emission for the sample after heating at 800 °C was around 430 nm in the range of UV-blue-green. The spectrum of the spinel heated at 1000 °C seems to consist of more than two main broad band emissions with center wavelength around 360 and 430 nm, and the emission intensity became low.

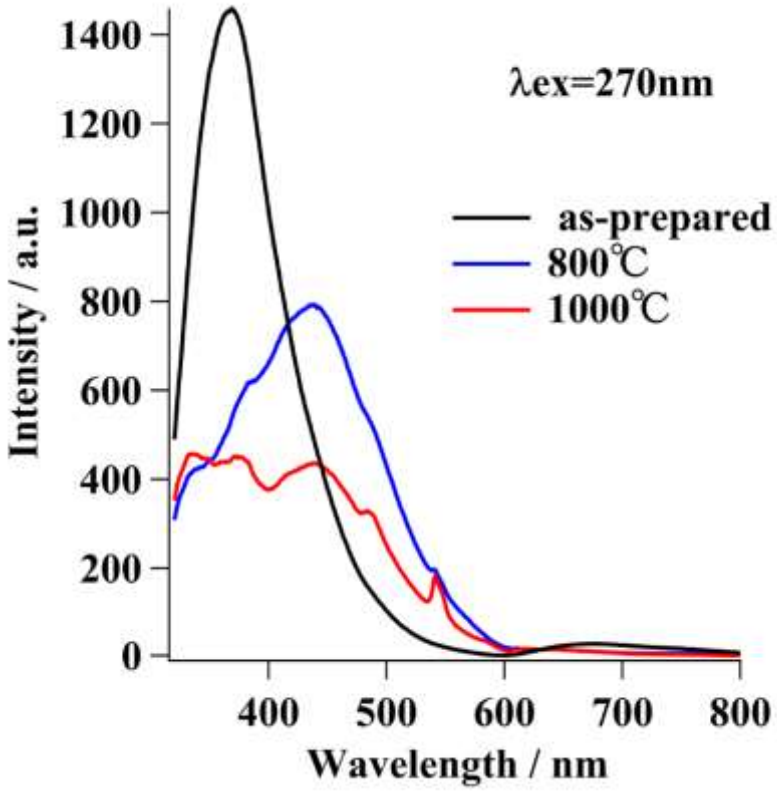

Fig.12 Emission spectra of samples as-prepared at 180 °C and after heating at 800 and 1000 °C for 1 h. (λ_{ex} = 270 nm)

Concerning two main broad bands, a model in which the origin of 360 nm emission is the Ga-O transition at octahedral sites distorted owing to single oxygen vacancies (V^*_O) generation in $ZnGa_2O_4$, whereas 430 nm emission originates from the Ga-O transition of regular octahedral sites without V^*_O in $ZnGa_2O_4$ has been proposed [46]. The observed broad bands are assigned to the charge transfer between Ga^{3+} or Al^{3+} ions at octahedral sites and its surrounding O^{2-} ions [45]. These transitions may originate from the inter-band-gap defects, such as oxygen vacancies. These defects provide donor levels near the conduction band edge of the oxide according to the literature [8, 10, 47, 48] although the origins of the emissions of nano-sized oxides, e.g. spinel-type γ-Ga_2O_3 [49] and γ-Al_2O_3 [50] are still a matter of discussion.

4-4 Summary

$ZnAlGaO_4$ spinel nanocrystals were formed via the hydrothermal route at 150-240 °C for 5 h in the presence of tetramethylammonium hydroxide. The structure, cell size, crystallite size, optical band gap, and luminescence of $ZnAlGaO_4$ spinel were investigated and discussed using as-prepared and post-heated samples. The cell size of as-prepared spinel phase changed slightly as the hydrothermal treatment temperature rose from 150 to 240 °C. The crystallite size of spinel obtained after hydrothermal treatment at 180 °C was around 8 nm. The crystallite growth was accelerated by heating at temperatures higher than 800 °C. The resultant crystallite size of the spinel after heating at 1000 °C was around 44 nm. The cell size of the as-prepared spinel decreased slightly and linearly as the heating temperature rose from 400 to 800 °C. After heating at temperature higher than 800 °C, the cell size reached almost the constant of ideal value, which is intermediate value between the JCPDS data of $ZnAl_2O_4$ spinel and that of $ZnGa_2O_4$ spinel. The optical band gap of the $ZnAlGaO_4$ spinel was around 4.5 eV. The relatively high intensity of UV-visible blue light emissions centered at around 360 and 450 nm were obtained under excitation at 270 nm for $ZnAlGaO_4$ spinel as-prepared and that heat-treated at 800 °C, respectively.

References

1. R. N. C. Rao, C. R. S. Vivekchand, K. Biswasa, Govindaraja, *Dalton Trans.,* **34**:3728–49, (2007)
2. J. W. Dawson, *Am. Ceram. Soc. Bull.,* **67**:1673–78, (1988)
3. M. Hirano, H. Morikawa, M. Inagaki, M. Toyoda, *J. Am. Ceram. Soc.,* **85**:1915-20, (2002)
4. M. Hirano, K. Matsushima, *J. Am. Ceram. Soc.,* **89**:110-17, (2006)
5. M. Hirano, H. Dozono, *J. Solid State Chem.,* **204**:335–40, (2013)
6. T. Minami, *MRS Bull.,* **25**:38-44, (2000)
7. T. Omata, N. Ueda, K. Ueda, H. Kawazoe, *Appl. Phys. Lett.,* **64**:1077-78, (1994)
8. E. L. Shea, K. R. Datta, Brown Jr., J. J. Jr., *J. Electrochem. Soc.,* **141**:1950-54, (1994)
9. G. J. Kho, D. H. Park, P. D. Kim, *Bull, Korean. Chem. Soc.,* **20**:1035-39, (1999)
10. S. Itoh, H. Toki, Y. Sato, K. Morimoto, T. Kishino, *J. Electrochem. Soc.,* **138**:1509-12, (1991)
11. K. T. Tran, W. Park, W. J. Tomm, K. B. Wagner, M. S. Jacobsen, J. C. Summers, N. P. Yocom, K. S. McClelland, *J. Appl. Phys.,* **78**:5691-95, (1995)
12. T. Minami, Y. Kuroi, S. Takata, *J. Vac. Sci. Technol. A,* **14**:1736-40, (1996)
13. X. Zhang, J. Huang, K. Ding, Y. Hou, X. Wang, X. Fu, *Environ. Sci. Technol.,* **43**:5947-51, (2009).
14. Y. X. Chen, C. Ma, J. Z. Zhang, N. B. Wang, *Mater. Res. Bull.,* **45**:1889-93, (2010)
15. L. Mu, J. Wan, Z. Wang, Y. Gao, Y. Qian, *J. Nanosci. Nanotechnol.,* **6**:863-67, (2006)
16. R. A. Phani, M. Passacantando, S. Santucci, *Mater. Chem. Phys.,* **68**:66-71, (2001)
17. K. S. Sampsth, F. J. Cordaro, *J. Am. Ceram. Soc.,* **81**:649-54, (1998)
18. X. Li, Z. Zhu, Q. Zhao, L. Wang, *J. Hazardous Mater.,* **186**:2089-96, (2011)
19. K. T. Shioyama, *U. S. Patent* 4,260,845 (1981)
20. G. Rios Aquilar, M. Valenzuela, P. Salas, H. Armendariz, P. Bosch, G. Del Toro, R. Sila, V. Bertin, S. Castillo, I. A. Schifter, *Appl. Catal. A: General,* **127**:65-75, (1995)
21. T. Nabarany El, A. A. Attia, N. M. Alayn, *Matter. Lett.,* **24**:319-25, (1995)
22. R. Roesky, J. Weiguny, H. Bestgen, U. Dingerdissen, *Appl. Catal. A: General,* **176**:213-20, (1999).
23. Z. Yan, H. Takei, *J. Cryst. Growth,* **171**:131-35, (1997)
24. Z. Yan, H. Takei, H. Kawazoe, *J. Am. Ceram. Soc.,* **81**:180-86, (1998)
25. T. Sei, Y. Nomura, T. Tsuchiya, *J. Non-Cryst. Solids,* **218**:135-38, (1997)
26. M. Hirano, S. Okumura, Y. Hasegawa, M. Inagaki, *Int. J. Inorg. Mater.,* **3**:809-11, (2001)
27. M. Hirano, S. Okumura, Y. Hasegawa, M. Inagaki, *J. Solid State Chem.,* **168**:5-10, (2002)
28. L. Zou, X. Xiang, M. Wei, F. Li, G. D. Evans, *Inorg. Chem.,* **47**:1361-69, (2008)
29. C. A. Tas, J. P. Majewski, F. Aldinger, *J. Mater. Res.,* **17**:1425-33, (2002)
30. M. Hirano, *J. Mater Chem.,* **10**:469-72, (2000)

31. M. Hirano, N. Sakaida, *J. Am. Ceram. Soc.,* **85**:1145-1150, (2002)
32. Y. J. Kim, H. J. Kang, C. D. Lee, Y. D. Jeon, *J. Vac. Soc. Technol.B,* **21**:532-35, (2003)
33 S. W. Hong, L. J. De, X. Yang, N. M. Rahaman, *J. Am. Ceram. Soc.,* **78**:3217-24, (1995)
34. F. G. Huttig, H. Worl, H. H. Weitzer, *Z. Anorg. Allg. Chem.,* **283**:207-16, (1956)
35. K. L. Kurihara, L. S. Suib, *Chem. Mater.,* **5**:609-13, (1993)
36. S. Mathur, M. Veith, M. Haas, H. Shen, N. Lecerf, V. Huch, *J. Am. Ceram. Soc.,* **84**:1921-28, (2001)
37. Y. Wang, K. Wu, : As a whole, *J. Am, Chem. Soc.,* **127**:9686-87, (2005)
38. T. Takeguchi, Y. Kani, M. Inoue, K. Eguchi, *Catal. Lett.,* **83**:49-53, (2002)
39. M. Zawadzki, J. Wrzyszcz, *Mater. Res. Bull.,* **35**:109-14, (2000)
40. Z. Chen, E. Shi, Y. Zheng, W. Li, N. Wu, W. Zhong, *Mater. Lett.,* **56**, 601-605, (2002)
41. P. Kubelka, F. Munk, *Zeits. f. Techn. Physik.,* **12**:593-601, (1931)
42. L. Zhang, F. G. Ji, F. Zhao, Z. Z. Gong, *Chin. Phys. B.,* **20**:047102, (2011)
43. H. Dixit, N. Tandon, S. Cottenier, R. Saniz, D. Lamoen, B. Partoens, V. V. Speybroecl, M. Waroquier, *New J. Phys.,* **13**, 063002, (2011)
44. K. S. Sampath, G. D. Kanhere, R. J. Pandey, *J. Phys. Cond. Matt.* **11**, 3635-44, (1999)
45. K. I.Jeong, L. H. Park, I. S. Mho, *Solid State Commun.,* **105**:179-83, (1998)
46. S. J. Kim, I. H. Kang, N. W. Kim, I. J. Kim, C. J. Choi, L. H. Park, C. G. Kim, W. T. Kim, H. Y. Hwang, I. S. Mho, C. M. Jung, M, Han, *Appl. Phys. Lett.,* **82**:2029-31, (2003)
47. Y. S. Bae, W. H. Seo, W. C. Na, J. Park, *Chem. Commun,* 1834-35, (2004).
48. A. A. Da Silva, S. A. Goçalves, R. M. Davolos, *J. Sol-Gel Sci Technol.,* **49**:101-105, (2009).
49. T. Wang, V. P. Radovanovic, *J. Phys. Chem. C.,* **115**:18473-78, (2011)
50. A. Anjiki, T. Uchino, *J. Phys. Chem. C.,* **116**:15747-55, (2012)

Chapter 5

Low-temperature synthesis of $Zn(Al,Ga)_2O_4$ nanoparticles and thermal change in their structures

5-1 Introduction

Recently, wide-band-gap semiconductor materials such as ZnO, In_2O_3, Ga_2O_3, SnO_2, and TiO_2 have attracted much interest due to superior optical, electric, chemical, photocatalytic, and structural properties [1]. Among oxide spinel compounds, zinc aluminum oxide (zinc aluminate, $ZnAl_2O_4$) and zinc gallium oxide (zinc gallate $ZnGa_2O_4$), both of which exist as an intermediate compound in the ZnO and Al_2O_3 system and in the ZnO and Ga_2O_3 system, respectively, are members of the wide-band-gap semiconductors [2, 3]. The zinc gallate is an ultraviolet-transport electro conductive oxide [2-4] and is proposed as one of low-voltage phosphor materials [5] because of its applications in different areas, e.g. vacuum florescent display [6], field emission display [7], and thin film electroluminescence display [8]. The zinc aluminate is mainly applied for reflective optical coatings [9], UV-transport electro conductive oxide [2], phosphor materials [10], catalysts [11-14] and photocatalyst for the degradation of toluene [15] due to its good properties, e.g. thermomechanical resistance, chemical stability, high thermal stability, and photoluminescence property [16, 17].

A great deal of research effort has been devoted to wet chemical synthesis technique to produce nanometer-sized crystals of inorganic materials [18] because the investigation on their formation techniques as well as controlling their compositions and microstructures can lead to improve their performance. The direct formation of nanocrystalline metal oxides, solid solutions, and complex oxides at low temperatures is also technologically interesting [19]. Although a variety of wet chemical synthesis techniques have been developed to prepare inorganic materials, it is well-known that homogeneous nanocrystalline inorganic materials, e.g. new compounds [20], complex oxides [21], metastable phases [22], and solid solutions [23] can be directly synthesized from aqueous precursor solutions by the mild hydrothermal synthesis method at relatively low temperatures less than 250 °C.

Many studies on the preparation of $ZnGa_2O_4$ spinel, e.g. the solid-state reaction [2, 3, 6], flux method using Li_3PO_4 at high temperature [4, 24, 25], sol-gel method [26], low-temperature direct synthesis [27, 28], co-precipitation [29, 30], homogeneous precipitation [31], hydrothermal method [32, 33], and combustion synthesis [34] have been reported. Various

methods, e.g. solid-state reaction [35], co-precipitation [36], sol-gel [37, 38], template-assisted synthesis [39], hydrothermal synthesis[15-17, 40, 41], and glycothermal synthesis [42] have also been employed to prepare $ZnAl_2O_4$ spinel particles.

In most reports on the hydrothermal preparation of $ZnAl_2O_4$ spinel, the post-heat treatment of samples have been carried out at temperature around 500-800 °C. Although $ZnAl_2O_4$ nanocrystals have been synthesized through hydrothermal method using urea at 180-220 °C for 24-96 h [43], the details on the structures such as lattice parameter and optical band gap of as-prepared $ZnAl_2O_4$ precipitates before post-heat treatment have not been apparent. Furthermore only few studies have been reported concerning the direct formation of spinel-type solid solution nanocrystals in the $ZnAl_2O_4$-$ZnGa_2O_4$ system through hydrothermal route. In addition, there are few works on their hydrothermal synthesis in the presence of tetramethylammonium hydroxide.

There are possibilities that the luminescence properties of $ZnGa_2O_4$ can be controlled via the formation of solid solutions through the substitutional incorporation of aluminum ion into the spinel lattice in the $ZnAl_2O_4$-$ZnGa_2O_4$ system, and what is more, to substitute aluminum for gallium is useful and economical because aluminum is the second most abundant metallic element in the Earth's crust after silicon. The aim of this paper is to prepare luminescent spinel solid solution nanocrystals in the $ZnAl_2O_4$-$ZnGa_2O_4$ system from the aqueous precursor solutions of inorganic metal salts using mild hydrothermal technique at low temperature of 180 °C in a short time. The compositional dependence of the structure and optical and luminescence properties of as-prepared spinel solid solutions has been investigated through comparing those of heat-treated samples.

5-2 Experimental

5-2-1 Sample preparation

The hydrothermal treatment of precursor solutions was carried out at 180 °C for 5 h in the presence of tetramethylammonium hydroxide ($N(CH_3)_4OH$, TMAH). In a Teflon container, a mixture of an aqueous solution of reagent-grade $ZnSO_4$, $Al(NO_3)_3$ and $Ga(NO_3)_3$ in different ratios of Zn/Al/Ga (that was controlled to be the composition: $ZnAl_xGa_{1-x}O_4$, x=0-1.0) was prepared. Before hydrothermal treatment, $N(CH_3)_4OH$ solution was added into the solution mixture until the pH of the solution which was hydrothermally treated became weakly basic. The concentration of TMAH in the solution mixture of samples (x=0-1.0) was 1.33 mol/dm^3. This solution mixture with total cation concentrations (Zn + Al + Ga) of 0.20 mol/dm^3 in the Teflon container was then placed in a stainless-steel vessel. The vessel was tightly sealed and it was heated at 180 °C for 5 h under rotation at 1.5 rpm. After hydrothermal treatment, the precipitates were washed with distilled water until the pH value of the rinsed water became 7.0,

separated from the solution by centrifugation, and dried in an oven at 60 °C. The prepared powders were heated in an alumina crucible at heating rate 200 °C/h, held at 1000 °C for 1 h in air, and then cooled to room temperature in a furnace.

5-2-2 Characterization

The powder X-ray diffraction (XRD) measurement was done at room temperature for the as-prepared and heat-treated powders using CuKα radiation (XRD; RINT-2000, Rigaku, Tokyo, Japan). The morphology of the samples was characterized with transmission electron microscopy (TEM; JEM-2010, JEOL, Tokyo, Japan). The crystallite size of cubic spinel phase was calculated from the line broadening of 311 diffraction peak, according to the Scherrer equation, $D_{XRD} = K\lambda / \beta\cos\theta$, where θ is the Bragg angle of diffraction lines; K is a shape factor ($K = 0.9$ in this work); λ is the wavelength of incident X-rays, and β is the corrected half-width given by $\beta^2 = \beta_m^2 - \beta_s^2$, where β_m is the measured half-width and β_s is the half-width of a standard sample. The lattice parameter of spinel phase was measured using silicon as the internal standard. The specific surface area of the prepared samples was calculated from the adsorption isotherm of nitrogen at 77 K based on the Brunauer-Emmett-Teller method (BET, model; NOVA 1200, Yuasa Ionics, Osaka, Japan).

UV-vis absorption spectroscopy (diffuse reflectance) of the prepared powders was performed at room temperature and in air by means of ultraviolet-visible spectrophotometer with an integrating sphere attachment (V-560, Nihon Bunko, Tokyo, Japan). The spectra were derived from the measured ones using the Kubelka-Munk equation [44]. The measurement of the photoluminescence (PL) emission spectra of samples was carried out at room temperature using a fluorescence spectrophotometer (F-2700, Hitachi High-Tech, Japan) with Xe lamp. Sample powders were excited with 270 nm radiation from a 150 W xenon lamp. The emission wavelength was scanned from 280 nm to 800 nm at a scanning rate of 60 nm/min.

5-3 Results and discussion

5-3-1 Low-temperature formation and heat treatment of $Zn(Al,Ga)_2O_4$ nanoparticles

The hydrothermal treatment of the precursor solution mixtures with compositions: $Zn(Al_xGa_{1-x})_2O_4$, x=0-1.0 was carried out under weakly basic conditions at 180 °C for 5 h in the presence of TMAH. We consider that there is hardly any presence of unreacted metal cations left in the ultrafiltrated solution since there was no presence of the formation of precipitation in the ultrafiltrated solution after hydrothermal treatment by controlling the pH to be 8-9. The XRD patterns of precipitates formed under hydrothermal conditions at 180 °C are shown in Fig. 1(a). Only a single phase corresponding to spinel-type cubic structure was detected in the

precipitates with compositions ranging from $ZnAl_2O_4$ to $ZnGa_2O_4$ and no diffraction peaks due to another crystalline phase was detected. The sharpness in XRD lines corresponding to the crystallinity of products changed depending on the composition between $ZnAl_2O_4$ and $ZnGa_2O_4$. In the composition $ZnGa_2O_4$, a spinel-type product with good crystallinity was prepared. On the other hand, a spinel-type product with very fine crystallite was formed in the composition $ZnAl_2O_4$. Thus, the crystallinity of the as-prepared spinel particles decreased with increased $ZnAl_2O_4$ concentration though spinel-type products were formed in the whole composition range.

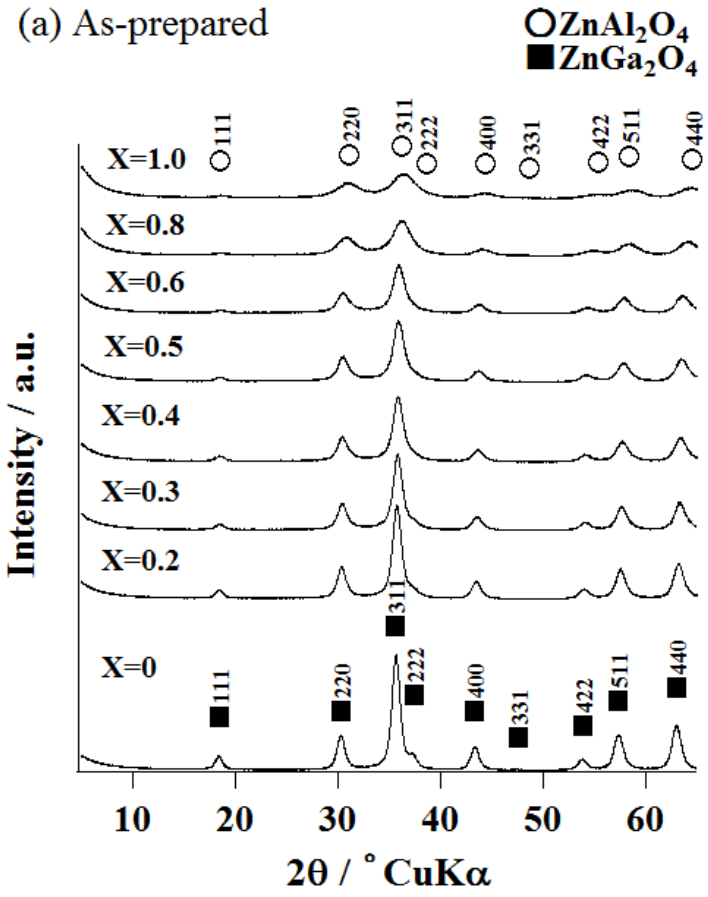

Fig.1 X-ray diffraction patterns of (a) as-prepared samples ($Zn(Al_xGa_{1-x})_2O_4$: x=0~1.0) obtained under hydrothermal conditions at 180 °C for 5 h.

The XRD patterns of the samples with compositions: $Zn(Al_xGa_{1-x})_2O_4$ after heating at 1000 °C for 1 h in air are presented in Fig. 1(b). The diffraction peaks observed in all the recorded XRD patterns corresponded to those of spinel-type cubic structure. No other crystalline phases were detected in the samples. It is found that the XRD lines became fairly sharp and the diffraction peak widths decreased after heat treatment of the as-prepared spinel products. This means that the crystallinity of the spinel phase of the samples was fairly improved via heat treatment. In Figs. 1 (a) and (b), slight and gradual shifts of the XRD lines, e.g. 440 diffraction line of the spinel phase are clearly observed with the change in the composition between $ZnAl_2O_4$ and $ZnGa_2O_4$.

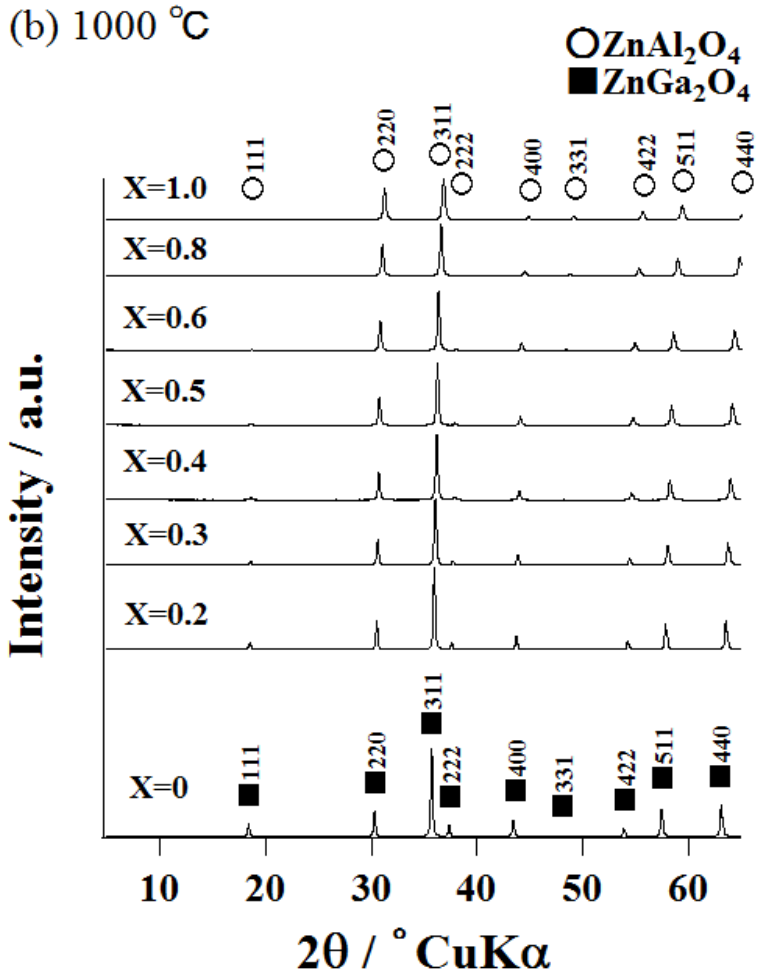

Fig.1 X-ray diffraction patterns of (b) heat-treated samples obtained via heating the as-prepared samples at 1000 °C for 1 h in air.

The TEM images of the as-prepared spinels with compositions x =0, 0.50, and 1.0 formed under hydrothermal conditions at 180°C for 5 h and the spinel with composition x =0.50 after heating at 1000 °C for 1 h are shown in Figures 2(a)~(d), respectively. The particle size of the as-prepared $ZnGa_2O_4$ spinel (x=0, Fig. 2 (a)) is around 10 nm and the lattice fringes of the $ZnGa_2O_4$ spinel are clearly observed since the particles have relatively good crystallinity. On the other hand, the lattice fringes of the as-prepared $ZnAl_2O_4$ spinel (x=1.0, Fig. 2 (c)) are barely observed due to their low crystallinity. The micrographs reveal that the particle size and the crystallinity of the as-prepared spinel precipitates gradually increases when the ratio $ZnGa_2O_4/(ZnGa_2O_4+ZnAl_2O_4)$ increases. The agglomerated particles that were grown up to be 30-50 nm are observed in the $ZnAlGaO_4$ (x=0.50, Fig. 2 (d)) spinel after heating at 1000 °C.

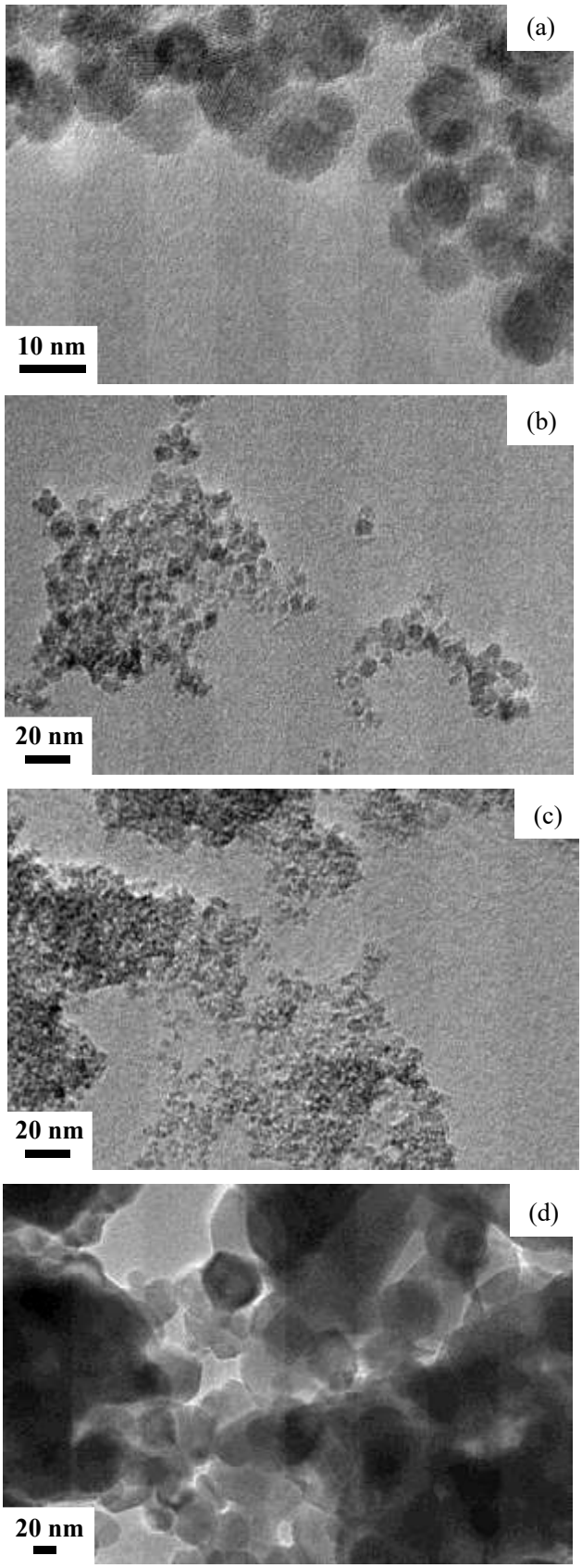

Fig.2 Transmission electron microscopy images of as-prepared $Zn(Al_xGa_{1-x})_2O_4$ samples: (a) x=0, (b) x=0.50, and (c) x=1.0 obtained under hydrothermal conditions at 180 °C for 5 h and heat-treated sample: (d) x=0.50 obtained via heating at 1000 °C for 1 h in air.

The change in the crystallite size of the as-prepared spinel-type precipitates in the $ZnAl_2O_4$–$ZnGa_2O_4$ system, which is estimated from the XRD line broadening, is shown against the composition (Al atomic ratio) of the samples in Fig. 3 (a). This figure indicates that the crystallite size of the as-prepared spinel almost linearly decreases from about 9 to 3 nm as the Al atomic ratio increases from x=0 to 1.0.

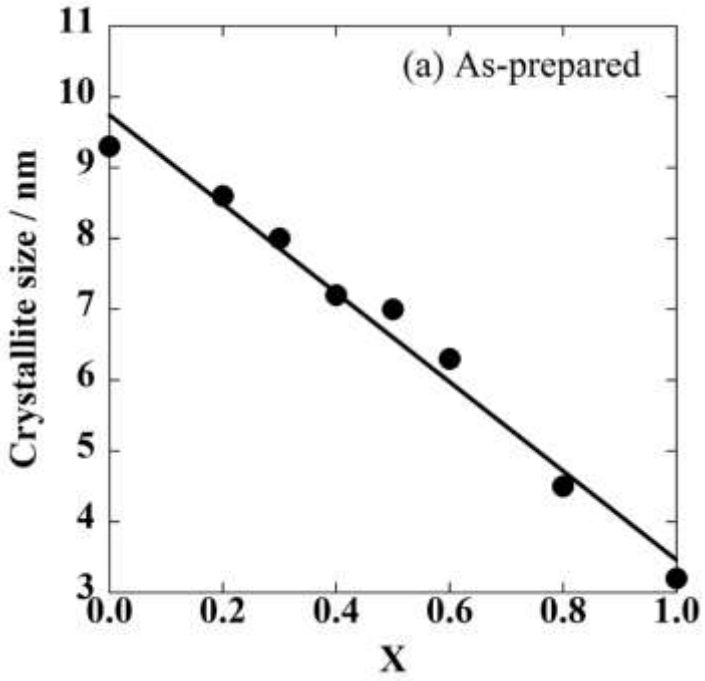

Fig.3 Crystallite size of $Zn(Al_xGa_{1-x})_2O_4$ spinel: (a) as-prepared under hydrothermal conditions at 180 °C for 5 h.

The crystallite sizes of the $Zn(Al_xGa_{1-x})_2O_4$ spinel after heating at 1000 °C for 1 h in air are also indicated in Figure 3(b). The similar relationship between crystallite size and the concentration, Al atomic ratio is observed. The crystallite size of the heat-treated spinel decreased from 52 to 32 nm with increased Al atomic ratio. The growth behavior of crystallite of the as-prepared spinel nanocrystals is observed by comparing the crystallite size of the spinel before and after heating at 1000 °C. The particle sizes of the spinel observed in the TEM micrographs correspond relatively well to the crystallite sizes of spinel phases estimated from the XRD line broadening.

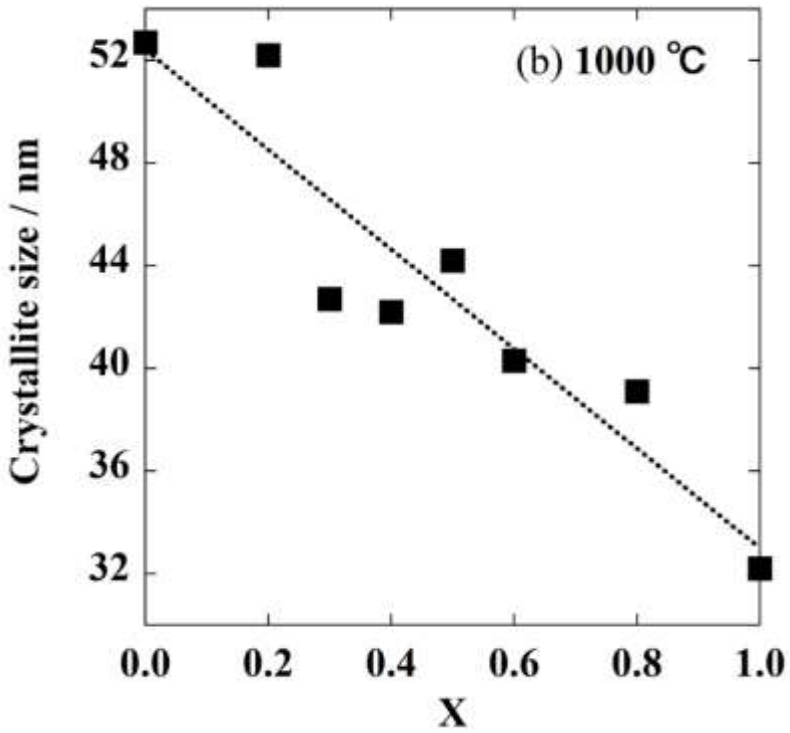

Fig.3 Crystallite size of $Zn(Al_xGa_{1-x})_2O_4$ spinel: (b) heat treated at 1000 °C for 1 h in air.

The specific surface areas of the spinel samples as-prepared and heat treated at 1000 °C are shown as a function of Al atomic ratio in Figures 4(a) and (b), respectively. In both samples, the specific surface areas increased linearly as Al atomic ratio increased corresponding to the behavior of change in the crystallite size of spinel phase, i.e. the compositional dependence of crystallite size. The specific surface areas of the as-prepared spinel precipitates are in the range of 100-235 m^2/g depending on the composition. The incorporation of aluminum component into the lattice, $Zn(Al_xGa_{1-x})_2O_4$ resulted in lower crystallinity of the spinel, which is considered to be due to lower mass transfer of Al component. This is explained by the fact that the component of Al_2O_3 in $ZnAl_2O_4$ has higher refractoriness and higher melting temperature than those of Ga_2O_3 component in $ZnGa_2O_4$. The specific surface area of the samples after the heat treatment at 1000 °C showed relatively small value, which is considered to be due to the formation of agglomerate particles containing closed pores by coagulation and sintering.

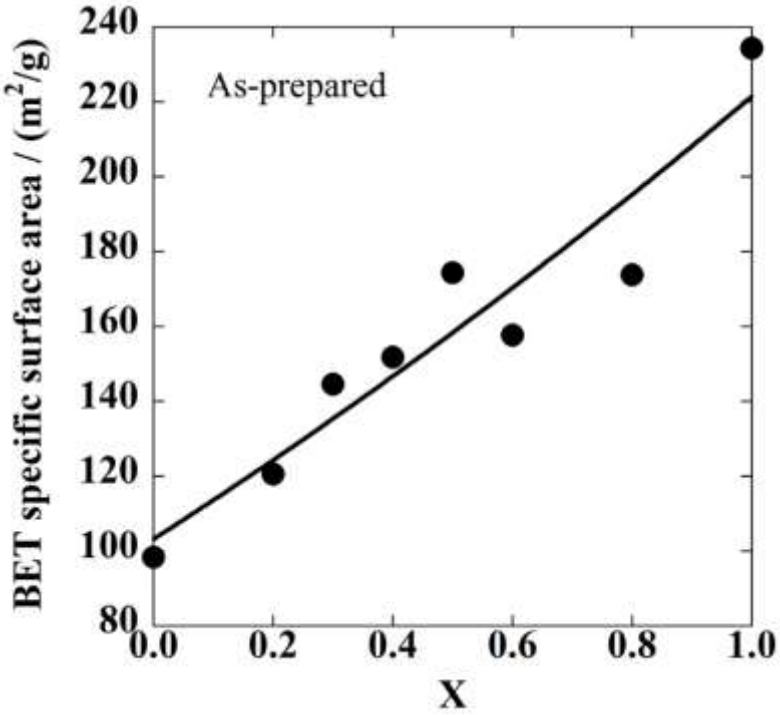

Fig.4 BET specific surface area of $Zn(Al_xGa_{1-x})_2O_4$ spinel: (a) as-prepared under hydrothermal conditions at 180 °C for 5 h.

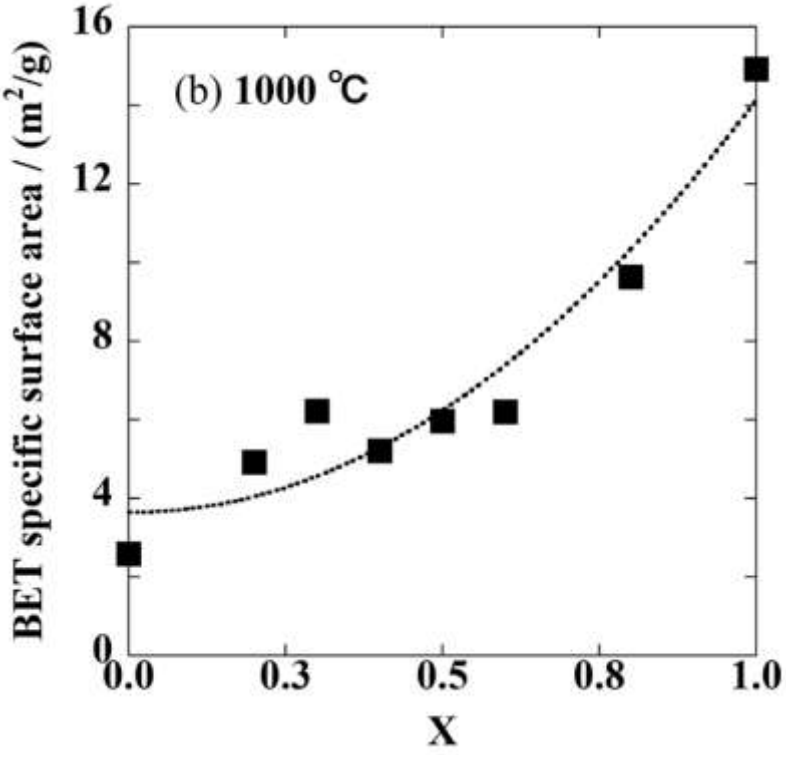

Fig.4 BET specific surface area of $Zn(Al_xGa_{1-x})_2O_4$ spinel: (b) heat treated at 1000 °C for 1 h in air.

5-3-2 Structural of $Zn(Al,Ga)_2O_4$

Figure 5(a) shows the details of region around 56-70 ° 2θ, i.e., the compositional dependence and shifting of the 511 and 440 lines in the XRD patterns of the spinel-type $Zn(Al_xGa_{1-x})_2O_4$ precipitates, together with the XRD lines of the internal standard Si around 56 ° and 69 ° 2θ. It is observed that the XRD lines of the $ZnGa_2O_4$ spinel phase gradually shift into $ZnAl_2O_4$ spinel phase as Al atomic ratio increases in the $Zn(Al_xGa_{1-x})_2O_4$ precipitates.

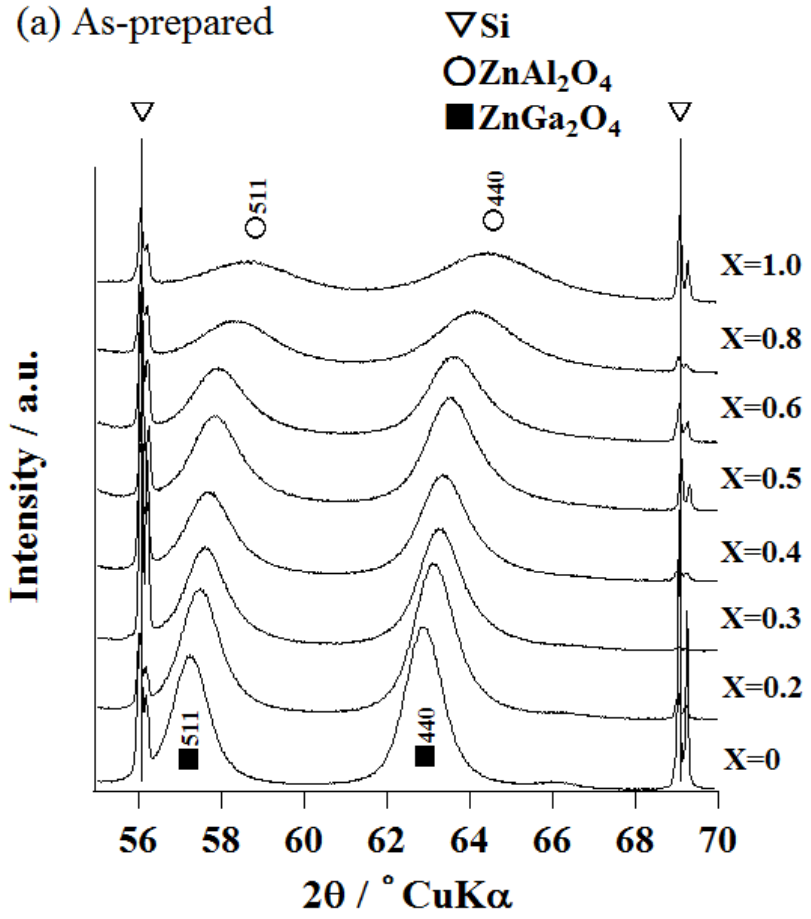

Fig.5 Close-up of the region around 58-64° 2θ of the X-ray diffraction patterns of $Zn(Al_xGa_{1-x})_2O_4$ spinel: (a) as-prepared under hydrothermal conditions at 180 °C for 5 h.

The similar shifting of the 511 and 440 lines in the XRD patterns of the $Zn(Al_xGa_{1-x})_2O_4$ spinel heat treated at 1000 °C is also shown in Fig. 5(b). A clearer gradual shift in the XRD lines of the spinel phases corresponding to the compositional change is observed in the heat-treated samples. These continuous shifting in XRD lines of the spinel phases corresponding to

the change in composition between $ZnAl_2O_4$ and ZnG_2O_4 suggest the formation of spinel-type solid solutions.

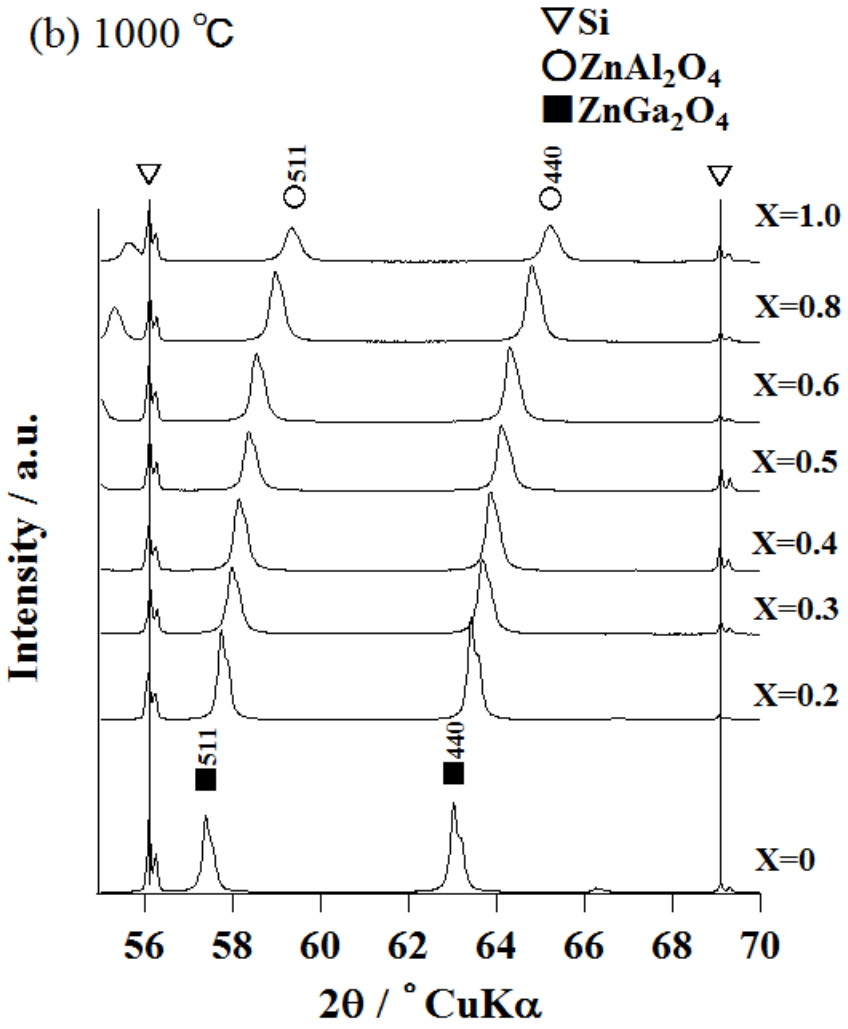

Fig.5 Close-up of the region around 58-64° 2θ of the X-ray diffraction patterns of $Zn(Al_xGa_{1-x})_2O_4$ spinel: (b) heat treated at 1000 °C for 1 h in air.

In Fig. 6, the values of the lattice parameter a_0 of both the as-prepared and heat-treated cubic spinel-type $Zn(Al_xGa_{1-x})_2O_4$ that were determined by XRD using silicon as the internal standard are plotted as a function of Al atomic ratio. The lattice parameter of as-prepared spinel gradually decreased with increased Al atomic ratio. As Al atomic ratio increased in the $Zn(Al_xGa_{1-x})_2O_4$ precipitates, the relationship between the lattice parameter of as-prepared samples and the Al atomic ratio, which is rounded slope line, exists slightly and gradually apart from the ideal linear relationship, i.e., a straight line drown via connecting with the lattice parameter of $ZnGa_2O_4$ spinel and that of $ZnAl_2O_4$ spinel that were heat treated at 1000 °C. This is suggested to be due to the presence of the component with low crystallinity in the range of composition

rich in Al atomic ratio as shown in the TEM image (Fig. 2 (c)). In the heat-treated $Zn(Al_xGa_{1-x})_2O_4$ spinel samples, it was proved that the lattice parameter linearly decreased with increased Al atomic ratio according to the Vegard's Law. The measured lattice parameters for the end members $ZnAl_2O_4$ spinel and $ZnGa_2O_4$ spinel showed perfect coincidence with the published JCPDS data [45, 46] in this case. These results prove that the spinel-type solid solutions between $ZnAl_2O_4$ and $ZnGa_2O_4$ were formed in the present study.

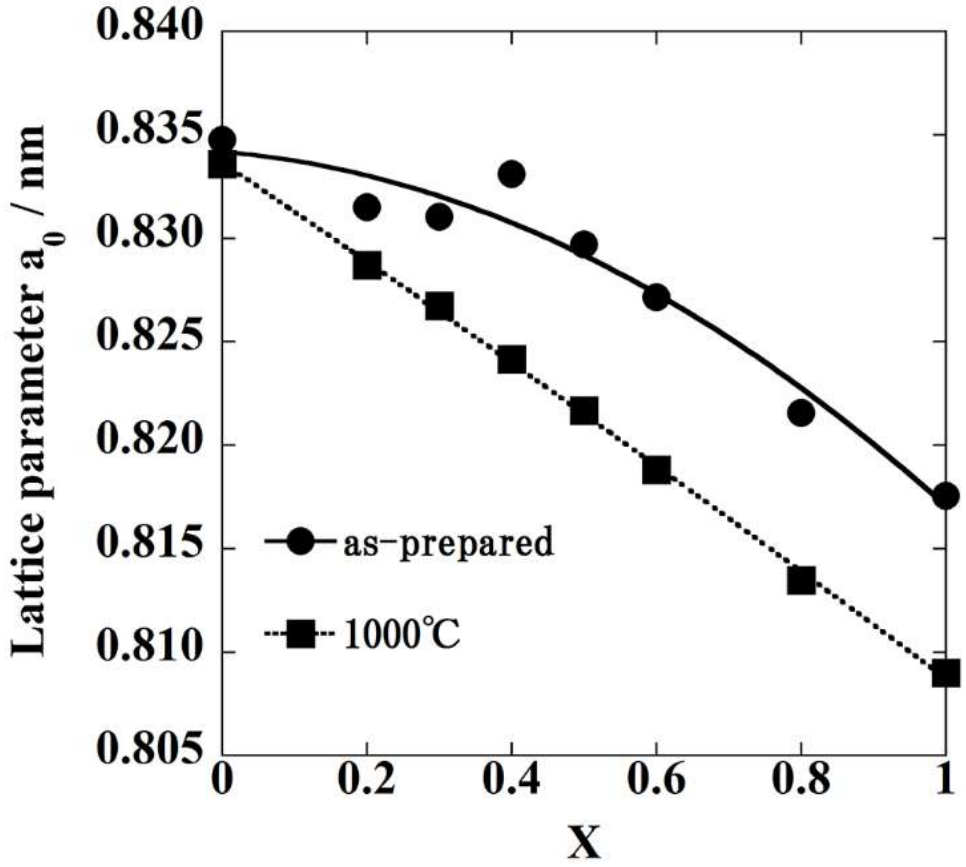

Fig.6 Lattice parameter of $Zn(Al_xGa_{1-x})_2O_4$ spinel: as-prepared under hydrothermal conditions at 180 °C for 5 h and after heating at 1000 °C for 1 h in air.

5-3-3 Optical properties of $Zn(Al,Ga)_2O_4$

The absorbance spectra of the $Zn(Al_xGa_{1-x})_2O_4$ spinels as-prepared and after heat treated were evaluated, respectively. In these spectra, onset of absorption slightly and gradually shifted to shorter wavelengths as the value x (i.e. Al atomic ratio) increases. The plots of transformed Kubelka–Munk function versus the energy of light absorbed of as-prepared $Zn(Al_xGa_{1-x})_2O_4$ spinel samples and heat-treated $Zn(Al_xGa_{1-x})_2O_4$ spinel samples are shown in Figs. 7 (a) and (b), respectively. A clear and gradual shift in the transformed Kubelka–Munk function curve corresponding to the change in Al atomic ratio is observed in both the as-prepared and heat-treated spinel solid solution samples.

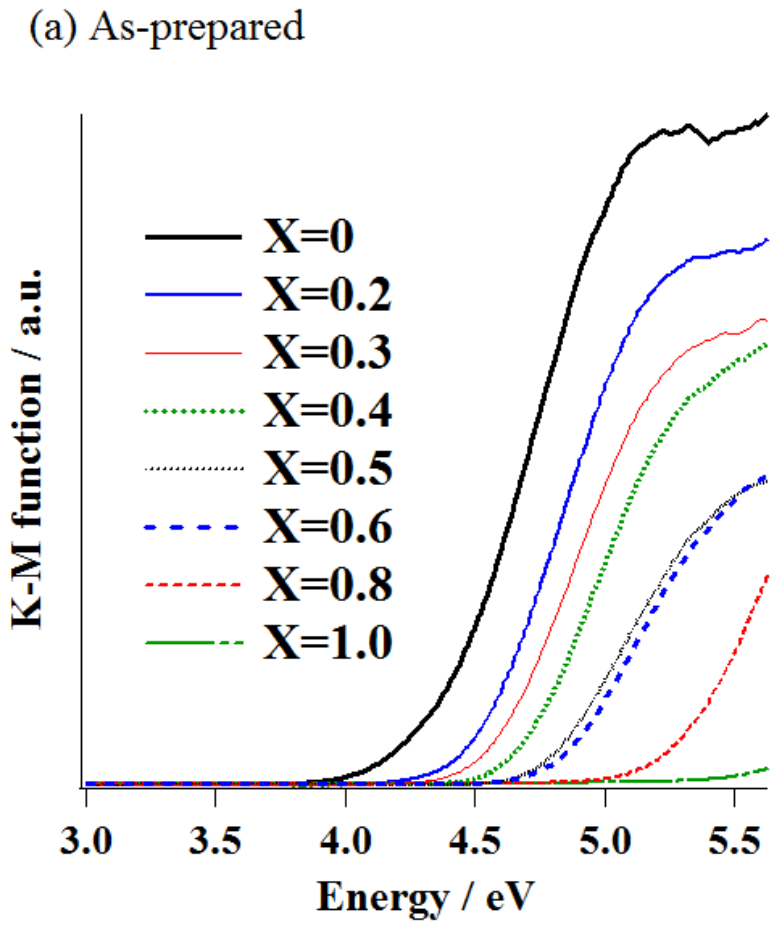

Fig.7 Plots of transformed Kubelka–Munk function vs. the energy of light absorbed of $Zn(Al_xGa_{1-x})_2O_4$ spinel: (a) as-prepared under hydrothermal conditions at 180 °C for 5 h.

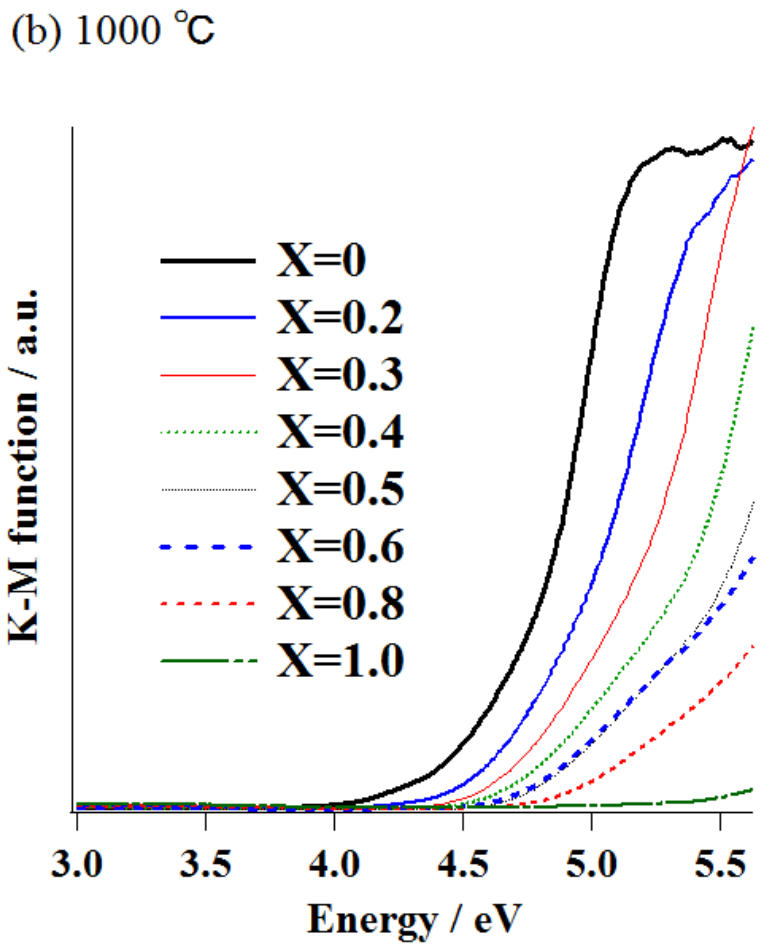

Fig.7 Plots of transformed Kubelka–Munk function vs. the energy of light absorbed of $Zn(Al_xGa_{1-x})_2O_4$ spinel: (b) heat treated at 1000 °C for 1 h in air.

In Figs. 8(a) and (b), the optical band gap values of $Zn(Al_xGa_{1-x})_2O_4$ spinel samples as-prepared and after heat treated at 1000 °C are both plotted as a function of the value x in $Zn(Al_xGa_{1-x})_2O_4$, respectively. Note that the optical band gap almost linearly increases as the value x, Al atomic ratio increases in both the as-prepared and heat-treated spinel samples.

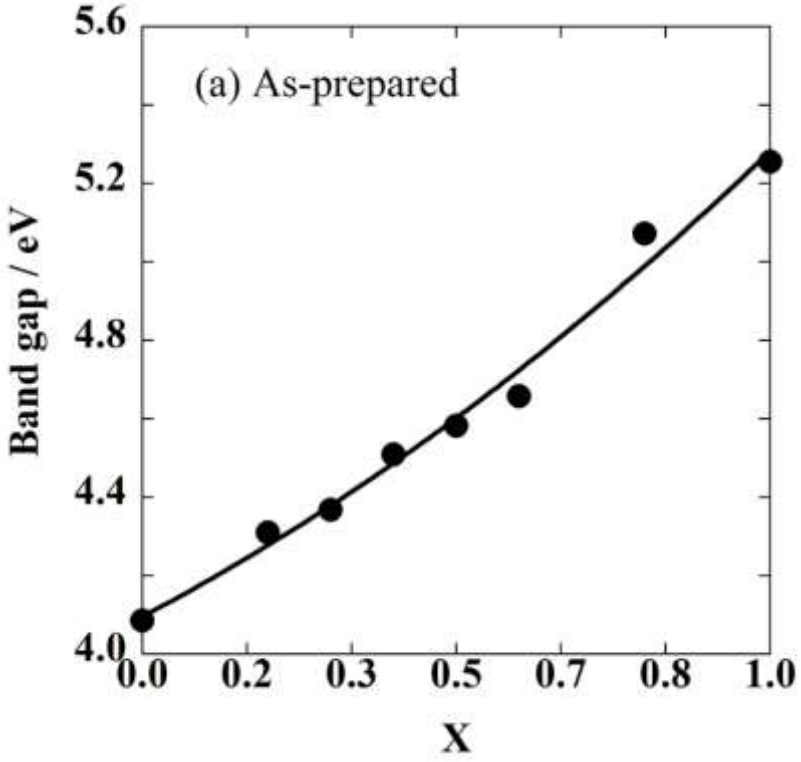

Fig.8 Optical band gap of $Zn(Al_xGa_{1-x})_2O_4$ spinel: (a) as-prepared under hydrothermal conditions at 180 °C for 5 h.

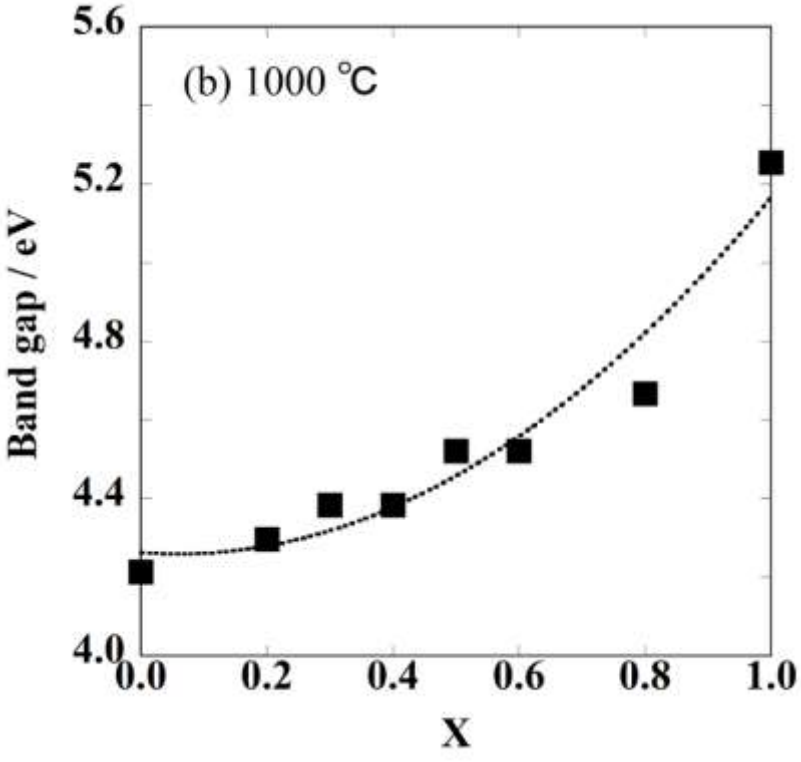

Fig.8 Optical band gap of $Zn(Al_xGa_{1-x})_2O_4$ spinel: (b) heat treated at 1000 °C for 1 h in air.

Both $ZnAl_2O_4$ spinel and $ZnGa_2O_4$ spinel are wide-band-gap semiconductors and there are reports on the calculation or estimation of their band gaps from their electronic and band structures using the tight-binding muffin-tin orbital method (TB-LMTO) [47], density functional theory (DFT) [48], the GW approximation [49], and the modified Becke-Johnson potential (MBJ) [50, 51]. The band gap values of $ZnAl_2O_4$ spinel and $ZnGa_2O_4$ spinel calculated using DFT are 4.25 and 2.82 eV, respectively [48]. The study using TB-LMTO shows that $ZnAl_2O_4$ and $ZnGa_2O_4$ are direct-band-gap materials with band gap of 4.11 and 2.79 eV, respectively [47]. The band gap values of $ZnAl_2O_4$ and $ZnGa_2O_4$ calculated using GW approximation are 6.55 and 4.57 eV, respectively [49]. The band gap values of $ZnAl_2O_4$ and $ZnGa_2O_4$ estimated using MBJ have been reported to be 6.18 and 4.71 eV, respectively [50, 51]. These above theoretical estimations show that the $ZnAl_2O_4$ spinel has a larger band gap value than $ZnGa_2O_4$ spinel. However, the experimental values of the band gap of spinel-type $ZnAl_2O_4$ and $ZnGa_2O_4$ have been reported to be 3.8-3.9 and 4.4-5.0 eV, respectively [3]. Since there are differences between these calculated values and experimental values, many investigations and discussions have been done [52].

In the present study, the results showed that the optical band gap of $Zn(Al_xGa_{1-x})_2O_4$ spinel solid solutions linearly increased from 4.1~4.2 eV for $ZnGa_2O_4$ spinel to 5.25 eV for $ZnAl_2O_4$ spinel with increased Al atomic ratio. Thus, it is obvious that the $ZnAl_2O_4$ spinel possesses a larger band gap value than $ZnGa_2O_4$ spinel. This experimental result corresponded well with the estimation derived from those theories above mentioned. The similar phenomenon, i.e., the increase in the band gap of spinel by the incorporation of aluminum ion into the lattice has been reported in the literature on the $Zn(Al_xGa_{1-x})_2O_4$ spinel synthesized based on the solid-state reaction [53].

The photoluminescence characteristics of the $Zn(Al_xGa_{1-x})_2O_4$ spinel solid solutions were investigated. The room temperature emission spectra of as-prepared $Zn(Al_xGa_{1-x})_2O_4$ spinels and those after heated at 1000 °C under excitation at 270nm are presented in Figs. 9(a) and (b), respectively. The emission spectra of those samples show broad-band emission in the range of UV-blue-green. The photoluminescence band of $ZnGa_2O_4$ spinel tended to show blue shifts by the incorporation of aluminum ion into the spinel lattice. The similar phenomenon has been reported in the $Zn(Al_xGa_{1-x})_2O_4$ spinels fabricated via solid-state reaction [53]. These shifts of photoluminescence band of $ZnGa_2O_4$ spinel via substitutional incorporation of Al into the $ZnGa_2O_4$ spinel, e.g., the shift from 360 to around 320 nm which are clearly observed in the heat treated samples at 1000 °C (in Fig. 9(b)), are considered to be the blue shifts due to wider band gap of Al-substituted $Zn(Al,Ga)_2O_4$ spinel (as shown in Fig. 8).

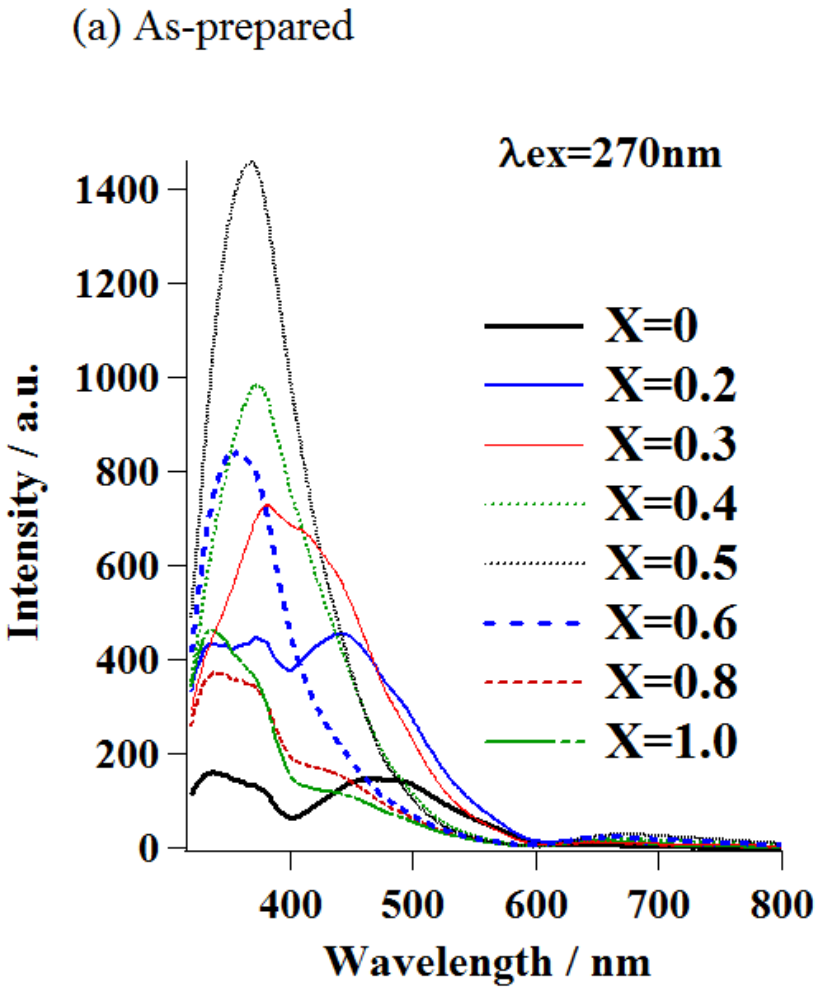

Fig.9 Emission spectra of $Zn(Al_xGa_{1-x})_2O_4$ spinel: (a) as-prepared under hydrothermal conditions at 180 °C for 5 h. (λ_{ex} = 270 nm)

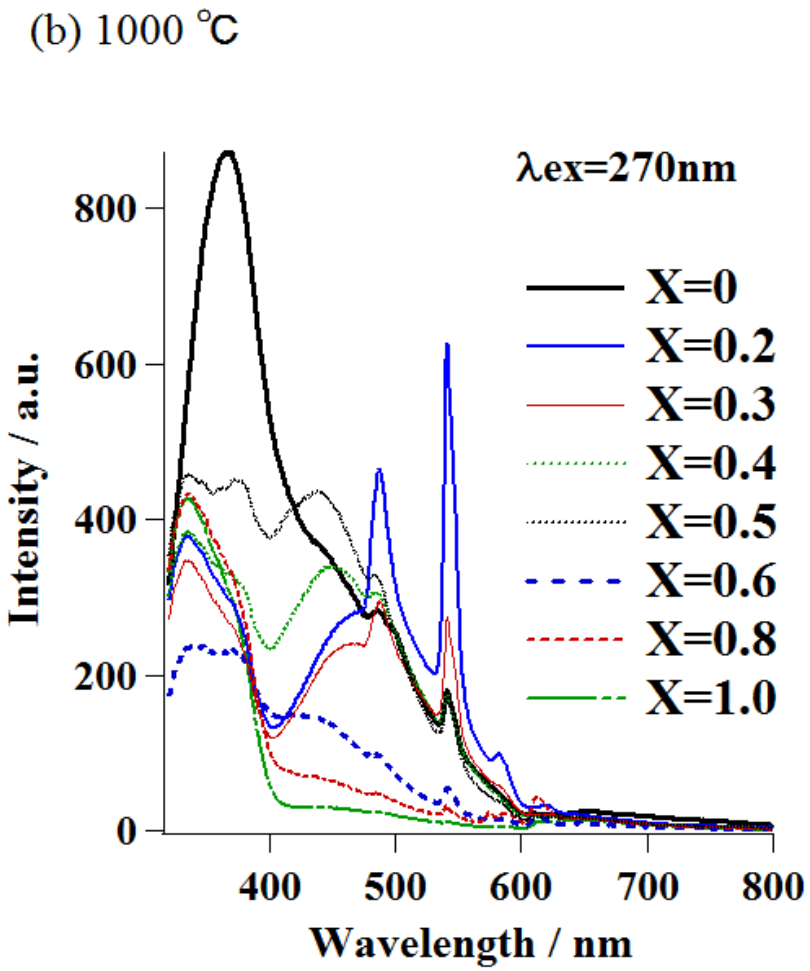

Fig.9 Emission spectra of $Zn(Al_xGa_{1-x})_2O_4$ spinel: (b) heat treated at 1000 °C for 1 h in air. (λ_{ex} = 270 nm)

It has been demonstrated that the blue emission of spinel oxide phosphors such as $ZnGa_2O_4$ and $ZnAl_2O_4$ originates from charge transfer between Al^{3+} or Ga^{3+} at octahedral sites and its surrounding O^{2-} and it is due to inter-band-gap defects, such as oxygen vacancies [53-55]. In general, the characteristic blue band emission around 430 nm from the self-activation center of Ga-O groups is observed in bulk $ZnGa_2O_4$ phosphors [53]. The broad-band emission spectra and their peak wavelengths subtly changed depending on the composition and heat treatment, and two main broad-band emission spectra centered at about 360 and 430 nm were observed in the present study. Some samples, e.g., especially the sample x=0.20 after heating at 1000 °C, show emission bands containing additional sharp peaks observed at around 480~580 nm, which is supposedly due to a certain discrete energy level. These additional sharp peaks in the solid solution samples with composition x =0.20 and 0.30 after heating at 1000 °C in air suggest that the existence of inter-band-gap defects corresponding to around 2.5 eV (490 nm) and 2.3 eV (540 nm) which provide donor level near the conduction band edge of the spinel oxide. In this

system, it is proper to think that the change in the bang gap relates to the structural condition of the octahedral $(Ga,Al)O_6$ group and the defects such as oxygen vacancies in $Zn(Al,Ga)_2O_4$ effect the emission band in the range of 300 and 600 nm.

It has been proposed that the origin of 360 nm emission is the Ga-O transition at distorted octahedral sites with single oxygen vacancies (V^*_O) in $ZnGa_2O_4$, whereas 430 nm emission originates from the Ga-O transition of regular octahedral sites without V^*_O in $ZnGa_2O_4$ [56]. We consider that the shift of the broad-band emission maximum into 360 nm observed in the pure $ZnGa_2O_4$ samples (x = 0) after heat treatment at 1000 °C (in Fig. 9(b)) is due to the increase in the Ga-O transition at distorted octahedral sites with single oxygen vacancies (V^*_O) in $ZnGa_2O_4$.

Although to find out the origins of the emissions is out of this study, the following recent discussions and suggestions on the origins of the emissions from spinel-type γ-Ga_2O_3 [57] and γ-Al_2O_3 [58] has been reported in addition to the above literatures since the origins of the emissions of nano-sized oxides are still a matter of discussion. A blue photoluminescence of spinel-type γ-Ga_2O_3 nanocrystals has been explained that it is associated with the presence of the vacancy-defect sites, and assigned to the donor (an oxygen vacancy)-acceptor (a gallium-oxygen vacancy pair) pair recombination. The defect sites on nanocrystals surfaces (OH^- or O^{2-}) also influence the donor-acceptor pair recombination by trapping photogenerated valence bond holes [57]. It has been demonstrated that the blue photoluminescence emission characterized by fast decay constants of spinel-type γ-Al_2O_3 nanocrystals results from the photoinduced excited state of O_2, and the slow photoluminescence emission observed at low temperature ~200 K results in a defect pair formed through the dehydration reaction of the residual OH^- groups at the surface of oxide nanoparticles such as γ-Al_2O_3 [58].

Each emission band of $Zn(Al_xGa_{1-x})_2O_4$ spines tended to shift to lower energies via heating at high temperature of 1000 °C in this study, which is considered to be due to the decrease in the quantum confinement effect in accordance with the increase in the particle size. A similar phenomenon has been reported in the UV and visible bands from ZnO nanocrystalline particles, in which emission bands shifted to higher wavelengths as the ZnO particle size increased [59].

5-4 Summary

Spinel-type solid solutions in the $ZnAl_2O_4$-$ZnGa_2O_4$ system were hydrothermally prepared as nanocrystals from the aqueous precursor solutions of inorganic metal salts at 180 °C for 5 h in the presence of tetramethylammonium hydroxide. The crystallite size of the as-prepared $Zn(Al,Ga)_2O_4$ nanoparticles linearly decreased from 9 to 3 nm as Al atomic ratio in the composition increased in the system. The lattice parameter of the as-prepared spinel-type nanoparticles with compositions rich in Al existed a little bit apart from that estimated from the Vegard's law as the Al atomic ratio increased in the composition. Each lattice parameter of

spinel solid solution in the whole range of composition perfectly accorded with the theoretical value via heat treatment at 1000 °C. The optical band gap of the spinel solid solutions linearly increased with increase in the aluminum ion incorporated into the lattice. The emission spectra of the spinel solid solutions showed broad band composed of two main peaks in the range of UV-blue-green (300~600 nm). The blue shifts of the photoluminescence band of $ZnGa_2O_4$ spinel were observed by the incorporation of the aluminum ion into the spinel lattice in accordance with their resultant wider band gaps.

References

1. R. G. Gordon, *MRS Bull.,* **25**:52-57, (2000)
2. T. Minami, *MRS Bull.,* **25**:38-44, (2000)
3. S. K. Sampsth, J. F. Cordaro, *J. Am. Ceram. Soc.,* **81**:649-54, (1998)
4. T. Omata, N. Ueda, K. Ueda, H. Kawazoe, *Appl. Phys. Lett.,* **64**:1077, (1994)
5. S. Itoh, H. Toki, Y. Sato, K. Morimoto, T. Kishino, *J. Electrochem. Soc.,* **138**:1509-1512, (1991)
6. L. E. Shea, R. K. Datta, J. J., Jr. Brown, *J. Electrochem. Soc.,* **141**:1950-1954, (1994)
7. T. K. Tran, W. Park, J. W. Tomm, B. K. Wagner, S. M. Jacobsen, C. J. Summers, P. N. Yocom, S. K. McClelland, *J. Appl. Phys.,* **78**:5691-5695, (1995)
8. T. Minami, Y. Kuroi, S. Takata, *J. Vac. Sci. Technol. A,* **14**:1736-1740, (1996)
9. A. R. Phani, M. Passacantando, S. Santucci, *Mater. Chem. Phys.,* **68**:66-71, (2001)
10. H. Matsui, C. N. Xu, H. Tateyama, *Appl. Phys. Lett.,* **78**:1068-1070, (2001)
11. T. K. Shioyama, *U. S. Patent,* 4,260,845, (1981)
12. G. Aquilar-Rios, M. Valenzuela, P. Salas, H. Armendariz, P. Bosch, G. Del Toro, R. Sila, V. Bertin, S. Castillo, A. I. Schifter, *Appl. Catal. A: General,* **127**:65-75, (1995)
13. T. El-Nabarany, A.A.Attia, M. N. Alayn, *Matter. Lett.,* **24**:319-325, (1995)
14. R. Roesky, J. Weiguny, H. Bestgen, U. Dingerdissen, *Appl. Catal. A: General,* **176**:213-220, (1999)
15. X. Li, Z. Zhu, Q. Zhao, L. Wang, *J. Hazardous Mater.,* **186**:2089-2096 (2011)
16. X. Y. Chen, C. Ma, Z. J. Zhang, B. N. Wang, *Mater. Res. Bull.,* **45**:1889-1893, (2010)
17. L. Mu, J. Wan, Z. Wang, Y. Gao, Y. Qian, *J. Nanosci. Nanotechnol.,* **6**:863-867, (2006)
18. D. J. Norris, A. L. Efros, S. C. Erwin, *Science,* **319**:1776-1779, (2008)
19. C. B. Murray, C. R. Kagan, M. G. Bawendi, *Annu. Rev. Mater. Sci.,* **30**:545-610, (2000)
20. M. Hirano, H. Morikawa, M. Inagaki, M. Toyoda, *J. Am. Ceram. Soc.,* **85**:1915-1920, (2002)
21. M. Hirano, H. Dozono, *Mater. Chem. Phys.,* **143**:860-866, (2014)
22. M. Hirano, K. Matsushima, *J. Nanosci. Nanotechnol.,* **6**:762-770, (2006)
23. M. Hirano, H. Dozono, *J. Am. Ceram. Soc.,* **96**:3394-3400, (2013)
24. Z. Yan, H. Takei, *J. Cryst. Growth,* **171**:131-35, (1997)
25. Z. Yan, H. Takei, H. Kawazoe, *J. Am. Ceram. Soc.,* **81**:180-86, (1998)
26. T. Sei, Y. Nomura, T. Tsuchiya, *J. Non-Cryst. Solids,* **218**:135-38, (1997)
27. M. Hirano, S. Okumura, Y. Hasegawa, M. Inagaki, *Int. J. Inorg. Mater.,* **3**:809-811, (2001)
28. M. Hirano, S. Okumura, Y. Hasegawa, M. Inagaki, M., *J. Solid State Chem.,* **168**:5-10, (2002)
29. J.-G. Kho, H.-D. Park, D.-P. Kim, Bull, *Korean. Chem. Soc.,* **20**:1035-1039, (1999)
30. L. Zou, X. Xiang, M. Wei, F. Li, D. G. Evans, *Inorg. Chem.,* **47**:1361-1369, (2008)

31. A. C. Tas, P. J. Majewski, F. Aldinger, *J. Mater. Res.,* **17**:1425-1433, (2002)
32. M. Hirano, *J. Mater Chem.,* **10**:469-472, (2000)
33. M. Hirano, N. Sakaida, *J. Am. Ceram. Soc.,* **85**:1145-1150, (2002)
34. J. Y. Kim, J. H. Kang, D. C. Lee, D. Y. Jeon, *J. Vac. Soc. Technol. B,* **21**:532-535, (2003)
35. W. S. Hong, J. L. De, X. Yang, M. N. Rahaman, *J. Am. Ceram. Soc.,* **78**:3217-3224, (1995)
36. G. F. Huttig, H. Worl, H. H. Weitzer, Z. Anorg, *Allg. Chem.,* **283**:207-2016, (1956)
37. L. K. Kurihara, S. L. Suib, *Chem. Mater.,* **5**:609-613, (1993)
38. S. Mathur, M. Veith, M. Haas, H. Shen, N. Lecerf, V. Huch, *J. Am. Ceram. Soc.,* **84**:1921-1928, (2001)
39. Y. Wang, K. Wu, *J. Am, Chem. Soc.,* **127**:9686-9687, (2005)
40. M. Zawadzki, J. Wrzyszcz, *Mater. Res. Bull.,* **35**:109-114, (2000)
41. Z. Chen, E. Shi, Y. Zheng, W. Li, N. Wu, W. Zhong, *Mater. Lett.,* **56**:601-605, (2002)
42. T. Takeguchi, Y. Kani, M. Inoue, K. Eguchi, *Catal. Lett.,* **83**:49-53, (2002)
43. X. Y. Chen, C. Ma, Z. J. Zhang, B. N. Wang, *Mater. Sci. Eng. B,* **151**:224-230, (2008)
44. P. Kubelka F. Munk, *Zeits. f. Techn. Physik.,* **12**:593-601, (1931)
45. JCPDS No. 05-0669
46. JCPDS No. 38-1240
47. S. K. Sampath, D. G. Kanhere, R. Pandey, *J. Phys. Cond. Matt.,* **11**:3635-364, (1999)
48. H. Dixit, N. Tandon, S. Cottenier, R. Saniz, D. Lamoen, B. Partoens, V. V. Speybroecl, M. Waroquier, *New J. Phys.,* **13**:063002, (2011)
49. W. G. Aulbur, L. Jönsson, J. W. Wilkins, *Solid State Phys.,* **54**:1-218, (1999)
50. F. Tran, P. Blaha, *Phys. Rev. Lett.,* **102**:226401, (2009)
51. F. Tran, P. Blaha, K. Schwarz, *J. Phys. Condens. Matter,* **19**:196208, (2007)
52. L. Zhang, G.-F. Ji, F. Zhao, Z.-Z. Gong, *Chin. Phys. B.,* **20**:047102, (2011)
53. I. K. Jeong, H. L. Park, S. I. Mho, *Solid State Commun.,* **105**:179-183, (1998)
54. M. Cao, I. Djerdj, M. Antonietti, M. Niederberger, *Chem. Mater.,* **19**:5830-5832, (2007)
55. A. A. D. Silva, A. S. Goçalves, M. R. Davolos, *J. Sol-Gel Sci Technol.,* **49**:101-105, (2009)
56. J. S. Kim, H. I. Kang, W. N. Kim, J. I. Kim, J. C. Choi, H. L. Park, G. C. Kim, T. W. Kim, Y. H. Hwang, S. I. Mho, M.-C. Jung, M. Han, *Appl. Phys. Lett.,* **82**:2029-2031, (2003)
57. T. Wang, P. V. Radovanovic, *J. Phys. Chem. C.,* **115**:18473-18478, (2011)
58. A. Anjiki T. Uchino, *J. Phys. Chem. C.,* **116**:15747-15755, (2012)
59. A. Van Dijken, E. A. Meulenkamp, D. Vanmaekelbergh, A. Meijerink, *J. Lumin,* **90**:123-128, (2000)

Chapter 6

Hydrothermal formation of spinel-type complete solid solution in the $ZnAl_2O_4$-$ZnGa_2O_4$ system

6-1 Introduction

Materials based on the spinel structure, AB_2O_4, which can be described by means of a cubic close packed arrangement of anions with one-half of the octahedral holes and one-eighth of the tetrahedral holes occupied by cations, possess high potentials and unique properties and have played an important part in various uses, e.g. the optical [1], magnetic [2], biomagnetic [3], electrochemical [4], electrocatalytic [5], and catalytic [6] fields of applications. Zinc aluminate ($ZnAl_2O_4$) and zinc gallate ($ZnGa_2O_4$) have the same spinel structure of AB_2O_4 which belong to the wide-band-gap semiconductor materials [7], e.g. ZnO, In_2O_3, and SnO_2. Both of $ZnAl_2O_4$ and $ZnGa_2O_4$ are known to have a normal spinel structure with all the Zn^{2+} ions in tetrahedral sites and Ga^{3+} or Al^{3+} ions in octahedral sites [8].

In recent years, zinc gallate has attracted attention as one of excellent phosphor host materials for applications in thin film electroluminescent devices (TFED), vacuum fluorescent displays (VFD), and field emission displays (FED) [9-13]. A blue emission of $ZnGa_2O_4$ without any dopant via a self-activation center of Ga-O groups under excitation by both UV light and low-voltage electrons [10, 14] changes to green or up to red when it is activated with Mn^{2+}, Cr^{3+}, Eu^{3+}, and Tb^{3+} [15-17]. The zinc aluminate also possesses unique properties and has been used as phosphor materials [18-20], reflective optical coatings [21], UV-transport electro conductive oxide [22], photocatalyst for the degradation of toluene [23], and catalysts for dehydration, hydrogenation, dehydrogenation, and synthesis of fine chemicals [24-27].

These days, there is considerable interest in producing nanometer-sized crystals of inorganic materials [28] via wet chemical synthesis route, since the properties and performance of inorganic materials are closely linked to their synthesis routes in general. The direct formation of nanocrystals of solid solutions and complex oxides [29, 30] with a controlled size and various morphologies at low temperatures has been of technological and scientific interest. The hydrothermal method, which is one of representative wet chemical synthesis techniques, is known to be useful for the synthesis of fine inorganic materials, especially those based on oxide nanocrystals [31-33].

In the literature on the preparation of spinel-type $ZnGa_2O_4$, various synthetic methods such

as the flux method [11, 34, 35], solid-state reaction [12, 17], co-precipitation [11, 36], homogeneous precipitation [37], the sol-gel method [38], low-temperature and direct crystallization at 25-90 °C [39, 40], hydrothermal synthesis [41, 42], and combustion synthesis [43] have been reported. Many synthetic techniques, for instance, solid-state reaction [44], co-precipitation [45], sol-gel [46, 47], spray pyrolysis [20], hydrothermal synthesis [48-51], template-assisted synthesis [52], and glycothermal synthesis [53] have also been employed for the preparation of $ZnAl_2O_4$ spinel. However, in the most literature, the detail of the structure such as lattice parameter of as-prepared $ZnAl_2O_4$ spinel that was synthesized via hydrothermal route without post-heat treatment in air has not been shown. Moreover, the influence of the composition of $Zn(Al_xGa_{1-x})_2O_4$ on the structure and properties of the spinel nanocrystals formed through hydrothermal route has hardly been investigated. It has been reported that $ZnGa_2O_4$ has the optical band gap of approximately 4.4 eV [54, 55]. This value relatively agrees with theoretically calculated band gap values [56]. On the other hand, the optical band gap of $ZnAl_2O_4$ in the polycrystalline form has been reported to be 3.8-3.9 eV [22], which seems to be lower than the theoretical band gap values and does not so coincide with most band gap values derived from various kinds of theories [56-59].

Here, we present spinel-structured complete solid solutions: $Zn(Al_xGa_{1-x})_2O_4$, x=0-1.0 in the $ZnAl_2O_4$-$ZnGa_2O_4$ system directly formed as nanocrystals from the aqueous precursor solutions of inorganic metal salts under mild hydrothermal conditions in the presence of tetramethylammonium hydroxide for a short period of time. We report the effect of the substitutional incorporation of aluminum into the spinel lattice on the formation, microstructure, lattice parameter, optical band gap, and luminescence property of the hydrothermally prepared spinel-structured solid solutions.

6-2 Experimental

6-2-1 Synthesis

The spinel-type $Zn(Al_xGa_{1-x})_2O_4$ solid solutions were synthesized by a hydrothermal method using tetramethylammonium hydroxide ($N(CH_3)_4OH$, TMAH). In a typical synthesis, a mixture of an aqueous solution of reagent-grade $ZnSO_4$, $Al(NO_3)_3$ and $Ga(NO_3)_3$ in different ratios of Zn/Al/Ga (that was controlled to be the composition: $Zn(Al_xGa_{1-x})_2O_4$, x=0-1.0) was prepared in a Teflon container. Before hydrothermal treatment, $N(CH_3)_4OH$ solution was added into the solution mixture until the pH of the solution which was hydrothermally treated became weakly basic. This solution mixture with total cation concentrations (Zn + Al + Ga) of 0.20 mol/dm^3 in the Teflon container was then placed in a stainless-steel vessel. The vessel was tightly sealed and it was heated at 120-240 °C for 5 h under rotation at 1.5 rpm. After hydrothermal treatment, the precipitates were washed with distilled water until the pH value of the rinsed water became

7.0, separated from the solution by centrifugation, and dried in an oven at 60 °C.

6-2-2 Characterization

The powder X-ray diffraction (XRD) patterns were collected with a powder diffractometer using CuKα radiation (RINT-2000, Rigaku, Tokyo, Japan). The transmission electron microscopy (TEM) imaging of the as-prepared samples was performed with a microscope (JEM-2010, JEOL, Tokyo, Japan). The crystallite size of cubic phase was calculated from the line broadening of 311 diffraction peak, according to the Scherrer equation, $D_{XRD} = K\lambda / \beta\cos\theta$, where θ is the Bragg angle of diffraction lines; K is a shape factor (K = 0.9 in this work); λ is the wavelength of incident X-rays, and β is the corrected half-width given by $\beta^2 = \beta_m^2 - \beta_s^2$, where β_m is the measured half-width and β_s is the half-width of a standard sample. The lattice parameter was measured using silicon as the internal standard. The thermogravimetric analysis was carried out in the air with a heating rate of 5°C/min (Thermo plus TG8120, Rigaku, Tokyo, Japan).

UV-vis absorption (diffuse reflectance) spectra of the prepared powders were recorded at room temperature and in air by means of ultraviolet-visible spectrophotometer with an integrating sphere attachment (V-560, Nihon Bunko, Tokyo, Japan). The spectra were derived from the measured ones using the Kubelka-Munk equation [60]. Photoluminescence (PL) spectra of the samples were recorded with a fluorescence spectrophotometer (F-2700, Hitachi High-Tech, Japan) with Xe lamp. The sample powders were excited with 270 nm radiation from a 150 W xenon lamp. The emission wavelength was scanned from 280 nm to 800 nm at a scanning rate of 60 nm/min.

6-3 Results and discussion

6-3-1 Formation and structural characteristics of spinel solid solutions

The hydrothermal treatment of the precursor solution mixtures with compositions: $Zn(Al_xGa_{1-x})_2O_4$, x=0 and 1.0 was carried out under weakly basic and hydrothermal conditions at 120°C–240°C using TMAH to get the information on the formation and crystallization of $ZnGa_2O_4$ and $ZnAl_2O_4$ spinel phase, respectively. The XRD patterns of the precipitates formed from the precursor solutions with compositions: x = 0 and 1.0 under hydrothermal conditions at various temperatures are shown in Fig. 1(a) and (b), respectively. As the hydrothermal treatment temperature rises, the XRD lines become sharper and the crystallinity of the precipitates is improved. The precipitates formed at the temperature range of 120-240 °C (x = 0) and 180-240 °C (x = 1.0) were detected as almost a single phase of cubic spinel. The crystallite growth behavior of the cubic spinel phase of the samples (x = 0 and 1.0) are shown

in Fig. 2. It is evident that the crystallite growth of the spinel phase in the composition x = 0 ($ZnGa_2O_4$) is pretty accelerated at lower temperature than that of x = 1.0 ($ZnAl_2O_4$).

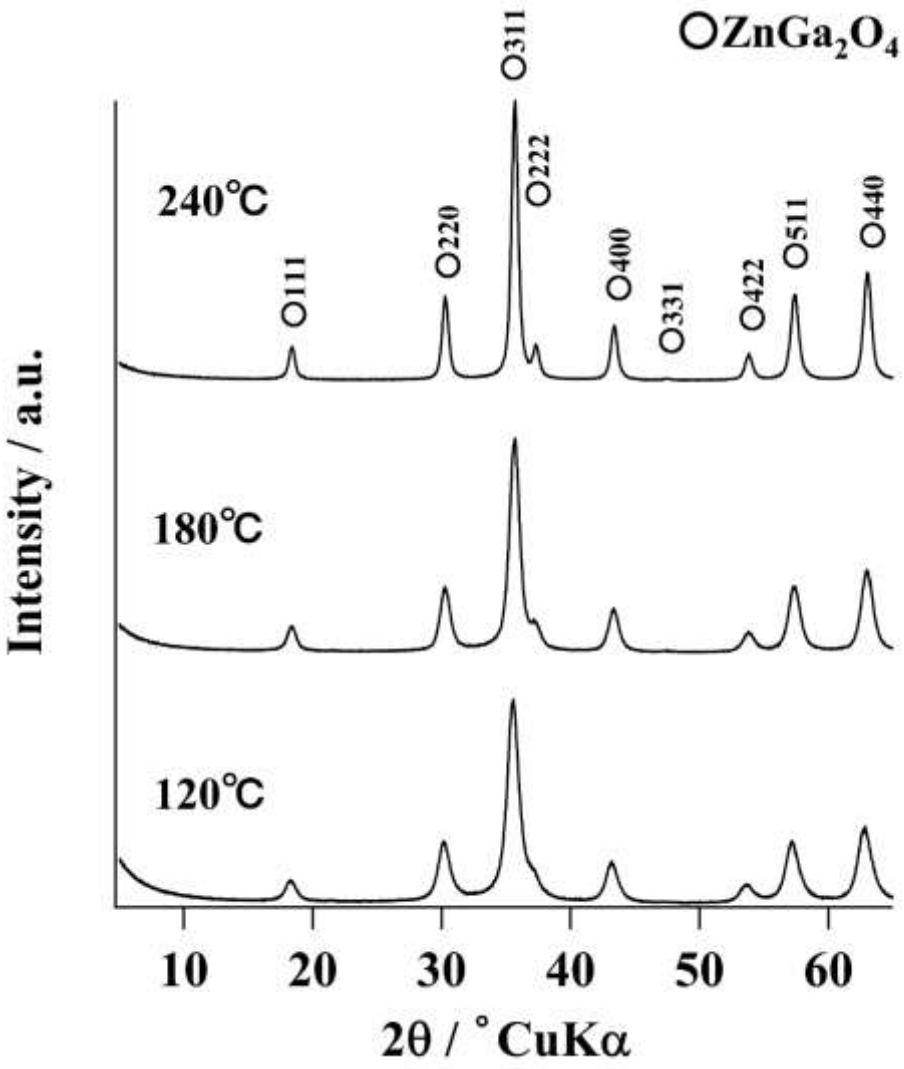

Fig.1(a) X-ray diffraction patterns of precipitates obtained at compositions of $ZnGa_2O_4$, x=0 under hydrothermal conditions at various temperatures for 5 h.

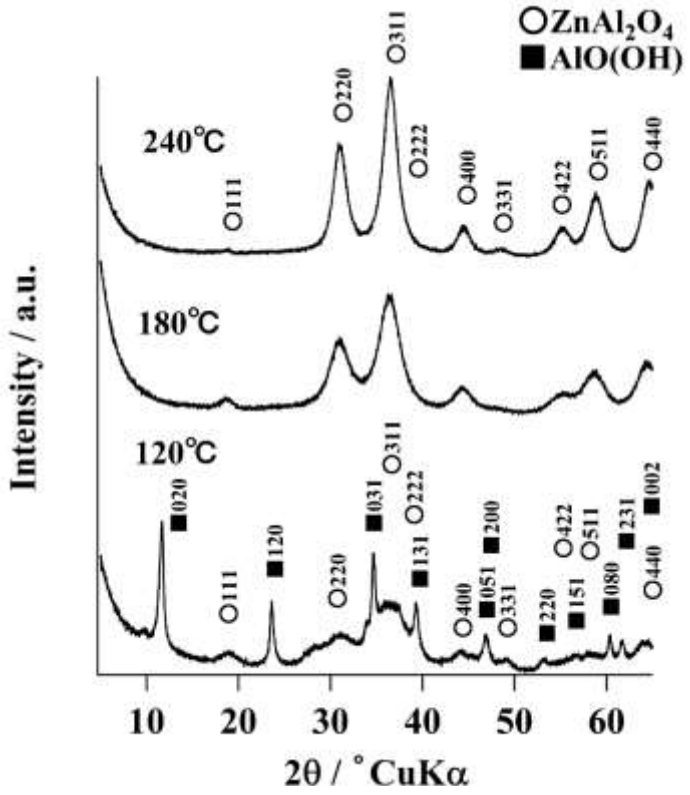

Fig.1(b) X-ray diffraction patterns of precipitates obtained at compositions of $ZnAl_2O_4$, x=1.0 under hydrothermal conditions at various temperatures for 5 h.

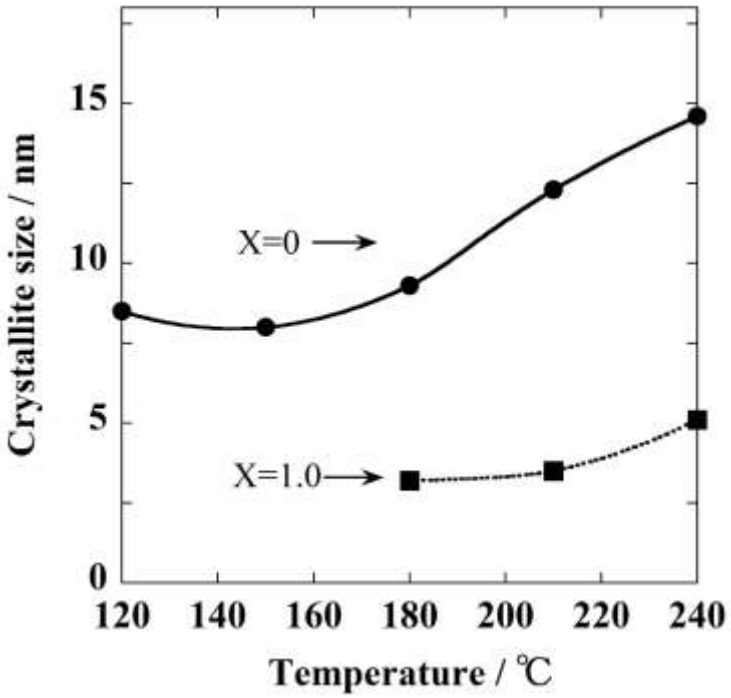

Fig.2 Crystallite size of spinel phase in the precipitates obtained at compositions of $ZnGa_2O_4$, x=0 and $ZnAl_2O_4$, x=1.0 under hydrothermal conditions at various temperatures for 5 h.

The effect of the substitutional incorporation of aluminum component into the lattice, $Zn(Al_xGa_{1-x})_2O_4$ on the formation and structure of spinel-type solid solutions has been investigated. There was no presence of unreacted components of Zn, Al, and Ga in the ultrafiltrated solution after hydrothermal treatment in all samples. Fig. 3 shows the XRD patterns of the as-prepared samples with different Al atomic ratio x from x=0 to 1.0 that were formed under hydrothermal condition at 240 °C for 5 h. As it can be seen, all the patterns are identified as a single phase corresponding to spinel-type cubic structure, and no trace of extra peaks has been detected. Via hydrothermal treatment at 240 °C for 5 h, spinel-type precipitates are formed in the whole composition range from the precursor solutions of inorganic metal salts under weakly basic condition in the presence of TMAH. The XRD data shows a significant decrease in crystallinity of the spinel-type precipitates corresponding to the increase in Al atomic ratio (i.e. the decrease in Ga atomic ratio) in the composition. It is obviously found that the XRD lines, e.g. the 440 diffraction line of the spinel phase slightly and gradually shift to higher degree of 2θ as the Al atomic ratio increases from x=0 to 1.0.

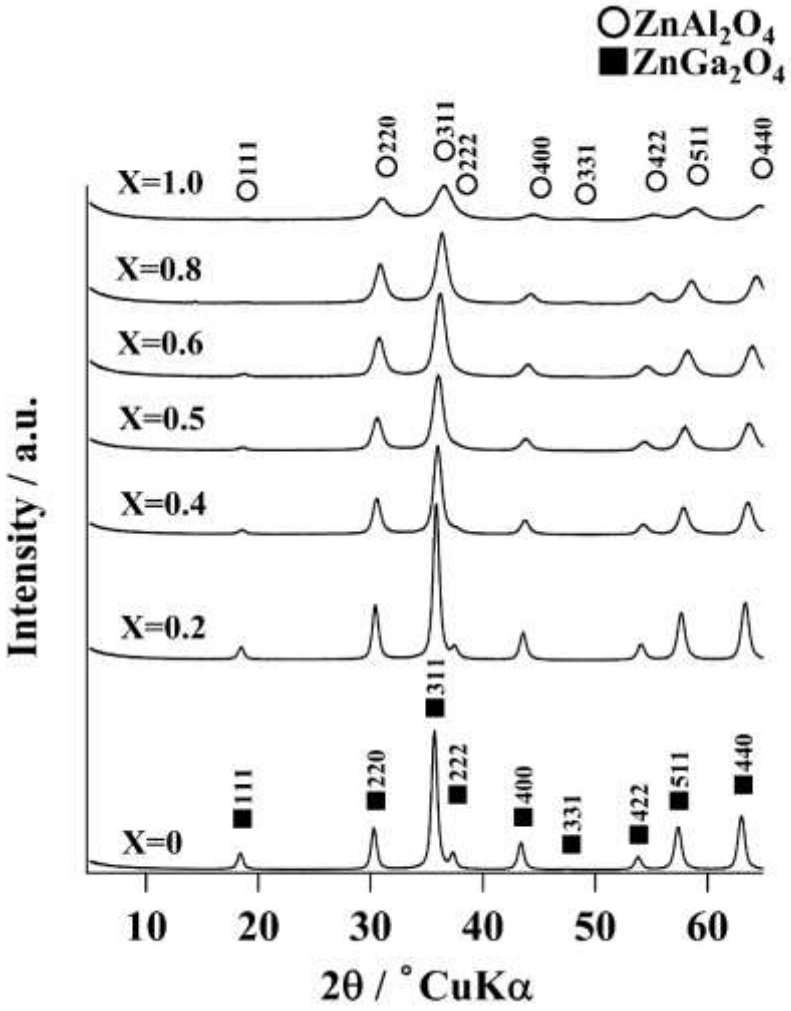

Fig.3 X-ray diffraction patterns of precipitates obtained at various compositions of x=0-1.0 in $Zn(Al_xGa_{1-x})_2O_4$ under hydrothermal conditions at 240 °C for 5 h.

The crystallite size of the spinel phase as-prepared at 240 °C for 5 h is plotted in Fig. 4 as a function of Al atomic ratio x. The products formed in the whole composition range in this study were spinel crystals in the range of nanosize. It is evident that the crystallite size of the spinel almost linearly decreases from 14.5 to 5 nm with the increase in Al atomic ratio. This phenomenon is considered to be due to the fast mass transfer of Ga component, which is suggested by the fact that metallic Ga has a very low melting temperature (29.8 °C) in comparison with Al (660 °C)

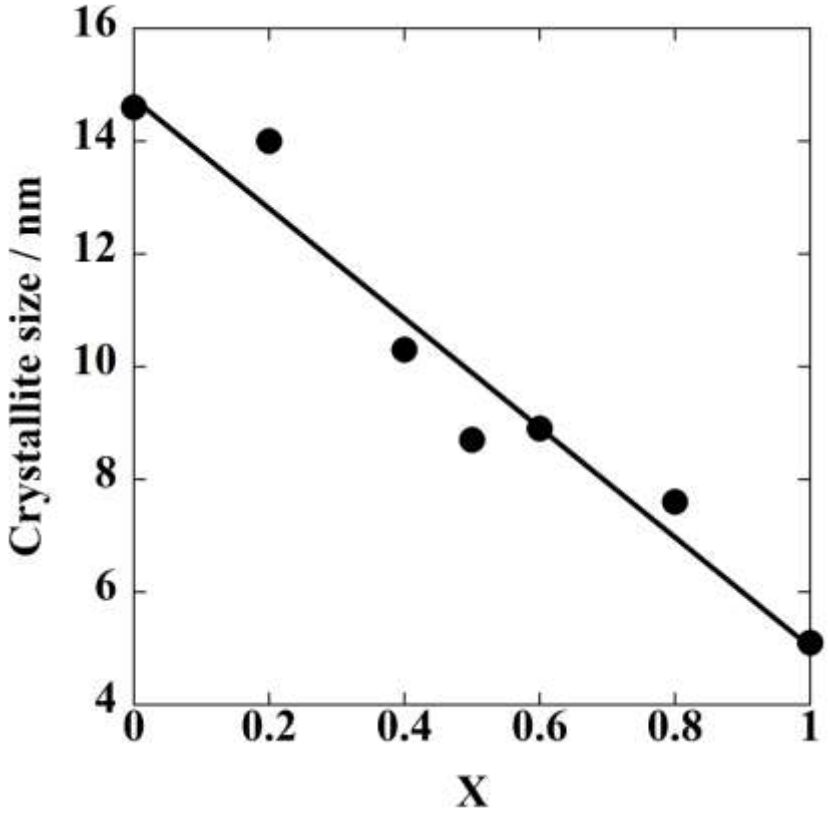

Fig.4 Crystallite size of $Zn(Al_xGa_{1-x})_2O_4$ spinel samples obtained under hydrothermal conditions at 240 °C for 5 h.

Figures 5(a), (b), and (c) present the TEM images of the as-prepared spinel nanocrystals formed under hydrothermal condition at 240°C for 5 h from the precursor solutions with the composition of Al atomic ratio x=0, 0.5, and 1.0, respectively. In Fig. 5(a), the $ZnGa_2O_4$ spinel shows clear lattice fringes due to relatively high crystallinity. Its particle size is approximately 12-15 nm, which agrees with the crystallite size data calculated from the XRD line broadening. This fact implies that these spinel particles are single crystals of spinel. The observed spinel particle size decreases from around 8 to 5 nm when the Al atomic ratio, x increases from x=0.5 to 1.0 as shown in Figs. 5(b) and (c). The phenomenon that the crystallinity of the spinel

particles is decreased by the incorporation of aluminum component into the lattice, $Zn(Al_xGa_{1-x})_2O_4$ is also definitely observed from these TEM images. These spinel particles are relatively homogeneous in size and show narrow particle-size distributions. The crystallite growth rate of the spinel seems to be slow down by the incorporation of aluminum component into the lattice, $Zn(Al_xGa_{1-x})_2O_4$, which is considered to be due to lower mass transfer of Al component under hydrothermal conditions.

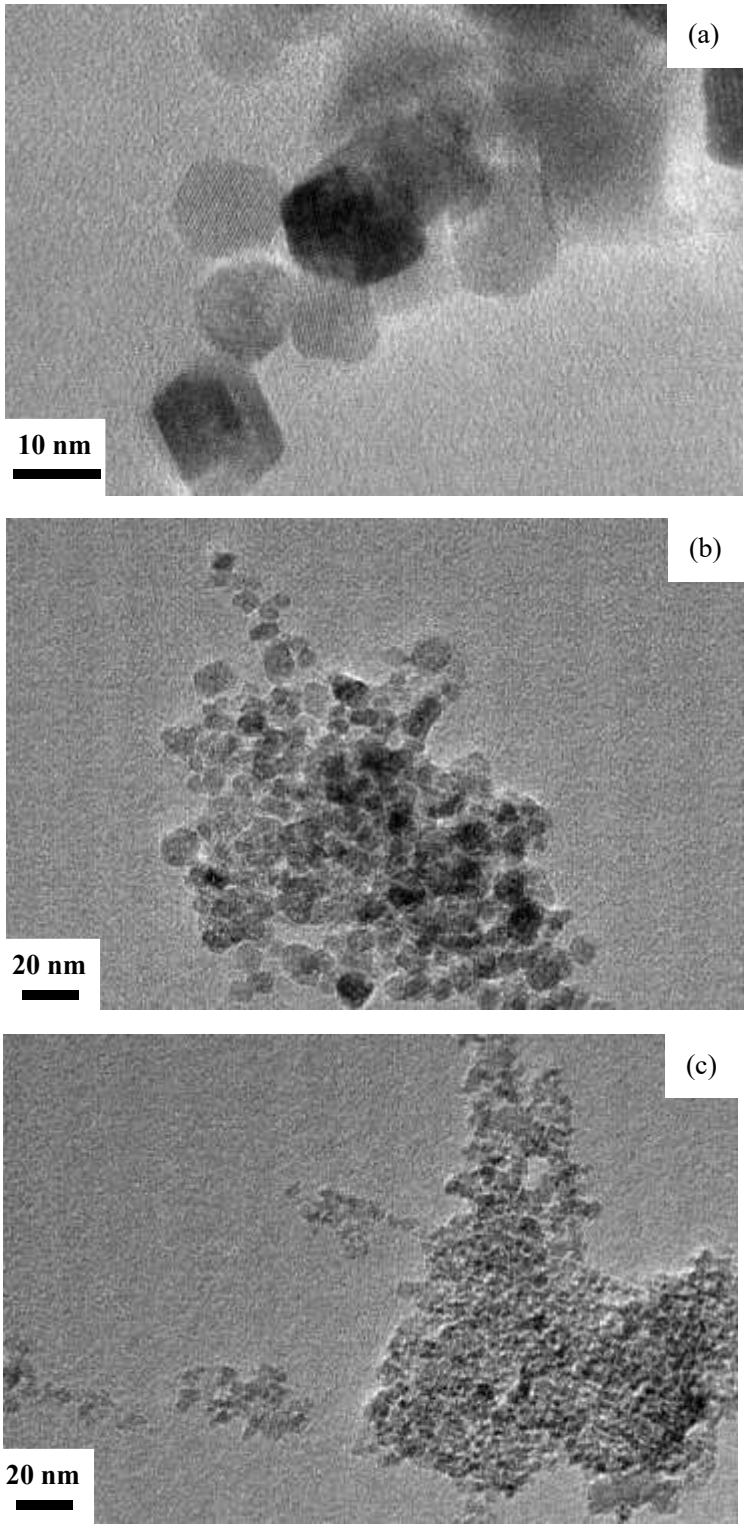

Fig.5 Transmission electron microscopy images of $Zn(Al_xGa_{1-x})_2O_4$ samples: (a) x=0, (b) x=0.5, and (c) x=1.0 obtained under hydrothermal conditions at 240 °C for 5 h.

The details of region around 56-70 ° 2θ, i.e. shifting of the 511 and 440 lines in the XRD patterns of the as-prepared spinel-type $Zn(Al_xGa_{1-x})_2O_4$ precipitates, together with the XRD lines of the internal standard Si around 56 ° and 69 ° 2θ are presented in Fig. 6. It is clearly seen that the 511 and 440 lines shift little by little as the Al atomic ratio increases. This fact is positive evidence that the spinel-type solid solutions were directly formed under mild hydrothermal conditions.

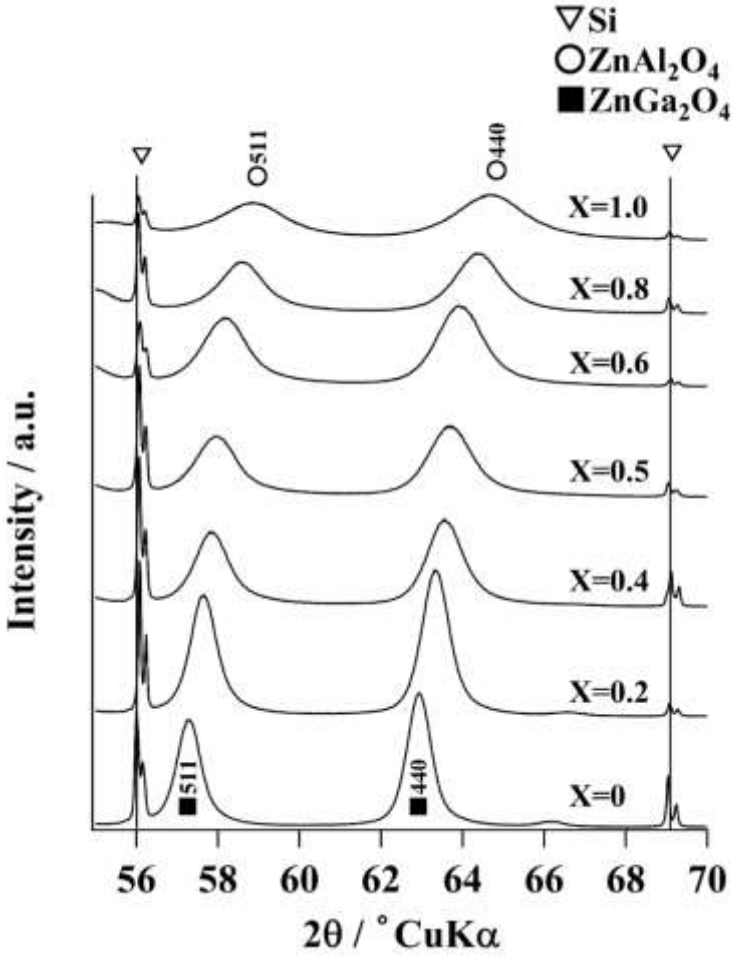

Fig.6 Close-up of the region around 57-65 ° 2θ of the X-ray diffraction patterns of $Zn(Al_xGa_{1-x})_2O_4$ samples prepared under hydrothermal conditions at 240 °C for 5 h.

The change in the lattice parameter a_0 of the cubic phase of the as-prepared nanocrystals with spinel-type structure in the $ZnAl_2O_4$-$ZnGa_2O_4$ system is shown in Fig. 7. Nearly linear decrease in the lattice parameter is observed as the Al atomic ratio increases. The change in the lattice parameter of the spinel solid solutions nearly followed the Vegard's Law. But the line drawn on the figure, which exists slightly apart from the straight line drawn connecting between the lattice

parameter of $ZnGa_2O_4$ spinel (JCPDS No. 38-1240) and that of $ZnAl_2O_4$ spinel (JCPDS No. 05-0669), shows slight and positive departure from the Vegard's Law. Thus, the spinel-type solid solutions in the whole composition range were directly formed under mild hydrothermal conditions.

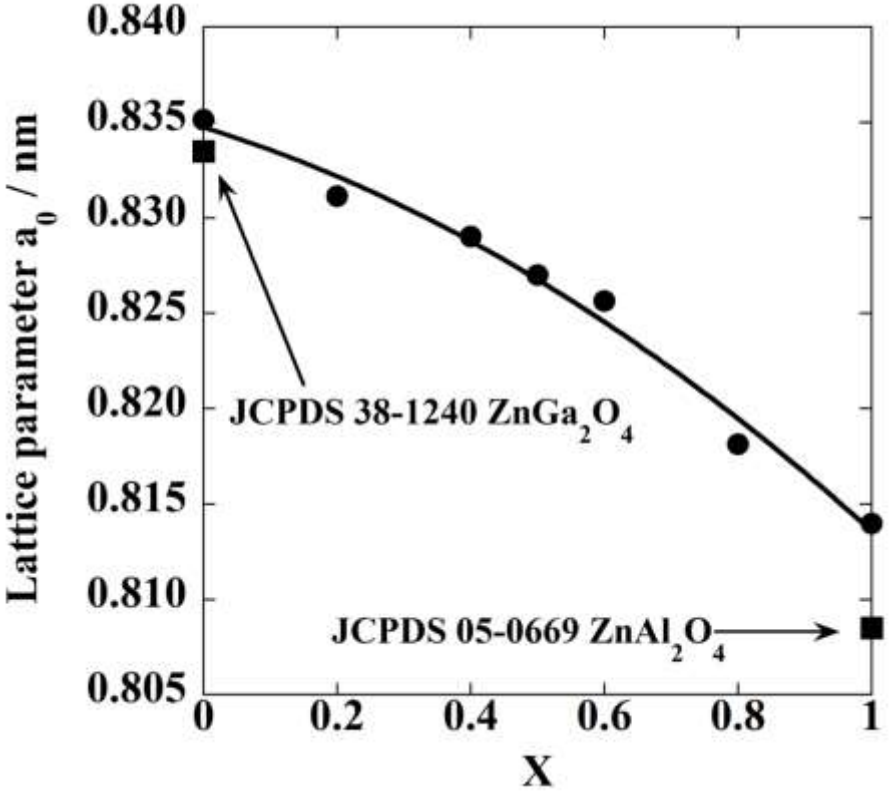

Fig.7 Lattice parameter of $Zn(Al_xGa_{1-x})_2O_4$ samples prepared under hydrothermal conditions at 240 °C for 5 h.

Since the difference between the experimental values and the JCPDS data on the lattice parameter of $ZnGa_2O_4$ and $ZnAl_2O_4$ suggests that the spinel solid solutions formed under hydrothermal conditions may hold small amounts of OH^- species in their structures, TG analysis with heating rate of 5°C/min was carried out for the as-prepared spinel samples. The results are shown in Fig. 8. The TG curves observed on the present samples show weight loss in two steps. It has been reported that the surface of ferrite grains synthesized under hydrothermal conditions was covered with a thin film of water that was chemically bound to the ferrite surface and it was released in the temperature range up to 500°C [61]. Taking this literature into consideration, the TG analysis suggests that the as-prepared samples include small amounts of water, though the total weight loss which depended on their composition was only a little more than 0.2-1.4 mass%. It is evident that the total weight loss of the sample gradually increases as the Al atomic

ratio increases. The $ZnAl_2O_4$ nanocrystals showed the largest amount of weight loss, which may be a reason why the lattice parameter of $ZnAl_2O_4$ was mostly apart from the JCPDS data. The first weight loss (0.1-0.8 mass%) occurs from room temperature to a little above 100 °C, which is due to the release of adsorbed water on the surface. The weight loss at this step is considered to be different from sample to sample. The weight loss at the second step occurs between 200 and 550 °C and is about 0.1-0.55 mass%. The total weight loss of the sample concluded at 500°–600 °C.

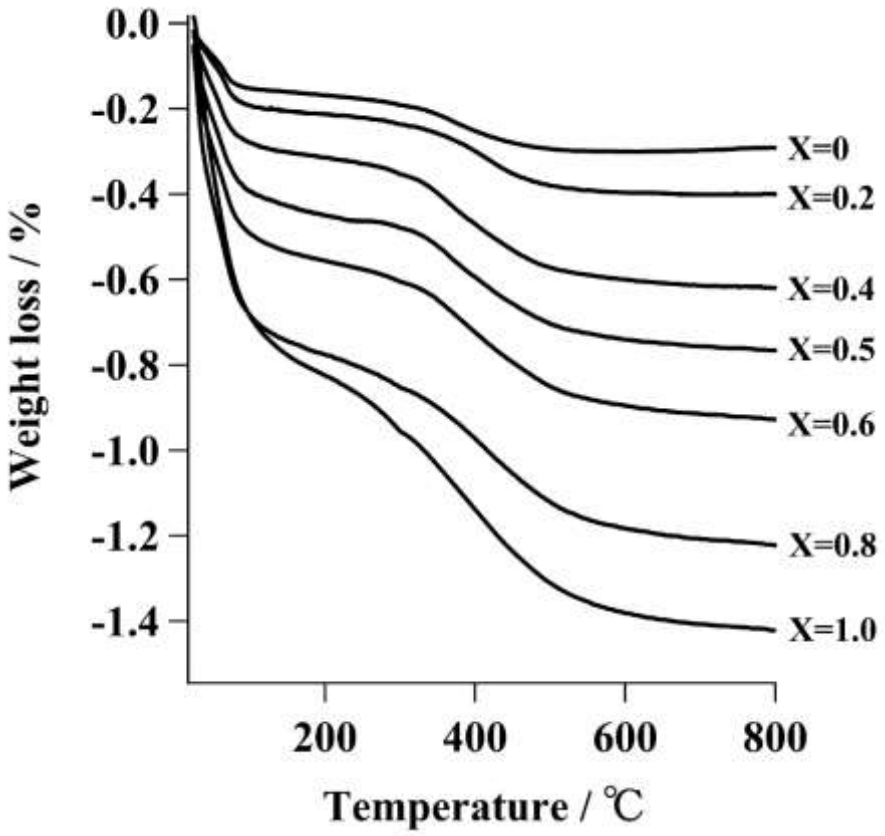

Fig.8 TG curves of $Zn(Al_xGa_{1-x})_2O_4$ samples prepared under hydrothermal conditions at 240 °C for 5 h.

6-3-2 Optical characteristics of spinel solid solutions

The optical properties of the as-prepared spinel solid solutions were evaluated from the measurements of UV-vis absorption spectra and emission spectra. The UV-vis absorption spectra of the as-prepared $Zn(Al_xGa_{1-x})_2O_4$ spinel samples are presented in Fig. 9. It is evidently observed that the absorption edge in the spectra slightly and gradually shifts into shorter wavelengths as the Al atomic ratio in $Zn(Al_xGa_{1-x})_2O_4$ spinel increases. This phenomenon suggests that the increase in the optical band gap of the spinel solid solutions by the substitutional incorporation of Al into the lattice, $Zn(Al_xGa_{1-x})_2O_4$, that is to say, $ZnAl_2O_4$ has a larger band gap than $ZnGa_2O_4$.

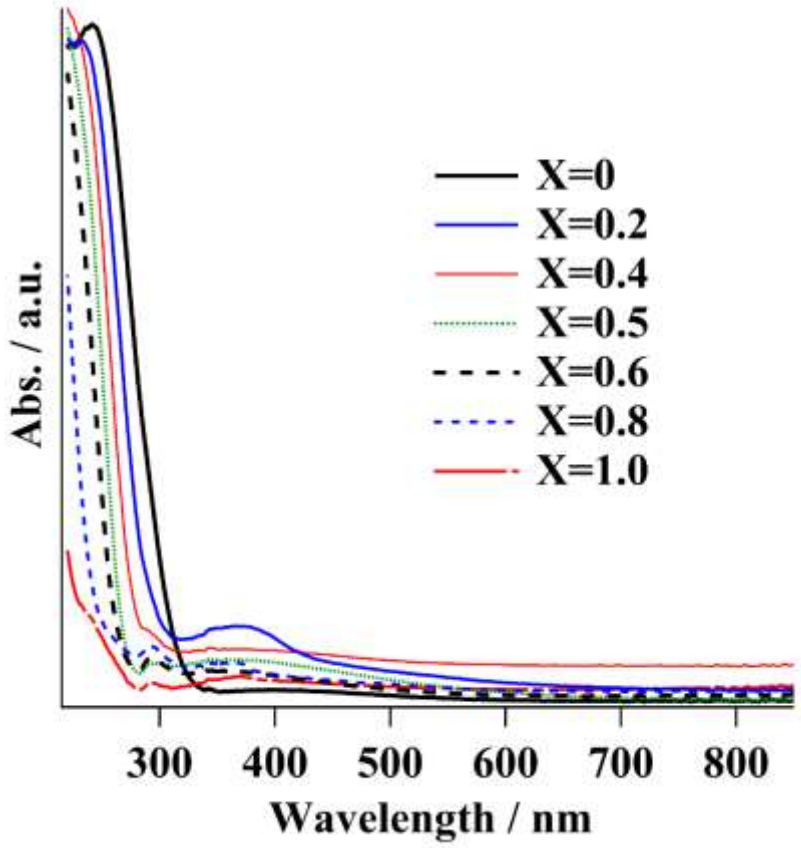

Fig.9 Diffuse reflectance spectra of $Zn(Al_xGa_{1-x})_2O_4$ samples prepared under hydrothermal conditions at 240 °C for 5 h.

The optical band gap was estimated from the plots of transformed Kubelka-Munk function vs. the energy of light absorbed of samples. In Fig. 10, the optical band gap of the as-prepared $Zn(Al_xGa_{1-x})_2O_4$ spinel is plotted against the value x (i.e. Al atomic ratio). It is obviously

observed that the optical band gap almost linearly increases as the Al atomic ratio in $Zn(Al_xGa_{1-x})_2O_4$ spinel increases. The substitutional incorporation of Al into $ZnGa_2O_4$ widens its band gap, leading to a blue shift in the band gap absorption.

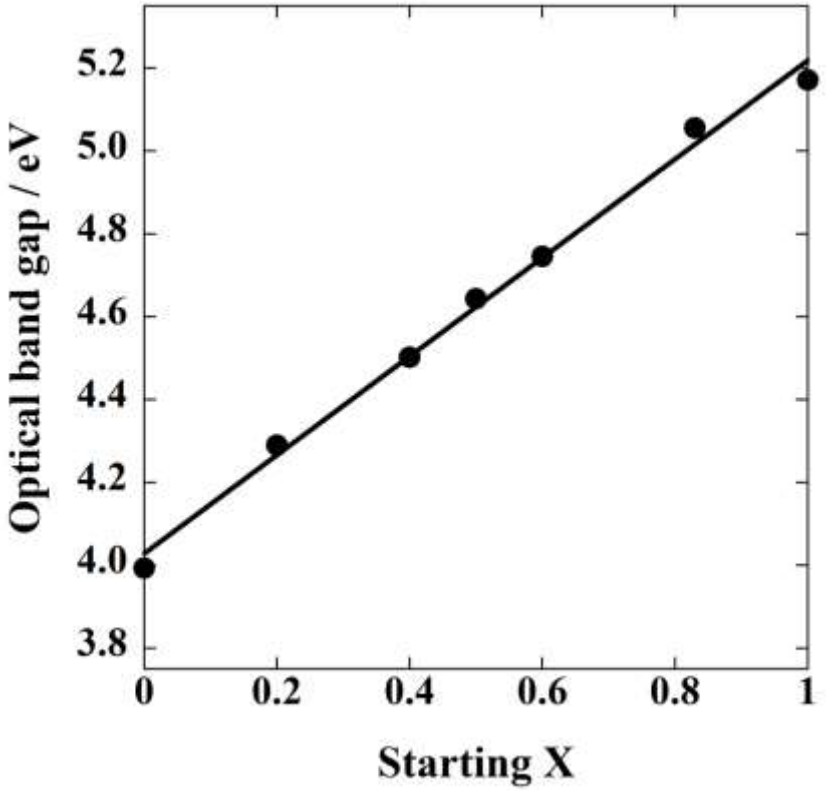

Fig.10 Optical band gap of $Zn(Al_xGa_{1-x})_2O_4$ samples prepared under hydrothermal conditions at 240 °C for 5 h.

Regarding the band gap of spinel-type $ZnAl_2O_4$ and $ZnGa_2O_4$, different estimations of their theoretical band gaps have been done from their electronic and band structures using the tight-binding muffin-tin orbital method (TB-LMTO) [62], the density functional theory (DFT) [56], the GW approximation [57], and the modified Becke-Johnson potential (MBJ) [58, 59]. All these theoretical estimations have shown that $ZnAl_2O_4$ has a larger band gap than $ZnGa_2O_4$, though the experimental values of the band gap of spinel-type $ZnAl_2O_4$ and $ZnGa_2O_4$ have been reported to be 3.8-3.9 and 4.1-4.3, respectively in the literature [22]. However, in this literature it has been stated that "Given the same crystal structures, the compounds that contain the heavier atoms–i.e., the gallates–must have the smaller energy band gaps" [22]. It is evident from the present study that the $ZnAl_2O_4$ spinel has a wider band gap than $ZnGa_2O_4$ spinel in accordance with the suggestions from those theoretical calculations, even if taking the quantum size effect into consideration. It has been clearly shown in this study that the optical band gap

of $Zn(Al_xGa_{1-x})_2O_4$ spinel solid solutions increases as the substitutional incorporation amount of Al into the lattice, $Zn(Al_xGa_{1-x})_2O_4$ increases.

The effect of the composition on the photoluminescence property of the $Zn(Al_xGa_{1-x})_2O_4$ spinel solid solutions formed at 240 °C was investigated. Fig. 11 shows the room temperature emission spectra of the $Zn(Al_xGa_{1-x})_2O_4$ spinel solid solutions under excitation at 270nm Xe lamp. The $ZnGa_2O_4$ spine showed a broad-band UV-visible blue light emission centered at around 480 nm. The blue emission of $ZnGa_2O_4$ spinel has been explained that it originates from the self-activation center of the octahedral GaO_6 group in the spinel lattices and the Ga^{3+} ions combine with UV-generated free electrons produced in oxygen vacancies [11, 36, 54]. The shifts of the emission band were observed corresponding to the compositional change of the spinel. The substitutional incorporation of Al into $ZnGa_2O_4$ results in the blue shifts of the absorption and photoluminescence bands of $ZnGa_2O_4$, which is explained by the wider band gap of solid solutions formed by the incorporation of Al.

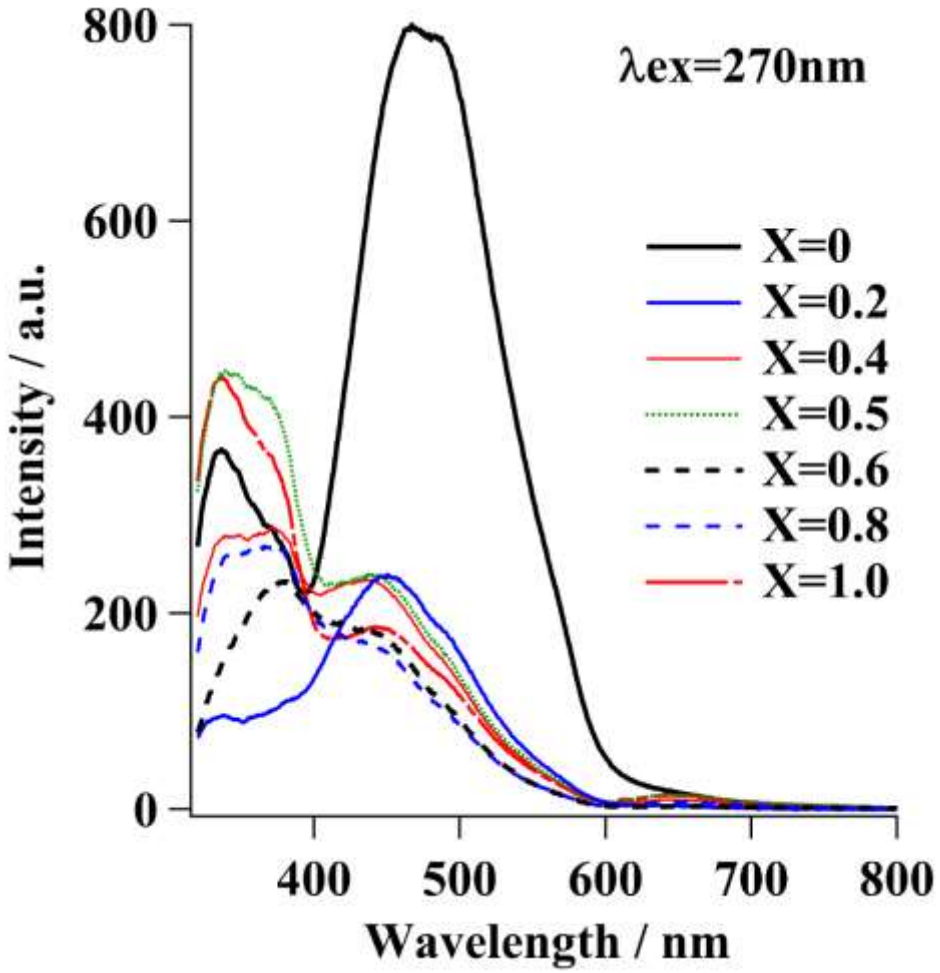

Fig.11 Emission spectra of $Zn(Al_xGa_{1-x})_2O_4$ samples prepared under hydrothermal conditions at 240 °C for 5 h. (λ_{ex} = 270 nm)

6-4 Conclusion

Nanocrystalline spinel-structured $Zn(Al_xGa_{1-x})_2O_4$ solid solutions were hydrothermally formed from the aqueous precursor solutions of $ZnSO_4$, $Al(NO_3)_3$ and $Ga(NO_3)_3$ at 240 °C for 5 h in the presence of tetramethylammonium hydroxide. The crystallite growth of the spinel under hydrothermal condition was lowered by the substitutional incorporation of Al into $ZnGa_2O_4$. As the Al atomic ratio, x in the system increased from x=0 to 1.0, the lattice parameter of the spinel gradually decreased, and the change in the lattice parameter of the spinel nearly followed the Vegard's law. The optical band gap of the $Zn(Al_xGa_{1-x})_2O_4$ spinel solid solutions increased as the incorporation amount of Al into the spinel lattice increased. The substitutional incorporation of Al into $ZnGa_2O_4$ resulted in the blue shifts of the absorption and photoluminescence bands of $ZnGa_2O_4$, which was due to the wider band gap of the solid solutions formed by the incorporation of Al.

References

1. Y. E. Lee, D. P. Norton, and J. D. Budai, *Appl. Phys. Lett*., **74**:3155-57, (1999)
2. S. Sun, H. Zeng, D. B. Robinson, S. Raoux, P. M. Rice, S. X. Wang, and G. Li, *J. Am. Chem. Soc*., **126**:273-9, (2004)
3. Y. P. He, S. Q. Wang, C. R. Li, Y. M. Miao, Z. Y. Wu, and B. S. Zou, *J. Phys. D: Appl. Phys*., **38**:1342-50, (2005)
4. M. M. Thackeray, W. I. F. David, P. G. Bruce, and J. B. Goodenough, *Mater. Res. Bull*., **18**:461-72, (1983)
5. G. Zhao, J.-J. Feng, Q.-L. Zhang, S.-P. Li, and H.-Y. Chen, *Chem. Mater*., **17**:3154-9, (2005)
6. C. Cabet, A. C. Roger, A. Kiennemann, S. Lakamp, and G. Pourroy, *J. Catal*., **173**:64-73, (1998)
7. T. Minami, *MRS Bull*., **25**:38-44, (2000)
8. A. F. Wells, *Structural Inorganic Chemistry*, p. 489. Oxford University Press, London, (1975)
9. T. Minami, Y. Kuroi, and S. Takata, *J. Vac. Sci*. Te*chnol. A*, **14**:1736-40, (1996)
10. L. E. Shea, R. K. Datta, and J. J., Jr. Brown, *J. Electrochem. Soc*., **141**:1950-4, (1994)
11. S. Itoh, H. Toki, Y. Sato, K. Morimoto and T. Kishino, *J. Electrochem. Soc*., **138**:1509-12, (1991)
12. T. K. Tran, W. Park, J. W. Tomm, B. K. Wagner, S. M. Jacobsen, C. J. Summers, P. N. Yocom, and S. K. McClelland, *J. Appl. Phys*., **78**:5691-5, (1995)
13. J. S. Kim, S. G. Lee, H. L. Park, J. Y. Park, and S. D. Han, *Mater. Lett*., **58**:1354-7, (2004)
14. T. Omata, N. Ueda, K. Ueda, and H. Kawazoe, *Appl. Phys. Lett*., **64**:1077-8, (1994)
15. J.-G. Kho, H.-D. Park, and D.-P. Kim, *Bull, Korean. Chem. Soc*., **20**:1035-9, (1999)
16. P. D. Rack, J. J. Peterson, M. D. Potter, and W. Park, *J.Mater. Res*., **16**:1429-33, (2001)
17. Z. Xu, Y. Li, Z. Liu, and D. Wang, *J. Alloys Comp*., **391**:202-5, (2005)
18. H. Matsui, C. N. Xu, and H. Tateyama, *Appl. Phys. Lett*., **78**:1068-70, (2001)
19. E. Martinez-Sanchez, M. Garcia-Hipolito, J. Guzman, F. Ramos-Brito, J. Santoyo Salazar, R. Martinez-Martinez, O. Alvarez-Fregoso, M. I. Ramos-Cortes, J. J. Mendez-Delgado, and C. Falcony, *Phys. Status Solidi A*, **202**:102-7, (2005)
20. Z. Lou and J. Hao, *Appl. Phys. A: Mater. Sci. Process*., **80**:151-4, (2005)
21. A. R. Phani, M. Passacantando, and S. Santucci, *Mater. Chem. Phys*., **68**:66-71, (2001)
22. S. K. Sampsth and J. F. Cordaro, *J. Am. Ceram. Soc*., **81**:649-54, (1998)
23. X. Li, Z. Zhu, Q. Zhao, and L. Wang, *J. Hazardous Mater*., **186**:2089-96, (2011)
24. T. K. Shioyama, *U. S. Patent* 4,260,845 (1981)
25. G. Aquilar-Rios, M. Valenzuela, P. Salas, H. Armendariz, P. Bosch, G. Del Toro, R. Sila, V. Bertin, S. Castillo, and A. I. Schifter, *Appl. Catal. A: General*, **127**:65-75, (1995)
26. T. El-Nabarany, A.A. Attia, and M. N. Alayn, *Matter. Lett*., **24**:319-25, (1995)
27. R. Roesky, J. Weiguny, H. Bestgen, and U. Dingerdissen, *Appl. Catal. A: General*, **176**:213-

20, (1999)
28. D. J. Norris, A. L. Efros, and S. C. Erwin, *Science*, **319**:1776-9, (2008)
29. M. Hirano and Y. Ichihashi, *J. Mater. Sci*., **44**:6135-40, (2009)
30. M. Hirano and H. Dozono, *Mater. Res. Bull*., **50**:213-20, (2014)
31. K. Byrappa and T. Adschiri, *Progr. Cryst. Growth .Charact. Mater*., **53**:117-66, (2007)
32. S. Feng and R. Xu, *Acc. Chem. Res*., **34**:239-47, (2001)
33. M. Hirano, H. Dozono, and T. Kono, *Mater. Res. Bull*., **46**:1384-90, (2011)
34. Z. Yan and H. Takei, *J. Cryst. Growth*, **171**:131-5, (1997)
35. Z. Yan, H. Takei, and H. Kawazoe, *J. Am. Ceram. Soc*., **81**:180-6, (1998)
36. L. Zou, X. Xiang, M. Wei, F. Li, and D. G. Evans, *Inorg. Chem*., **47**:1361-9, (2008)
37. A. C. Tas, P. J. Majewski, and F. Aldinger, *J. Mater. Res*., **17**:1425-33, (2002)
38. T. Sei, Y. Nomura, and T. Tsuchiya, *J. Non-Cryst. Solids*, **218**:135-8, (1997)
39. M. Hirano, S. Okumura, Y. Hasegawa, and M. Inagaki, *Int. J. Inorg. Mater*., **3**:797-801, (2001)
40. M. Hirano, S. Okumura, Y. Hasegawa, and M. Inagaki, *J. Solid State Chem*., **168**:5-10, (2002)
41. M. Hirano, *J. Mater Chem*. **10**:469-72, (2000)
42. M. Hirano and N. Sakaida, *J. Am. Ceram. Soc*., **85**:1145-50, (2002)
43. J. Y. Kim, J. H. Kang, D. C. Lee, and D. Y. Jeon, *J. Vac. Soc. Technol.B*, **21**:532-5, (2003)
44. W. S. Hong, J. L. De, X. Yang, and M. N. Rahaman, *J. Am. Ceram. Soc*., **78**:3217-24, (1995)
45. G. F. Huttig, H. Worl, and H. H. Weitzer, *Zeitschrift fuer Anorganische und Allgemeine Chemie*, **283**:207-16, (1956)
46. L. K. Kurihara, and S. L. Suib, *Chem. Mater*., **5**:609-13, (1993)
47. S. Mathur, M. Veith, M. Haas, H. Shen, N. Lecerf, and V. Huch, *J. Am. Ceram. Soc*., **84**:1921-8, (2001)
48. X. Y. Chen, C. Ma, Z. J. Zhang, and B. N. Wang, *Mater. Res. Bull*., **45**:1889-93, (2010)
49. L. Mu, J. Wan, Z. Wang, Y. Gao, and Y. Qian, *J. Nanosci. Nanotechnol*., **6**:863-7, (2006)
50. M. Zawadzki and J. Wrzyszcz, *Mater. Res. Bull*., **35**:109-14, (2000)
51. Z. Chen, E. Shi, Y. Zheng, W. Li, N. Wu, and W. Zhong, *Mater. Lett*., **56**:601-5, (2002)
52. Y. Wang and K. Wu, *J. Am, Chem. Soc*., **127**:9686-7, (2005)
53. T. Takeguchi, Y. Kani, M. Inoue, and K. Eguchi, *Catal. Lett*., **83**:49-53, (2002)
54. I. K. Jeong, H. L. Park, and S. I. Mho, *Solid State Commun*., **105**:179-83, (1998)
55. D. P. Dutta, R. Ghildiyal, and A. K. Tyagi, *J. Phys. Chem. C*., **113**:16954-61, (2009)
56. H. Dixit, N. Tandon, S. Cottenier, R. Saniz, D. Lamoen, B. Partoens, V. V. Speybroecl, and M. Waroquier, *New J. Phys*., **13**:063002 (2011)
57. W. G. Aulbur, L. Jönsson, and J. W. Wilkins, *Solid State Phys*., **54**:1-218, (1999)
58. F. Tran and P. Blaha, *Phys. Rev. Lett*., **102**:226401, (2009)
59. F. Tran, P. Blaha, and K. Schwarz, *J. Phys.: Condens. Matter*, **19**:196208, (2007)

60. P. Kubelka and F. Munk, *In Zeits. Für Techn. Physik*. **12**:593-601, (1931)
61. M. Rozman and M. Drofenik, *J. Am. Ceram. Soc*., **78**:2449–55, (1995)
62. S. K. Sampath, D. G. Kanhere, and R. Pandey, *J. Phys. Cond. Matt*. **11**:3635-44, (1999)

Chapter 7
Conclusions

Spinel compounds have been used in a wide variety of application areas as a main member of ceramic materials due to their various attractive properties. The electric, electronic, magnetic, semi-conductive, electrochemical, catalytic, and optical properties of some of the representative spinel members and their usages are described in addition to their structures in chapter 1. In general, particles in the range from 1 to 100 nanometers are referred to as nanoparticles. In recent years, the research on nanoparticles and nanocrystals is an area of intense scientific interest due to a variety of potential applications in optical, electronic, magnetic, and biomedical fields. The direct formation of spinel nanoparticles in the Al_2O_3-Ga_2O_3 and $ZnAl_2O_4$-$ZnGa_2O_4$ systems from aqueous precursor solutions of inorganic salts by means of a simple and mild hydrothermal method was conducted and the results obtained on this study are summarized.

7-1 Gallium oxide spinel nanoparticles

Hydrothermal treatment of the aqueous precursor solution of $Ga(NO_3)_3$ or $Ga_2(SO_4)_3$ was carried out under weakly basic conditions at 180~240 °C for 5 h in the presence of citric acid. When citric acid was not present in these weakly basic precursor solutions, a single phase of GaO(OH) was only formed after hydrothermal treatment. To inhibit the formation of GaO(OH) phase at low temperatures, citric acid effectively acted as chelating ligand. Gallium oxide (γ-Ga_2O_3) nanoparticles with a single-phase of spinel-type structure were directly formed in the precursor solution by inhibiting the formation of GaO(OH) phase using citric acid. The crystallite size of γ-Ga_2O_3 spinel that was hydrothermally formed was in the range from 5 to 9 nm. The optical band gap value of the as-prepared γ-Ga_2O_3 was 4.88 eV. The γ-Ga_2O_3 nanocrystals synthesized at 180 °C emitted a broad-band visible violet-blue light spectrum with a peak wavelength at 410 nm, centered at around 425 nm under excitation at 325 nm. The emission intensity of γ-Ga_2O_3 depended on hydrothermal treatment temperature. The γ-Ga_2O_3 maintained spinel structure after heating up to 600 °C for 1 h, and it fully transformed into β-Ga_2O_3 phase during heating at 800 °C. The luminescence intensity of gallium oxide decreased and the peak wavelength of emission spectrum shifted to lower wavelengths after heating at 600 and 800 °C for 1 h in air.

7-2 Gallium and aluminum oxide spinel nanoparticles

Spinel-type γ-Ga_2O_3-Al_2O_3 nanoparticles, i.e., $(Al_xGa_{1.00-x})_2O_3$, x=0~0.85 with crystallite size of spinel phase in the range of 4~5 nm were hydrothermally formed from the aqueous

precursor solutions of $Ga(NO_3)_3$ and $Al_2(SO_4)_3$ under weakly basic conditions using aqueous ammonia in the presence of citric acid at 180 °C for 5 h. Under the present hydrothermal conditions in the absence of citric acid, crystalline GaO(OH) and AlO(OH) phases were formed from the weakly basic precursor solutions. The direct formation of γ-Ga_2O_3-based spinel nanoparticles doped with alumina component was considered to be achieved when the presence of citric acid as chelating ligand prohibited the aluminum and gallium hydroxide phases from crystallizing in the precursor solutions in the early stage of hydrothermal treatment at low temperature. As-prepared $(Al_xGa_{1.00-x})_2O_3$ samples presented a broad-band visible violet-blue light emission with a peak wavelength at 410~415 nm under excitation at 325 nm. The most intense emission was obtained in the as-prepared nanoparticles with a composition $(Al_{0.50}Ga_{0.50})_2O_3$. The spinel phase of nanoparticles in all compositions except x=1.00 was maintained after heating at 600 °C for 1 h. After heating at 1000°C, there appeared the structure similar to the β-Ga_2O_3 phase that was transformed from the spinel phase in the nanoparticles with compositions from Ga_2O_3 to $(Al_{0.50}Ga_{0.50})_2O_3$. The spinel-phase was still preserved in the $(Al_{0.75}Ga_{0.25})_2O_3$ nanoparticles after heating at 1000 °C for 1 h, though a single phase of θ-Al_2O_3 in the case of pure Al_2O_3 composition was observed.

7-3 Zinc gallate and aluminate spinel nanoparticles

The mild hydrothermal treatment of the aqueous precursor solutions of $ZnSO_4$, $Al(NO_3)_3$ and $Ga(NO_3)_3$ was conducted using tetramethylammonium hydroxide at an intermediate composition, $ZnAlGaO_4$ in the $ZnAl_2O_4$-$ZnGa_2O_4$ system to form spinel-type nanoparticles. A slight decrease in the cell size of as-prepared spinel phase was observed with increased hydrothermal treatment temperature. The cell size of the as-prepared spinel nanoparticles that were formed at low hydrothermal treatment temperature slightly and gradually changed by heating up to 800 °C for 1 h in air, and it almost accorded with the ideal value reported in the reference after heating higher than 800 °C.

The low-temperature synthesis of spinel-type nanoparticles, in the $ZnAl_2O_4$-$ZnGa_2O_4$ system was done under hydrothermal condition at 180 °C for 5 h. Nanoparticles with spinel phase in the whole composition range were formed under wakly basic conditions in the presence of tetramethylammonium hydroxide. The relationship between the lattice parameter of as-prepared samples and the Al atomic ratio in the spinel composition was slightly apart from the ideal linear relationship that was obtained in the samples after heating at 1000 °C in air. The optical band gap value of both as-prepared nanoparticles and those after heating gradually changed from 4.1~4.2 to 5.25 eV by doping aluminum ion into the lattice, $Zn(Al_xGa_{1-x})_2O_4$. Two main broad-band emission spectra centered at around 360 and 430 nm were observed in the nanoparticles under excitation at 270 nm, but their broad-band emission spectra and their peak wavelengths subtly changed depending on the composition and heating in air.

Spinel-type nanoparticles: $Zn(Al_xGa_{1-x})_2O_4$, x=0~1.0 were directly formed as a complete solid solution from the aqueous precursor solutions of inorganic salts under hydrothermal condition at 240 °C for 5 h in the presence of tetramethylammonium hydroxide. The crystallite size of the spinel phase decreased from 14.5 to 5 nm with increased Al atomic ratio, x in the composition from x=0 to 1.0. The change in the lattice parameter of the spinel phase by the substitutional incorporation of Al into the lattice nearly followed the Vegard's Law though a slight positive departure from the Law was observed. The blue shift of absorption spectra was observed by the incorporation of Al into the lattice, $Zn(Al_xGa_{1-x})_2O_4$, which resulted in wider optical band gap. The broad-band UV-visible blue light emission of the $ZnGa_2O_4$ spinel that was observed under excitation at 270 nm shifted to lower wavelength by the incorporation of Al into the lattice, $Zn(Al_xGa_{1-x})_2O_4$.

List of publications

1. "Direct formation and phase stability of luminescent γ-Ga_2O_3 spinel nanocrystals via hydrothermal method"
   Masanori Hirano, **Kazuki Sakoda**, and Yoshiaki Hirose, *Journal of Sol-Gel Science and Technology,* vol. 77, No.2, pp. 348-354 (2016)

2. "Direct formation of spinel-structured γ-Ga_2O_3-Al_2O_3 nanoparticles by a mild hydrothermal method"
   Masanori Hirano, **Kazuki Sakoda**, Kento Souma, Hiroya Nishimoto, Kouki Jinno, and Yoshiaki Hirose, *Ceramics International*, Vol. 41, pp. 14285-14292 (2015)

3. "Hydrothermal Synthesis of $ZnAlGaO_4$ and the Effect of the Post-heat Treatment on the Enhancement in Crystallinity"
   Kazuki Sakoda and Masanori Hirano, *Journal of Ceramic Science and Technology*, Vol. 6 No. 1, pp. 9-16 (2015)

4. "Effect of Heat-treatment and Composition on Structure and Luminescence Properties of Spinel-type Solid Solution Nanocrystals"
   Kazuki Sakoda, Masanori Hirano, *Journal of Nanoscience and Nanotechnology*, Vol. 15, pp. 6069-6077 (2015)

5. "Formation of complete solid solutions, $Zn(Al_xGa_{1-x})_2O_4$ spinel nanocrystals via hydrothermal route"
   Kazuki Sakoda, Masanori Hirano, *Ceramics International*, Vol. 40, pp. 15841-15848 (2014)

Presentations at international conference

1. “Hydrothermal Formation of γ-$(Al,Ga)_2O_3$ Spinel Nanoparticles”,
   Kazuki Sakoda Yoshiaki Hirose, Kento Souma, Hiroya Nishimoto, Kouki Jinno, and Masanori Hirano,
   The 18th International Conference on Crystal Growth and Epitaxy, Nagoya, Japan, August 7-12 (2016)

2. “Hydrothermal Formation and Photoluminescence of Spinel Nanocrystals in the $ZnAl_2O_4$ $ZnAl_2O_4$-$ZnGa_2O_4$ system”
   Kazuki Sakoda and Masanori Hirano,
   XVIII International Sol-Gel Conference (Sol-Gel 2015), Kyoto, Japan, September 6-11 (2015)

3. “Synthesis of $Zn(Al_XGa_{1-X})_2O_4$ Spinel Solid Solutions through Hydrothermal Method”
   Kazuki Sakoda and Masanori Hirano,
   The 5th International Conference on the Characterization and Control of Interfaces for High Quality Advanced Materials, Kurashiki, Japan, July 7-10 (2015)

Acknowledgements

The present study has been performed at the Ceramics Laboratory, Department of Applied Chemistry, Aichi Institute of Technology in the period from 2012 to 2016.

I would like to give my best gratitude and acknowledgement to Prof. Masanori Hirano and Prof. Yuichi Kobayashi, my supervisors in my doctoral course, for their continuous encouragement, cordial guidance and suggestions during the course of this dissertation.

The author gratefully acknowledges Prof. Yoshimi Ohzawa (Aichi Institute of Technology) and Prof. Shinobu Hashimoto (Nagoya Institute of Technology) for their useful advices and encouragement.

I would like to acknowledge and thank Dr. Masaki Katayama, Mr. Yushuke Nunome, Mr. Hiroki Ichihashi, Mr. Hayato Dozono, Mr. Shinya Kondo, Mr. Takahiro Okamoto, Mr. Katuya Ishikawa, Mr. Toshiaki Omori, Mr. Tokifumi Iwata, Mr. Toshihiko Shimizu and Mr. Yuki Takagi for their many helps in my student life. Additionally, I thank all the students of Ceramics Laboratory.

Finally, the author expresses his gratitude to his parents for their continuous support and encouragement.

February 2017